

NORTHWESTERN UNIVERSITY

The Influence of Surface Chemistry on the Optoelectronic Properties of Semiconductor Quantum Dots

A DISSERTATION

SUBMITTED TO THE GRADUATE SCHOOL
IN PARTIAL FULFILLMENT OF THE REQUIREMENTS

for the degree

DOCTOR OF PHILOSOPHY

Field of Chemistry

By

Rachel Dory Harris

EVANSTON, ILLINOIS

September 2017

© Copyright by Rachel Dory Harris 2017
All Rights Reserved

“If there is an equation for a curve like a bell,
there must be an equation for one like a bluebell,
and if a bluebell, why not a rose?”

Arcadia (1.3)

ABSTRACT

The Influence of Surface Chemistry on the Optoelectronic Properties of Semiconductor Quantum Dots

Rachel Dory Harris

This dissertation describes the relationship between the surface chemistry of colloidal semiconductor nanocrystals (quantum dots, QDs) and their optoelectronic properties, such as photoluminescence and degree of quantum confinement. We primarily focus our efforts on one particular subset of ligands known to couple strongly to the inorganic core of the QD to decrease its quantum confinement, phenyldithiocarbamates (PTCs). We focus first on the development of quantitative Nuclear Magnetic Resonance (NMR) techniques to characterize the identity and quantity of ligands (such as PTCs and oleic acid) bound to nanocrystal surfaces. When we correlate the surface chemistry information obtained from NMR with the optical spectra of our QDs, we find that for strongly-delocalizing ligands like PTC, the spatial distribution of ligands on the QD surface affects the overall degree of delocalization. In the later chapters of this thesis, we describe two avenues for exploiting the relationship between surface coverage of exciton-delocalizing ligands and quantum confinement to design strongly coupled, hierarchical nanomaterials for efficient charge transport in films or in solution. We explore the treatment of thin lead sulfide QD films with a PTC derivative to improve their overall conductivity relative to benzoic acid, a similar molecule that does not affect confinement. Finally, we describe a potential strategy to improve the yield and rate of hole transfer to a tethered phthalocyanine molecule using dithiocarbamate and thiolate linkers.

ACKNOWLEDGEMENTS

The process of completing a Ph.D. is an intellectually, physically, and emotionally taxing experience. I have numerous individuals to thank for making this arduous journey worthwhile, and for encouraging me to continue on through periods of crippling self-doubt. I am grateful for the patient mentorship of Ken Aruda, Mark Peterson, Matthew Frederick, and most especially Victor Amin; their tough-love advice and sense of humor made me into the smarter, more curmudgeonly person I am today, and I am the better for it. I am also grateful for the friendship of David Weinberg and Kim Sung, whose companionship and sympathetic ears softened many blows, and particularly for the steadfast companionship of Kedy Edme, whose presence in the lab and in my life has been like that of the North Star on a tumultuous sea.

I would certainly not have attended graduate school at all had I not had phenomenal research experiences and advising in my undergraduate career. I thank Tara Meyer, George Bandik, and Michelle Ward for their encouragement in the earliest parts of my scientific career and beyond.

I have learned a lot from older students in the Weiss Group, but that knowledge pales in comparison to what I have learned from mentees I have worked with over the years. Shichen Lian and Dana Westmoreland have been instrumental in my development as a mentor, and their willingness to both give and receive advice has been a high point of my graduate career. I am also grateful to the undergraduates who have contributed to my research and helped to improve my management skills: Alex Kern, Carrington Cain, and Kali Williams.

This dissertation is the result of years of collaboration with other Weissians. I thank Ofer Kedem and Martin McPhail for their expertise and advice concerning the fabrication and characterization of quantum dot films, which is detailed in Chapter 4 of this dissertation. I am also deeply grateful for the

contributions of Stephanie Homan, Shengye Jin, Bryan Lau, Alec Nepomnyashchii, Nathaniel Swenson, Mohamad Kodaimati, Chen He, and Raul Calzada to my publications. I'd also like to thank everyone else in the Weiss group, past and present, I have interacted with; they number too many to list here, but I could not have asked for a better bunch of people which with to spend an inordinate amount of time.

I have been generously funded by the Hierarchical Materials Cluster Program at Northwestern, and by the National Science Foundation through a Graduate Research Fellowship. My research has been supported by the Department of Energy. Over the course of my studies, I made frequent use of the Integrated Molecular Structure Education and Research Center, as well as the Northwestern University Atomic and Nanoscale Characterization Experimental Center.

Graduate school, of course, is more than just research - I am fortunate to have been involved with several rewarding campus extracurriculars during my Ph.D. I am grateful to funding from The Graduate School, which made my two years leading the Northwestern Energy Technology Group possible; to the professors at the Kellogg School of Management for their enthusiasm in teaching a bunch of science nerds; and to the faculty of RSG, who helped me to rediscover my love of learning and improved my communication skills in the process. I would also like to thank the many administrative and support staff who work tirelessly behind the scenes in the business and main offices - they are the unsung heroes of the Chemistry Department.

I am immensely appreciative of the love and support I have received from my family. My parents have cheerfully ignored my deflections of praise and relentlessly reminded me of my past achievements (even sending a glowing report card from my kindergarten teacher - thanks, Mom and Dad!). I'm also thankful for (and continually impressed by) my younger sisters, Basha and Lainie Harris, who are living proof that you can be professionally successful and still have fun in your twenties. I am so, so grateful

for my boyfriend, Desmond Dean, for shouldering the bulk of domestic activities when I was frantically writing, and for his unconditional love and support. Thank you to my climbing family, within and without the university, for keeping me sane - you know who you are.

Finally, I would like to thank my advisor, Emily Weiss, who took a chance on me when I was a first-year grad student, and who believed in my ability years before I believed in myself. I attribute my success to her flexibility and willingness to support both my research and extracurricular pursuits. Over the last five years, she has invested massive amounts of time and energy in my critical thinking and communication skills. I greatly appreciate her approachability and invaluable counsel.

TABLE OF CONTENTS

| | |
|--|----|
| Abstract | 4 |
| Acknowledgements..... | 5 |
| Table of Contents | 8 |
| List of Figures..... | 11 |
| List of Schemes | 20 |
| List of Tables | 21 |
| 1 INTRODUCTION..... | 22 |
| 1.1 Chapter Summary..... | 22 |
| 1.2 What are Quantum Dots? ² | 22 |
| 1.3 The Importance of QD Surface Chemistry. | 24 |
| 1.4 The Role of Molecules in the Electronic Structure of Colloidal QDs. | 25 |
| 1.5 Characterization of QD Surface Chemistry by NMR..... | 27 |
| 1.6 Dissertation Outline..... | 29 |
| 2 USING NUCLEAR MAGNETIC RESONANCE TO CORRELATE THE SURFACE CHEMISTRY OF QUANTUM DOTS WITH THEIR PHOTOLUMINESCENCE | 30 |
| 2.1 Chapter Summary..... | 30 |
| 2.2 Correlation of the Surface Chemistry of QDs with Photoluminescence Enhancement. | 31 |
| 2.2.1. Introduction..... | 31 |
| 2.2.2. Results and Discussion..... | 32 |
| 2.2.3. Conclusions..... | 40 |
| 2.2.4. Supporting Information. | 40 |
| 2.3 The Composition and Permeability of Oleate Adlayers of CdS QDs upon Dilution to Photoluminescence-Relevant Concentrations..... | 46 |
| 2.3.1. Introduction..... | 46 |
| 2.3.2. The Effect of Dilution on the Surface Chemistry of Oleate-Capped CdS QDs..... | 48 |
| 2.3.3. The Photophysical Effects of Dilution..... | 53 |
| 2.3.4. The Effects of Dilution on the Permeability of the Ligand Shell to a Small Molecule. | 56 |
| 2.3.5. Conclusions..... | 57 |
| 2.3.6. Experimental Methods..... | 58 |

| | | |
|--------|--|-----|
| 2.4 | Summary of Methods for Quantitative Characterization of QD Surface Chemistry. | 60 |
| 2.4.1. | Direct measurement of spectrally resolved signals due to bound and free species..... | 60 |
| 2.4.2. | Measurement of bound species using signal subtraction. | 61 |
| 2.4.3. | Measurement of displaced native ligands to determine the number of bound species. | 62 |
| 3 | ROLE OF INTERLIGAND COUPLING IN DETERMINING THE INTERFACIAL ELECTRONIC STRUCTURE OF CDS QUANTUM DOTS | 64 |
| 3.1 | Chapter Summary..... | 64 |
| 3.2 | Introduction | 65 |
| 3.3 | Results and Discussion..... | 67 |
| 3.3.1 | Quantification of Exciton Delocalization and the Surface Coverage of C6-PTC on CdS QDs. | 67 |
| 3.3.2. | The Response of ΔR to the Surface Coverage of C6-PTC Ligands..... | 73 |
| 3.3.3. | The Contribution of Ligand Adjacency to Exciton Delocalization. | 76 |
| 3.3.4. | A Statistical Model for Estimating the Influence of Ligand Adjacency on Exciton Delocalization..... | 78 |
| 3.4 | Conclusions..... | 81 |
| 3.5 | Methods..... | 83 |
| 3.5.1 | Synthesis and Purification of CdS Quantum Dots. | 83 |
| 3.5.2. | Synthesis of the Ammonium Salts of 4-hexylphenyldithiocarbamate (C6-PTC). | 83 |
| 3.5.3. | Solution-phase Ligand Exchange. | 84 |
| 3.5.4. | Nuclear Magnetic Resonance (NMR) Spectroscopy..... | 84 |
| 3.5.5. | Ground State Absorption Spectroscopy..... | 85 |
| 3.6 | Supporting Information. | 85 |
| 3.6.1 | Experimental Methods..... | 85 |
| 3.6.2 | Computational Methods | 87 |
| 3.7 | Acknowledgements..... | 107 |
| 4 | EFFECT OF AN EXCITON-DELOCALIZING LIGAND ON THE CONDUCTIVITY OF THIN PBS NANOCRYSTAL FILMS | 108 |
| 4.1 | Chapter Summary..... | 108 |
| 4.2 | Introduction | 109 |
| 4.3 | Results and Discussion..... | 115 |
| 4.3.1. | The Effect of Film Thickness on the Optical and Electronic Properties of Ligand-Exchanged QD Films. | 115 |

| | |
|--|-----|
| 4.3.2. CH ₃ -PTC-exchanged PbS Films are More Conductive than BA-exchanged Films..... | 117 |
| 4.4 Conclusions and Outlook | 119 |
| 4.5 Experimental Methods | 122 |
| 5 INCREASED YIELD OF HOLE TRANSFER FROM CDS QDS TO A TETHERED ZINC PHTHALOCYANINE WITH AN EXCITON-DELOCALIZING LINKER..... | 126 |
| 5.1 Chapter Summary..... | 126 |
| 5.2 Introduction | 127 |
| 5.3 Experimental..... | 129 |
| 5.4 Preliminary Results and Discussion..... | 131 |
| 5.5 Conclusions and Future Work | 135 |
| 5.5.1. Alternatives to DCM. | 135 |
| 5.5.2. Chemical Functionalization of ZnPc | 136 |
| 6 CONCLUSIONS AND OUTLOOK | 137 |
| 6.1 Dissertation Summary | 137 |
| 6.2 Future Directions and Outlook..... | 138 |
| References..... | 140 |
| Vita..... | 154 |

LIST OF FIGURES

- Figure 1.1. A Plot of the surface area to volume ratio (SA/V) of a sphere as a function of radius. As the radius increases, the SA/V decreases rapidly, then levels off after ~ 10 nm. Inset: Pictographic representation of nanoparticles with increasing size, showing that as size increases, the fraction of atoms on the nanoparticle surface decreases. Adapted from ref ⁵.....24
- Figure 1.2. A schematic of the types of surface ligands on colloidal nanocrystals (NCs). Adapted from ref. ¹24
- Figure 1.3. The structure and corresponding 1D ¹H NMR spectra of A) free oleic acid and B) oleate-capped CdSe QDs. The NMR spectrum of free oleic acid has sharp, well-resolved proton signals. These signals are broadened in the NMR spectrum of oleate-capped CdSe QDs due to the restriction of motion for molecules bound to the surface of a (comparatively) large nanoparticle. This broadening is analogous to the broadening that occurs in the NMR of solids. NMR spectra adapted from ref. ²28
- Figure 2.1. Absorption spectra of CdSe QDs with radius $R=1.42$ nm in CH_2Cl_2 , and the same QDs treated with PTC for increasing amounts of time, which leads to increasing surface coverage of PTC on the QD. Spectra are scaled such that they have their first excitonic peaks have the same height. *Inset*: A plot of the apparent increase in excitonic radius, ΔR , for the QDs upon ligand exchange of native phosphonates for PTC, as a function of the ligand exchange time. The text describes the ligand exchange procedure and the calculation of ΔR from the absorption spectra in this figure.....33
- Figure 2.2. A) ¹H NMR spectra of PTC in CD_2Cl_2 at 0, 5, 16, 29, and 45 h. The PTC peaks decrease noticeably until they are undetectable after 16 h. The peaks attributable to aniline, a degradation product of PTC, increase continuously over the measured time period. Only one set of PTC peaks is shown for clarity; we believe that these peaks shift as PTC degrades because degradation proceeds, at least in part, through protonation of PTC by ammonium. Release of ammonia changes the pH of the solution. B) Relative normalized integrations of 2H peaks for aniline (red circles) and PTC (blank squares) showing the increase of aniline and decrease of PTC in solution over time relative to the residual solvent peak. C) Emission spectra of CdSe QDs ($R = 1.31$ nm) before and after treated with PTC to achieve a $\Delta R = 0.1$ nm at 0, 24 and 48 h. Recovery and eventual enhancement of the CdSe QD PL over time corresponds to the degradation of excess PTC. D) ¹H NMR spectra of a solution of $\text{NH}_4\text{-PTC}$ in d4-methanol added to either 0.8 mL CD_2Cl_2 or 0.8 mL (black) or to 0.8 mL of CdSe QDs in CD_2Cl_2 , after stirring for 10 min., to show the disappearance of NMR signals from PTC protons upon adsorption to the surfaces of QDs.....35
- Figure 2.3. (Top) Photograph showing the formation of a white precipitate (cadmium bis(phenyldithiocarbamate) $\text{Cd}(\text{PTC})_2$) upon addition of cadmium acetate ($\text{Cd}(\text{ac})_2$) to a solution of PTC in methanol and CH_2Cl_2 co-solvent. (Bottom) ¹H NMR spectra (in CD_3OD) of PTC and PTC + $\text{Cd}(\text{ac})_2$ after one and two filtrations. Upon addition of $\text{Cd}(\text{ac})_2$, the NMR signals due to free PTC disappear entirely. This is demonstrated by the disappearance of the doublet at 7.65 ppm, the overlaid triplets at 7.12 ppm resolving to a single triplet attributed to aniline, and the disappearance of the

triplet at 7.28 reappearing as a doublet attributable to either phenylisothiocyanate or the Cd(PTC)₂ complex. We also include spectra of (Cd(PTC)₂), as well as aniline, phenylisothiocyanate, and N,N'-diphenylthiourea, the degradation products of PTC.36

Figure 2.4. A) Emission spectra of a sample of CdSe QDs with no further treatment ("QDs only"), a sample of CdSe QDs treated with cadmium acetate ("QDs + Cd²⁺"), a sample of CdSe QDs treated with PTC to achieve $\Delta R = 0.05$ nm ("QDs + PTC with $\Delta R = .05$ nm"), and a set of samples of CdSe QDs treated first with PTC to achieve a series of ΔR values, and then with the same amount of cadmium acetate ("QDs + PTC + Cd²⁺"). All samples are in CH₂Cl₂ and are excited at 460 nm, and their photoluminescence intensities (PL) are scaled by their absorbances at 460 nm. Also shown on top of the spectra are photographs of three of the samples (as labeled) showing the quenching of PL by PTC, and the recovery of the PL of PTC-treated QDs by addition of cadmium acetate. Addition of cadmium acetate to the PTC-treated sample with $\Delta R = 0.05$ increases the PL intensity of the sample by a factor of 1.9, after accounting for the increase in absorption intensity. B) A plot of PL/PL₀ – the PL intensity of the sample of QDs treated with PTC and cadmium acetate divided by the PL intensity of the sample of QDs treated with cadmium acetate but with no added PTC – as a function of ΔR38

Figure 2.5. Emission spectra of Rhodamine B in CH₂Cl₂ and CdSe QDs in CH₂Cl₂ with 50 μ l MeOH. All samples are excited at 460 nm, and their photoluminescence intensities (PL) are scaled by their absorbance at 460 nm. The quantum yield (QY) of the QDs is calculated to be $\sim 2\%$ relative to Rhodamine B.42

Figure 2.6. Ground state absorption spectra of CdSe QDs (R=1.42 nm) (no PTC) and QDs at 24 h, 30 h and 48 h after treated with PTC to achieve a $\Delta R = 0.07$ nm. The first excitonic absorption peak of the QDs treated with PTC is almost unchanged, which indicates a stable ΔR over at least 48 h. .42

Figure 2.7. Ground state absorption spectra of PTC-treated QDs with a series of ΔR values before ("QD+PTC") and after ("QD+PTC+Cd²⁺") the treatment with cadmium acetate. The absorbance of the sample at wavelengths shorter than 400 nm – the region where PTC absorbs – significantly decreases due to the formation of cadmium *bis*-(phenyldithiocarbamate) precipitates. The addition of cadmium acetate also results in a 2-to-4 nm bathochromic shift.43

Figure 2.8. A) Absorption spectra of CdSe QDs with a radius R=2.5 nm in CH₂Cl₂, and the same QDs treated with PTC for increasing amounts of time. B) Emission spectra of a sample of CdSe QDs (R=2.5 nm) treated with cadmium acetate ("QDs + Cd²⁺") and a set of samples of CdSe QDs treated first with PTC with increasing amount of time, and then with the same amount of cadmium acetate ("QDs + PTC (1~12 h) + Cd²⁺"). All samples are in CH₂Cl₂ and are excited at 460 nm, and their photoluminescence intensities (PL) are scaled by their absorbances at 460 nm. We observe a small (~ 3 -4 nm) blue-shift of the absorbance and PL spectra of these samples due to etching of their surfaces by PTC. This blue-shift is apparent for these samples, and not for the samples of smaller QDs, since $\Delta R = 0$, but the etching may also occur in the samples of smaller QDs and lead to a systematic underestimating of ΔR . C) PL decay curves of the same set of samples shown in B). Black solid lines are the best fits of the decay curves to a multi-exponential function with the fitting parameters listed in Table 2.1.44

Figure 2.9. A) A two-dimensional slice of the three-dimensional hole wavefunction, taken through the center of the nanoparticle. The probability density is plotted against the x and y coordinate for four different ligand surface coverages. The electron wavefunction has spherical symmetry and is sketched as a radial slice (black curve). B) The square of the overlap integral between the hole and electron wavefunctions versus the fractional ligand surface coverage. The overlap increases to a maximum at 50% surface coverage, then decreases.45

Figure 2.10. The vinyl proton region of the NMR spectra of oleate-capped QDs (“CdS-OA QDs”); a mixture of Cd(oleate)₂, oleic acid, and CdO (“Cd-OA”); and free oleic acid (“Free OAc”) in (A) C₆D₆, (B) C₆D₁₂, (C) CDCl₃. The legends indicate the sample concentrations. The vertical lines are guides to the eye. The y-axes are intensity in arbitrary units. Note that the x-axes are not the same for each figure panel.....49

Figure 2.11. A), B), C) Comparison between ¹H NMR signal from oleate-capped CdS QDs (0.1 μM) and the background in C₆D₆, C₆D₁₂ and CDCl₃. D) Comparison between ¹H NMR signal from oleate-capped CdS QDs (10 nM) and the background in C₆D₆.50

Figure 2.12. FTIR spectra for 1 μM oleate-capped QDs (“CdS-OA QDs”, blue), 2 mM cadmium oleate with oleic acid impurity (“Cd-OA”, red), and 2 mM oleic acid (“Free OAc”, black), in C₆D₆. The y-axis is intensity in arbitrary units. The peak at 1709 cm⁻¹ corresponds to the C=O stretching mode of the carbonyl group in oleic acid. The peak at 1750 cm⁻¹ is its side-band. The peak at ~1530 cm⁻¹ corresponds to the O-C-O stretching modes of bridging and chelating carboxylates within cadmium-bound oleate. Resolution of the measurement is 2 cm⁻¹ for Cd-OA and oleic acid and 8 cm⁻¹ for CdS-OA QDs.51

Figure 2.13. ¹H NMR spectra of oleate-capped CdS QDs at 10 μM (black line), after dilution to 1 μM (red line) and after re-concentrating to 10 μM (green line).52

Figure 2.14. Ground state absorption (solid, left axis) and emission (dashed, right axis) spectra for oleate-capped CdS QDs in (A) C₆D₆, (B) C₆D₁₂ and (C) CDCl₃. The sample concentrations are 1 μM (black), 0.5 μM (red), 0.25 μM (green), 0.125 μM (blue), and 0.1 μM (cyan). Insets: plots of the difference between the integrated band-edge PL (centered at 490 nm) and the integrated “trap emission”, centered at 605 nm (scaled by the total PL intensity), vs. the concentration of the sample.54

Figure 2.15. A) Photoluminescence (PL) spectra of oleate-capped CdS QDs in CDCl₃ with and without 1000 equivalents of *p*-benzoquinone (BQ) added. The PL spectra are scaled in intensity by their absorbance at the excitation wavelength, 390 nm, and plotted relative to the intensity of the band-edge emission peak of the 1 μM CdS QD sample with no added BQ (black curve). *Inset*: A magnified version of the band-edge PL peak of A, which shifts to higher energy upon addition of BQ due to mild etching of the QD surface. B) Plot of PL/PL₀, the fraction of QDs that are still emissive after addition of 1000 equivalents of BQ, vs. the absolute concentration of QDs.....56

Figure 3.1. A) Schematic of the ligand exchange process, where each C6-PTC, added as either the DIPEA salt (shown) or the TEA salt (not shown), displaces, on average, one cadmium oleate complex (two oleate ligands) in order to bind to the core of the QD. The text explains how we determine the

stoichiometry of the ligand exchange. B) Ground state absorption spectra of CdS QDs ($R = 2.5$ nm) treated with increasing (black to red) molar equivalents of C6-PTC (0 – 717); the spectra are normalized to the height of the lowest-energy excitonic peak. We use the magnitude of the bathochromic shift of this peak and experimentally determined calibration curves of the size of the QD core vs. its bandgap to calculate the parameter ΔR , the apparent increase in excitonic radius upon ligand exchange, at each surface coverage of C6-PTC.....68

Figure 3.2. A) The vinyl proton region within ^1H NMR spectra of the oleate-coated CdS QDs ($R = 2.5$ nm) when treated with various concentrations of C6-PTC (increasing [C6-PTC] from black to red), in d_6 -benzene. The spectra are normalized to the height of a ferrocene internal standard (see Supporting Information for the full NMR spectra for these QDs and for the QDs with radii of 1.9 nm). *Inset*: NMR spectra of free DIPEA, DIPEA-C6-PTC, and CdS QDs with ~ 538 equivalents of DIPEA-C6-PTC. The peak shown is from the ethylene protons of the ethyl group. B) The number of C6-PTC molecules and its degradation products – 4-hexylaniline (AN), 4-hexylphenylisothiocyanate (ITC), and N,N' -bis(4-hexylphenyl)thiourea (TU) – in each sample of C6-PTC-treated CdS QDs ($R = 2.5$ nm), counted by NMR as described in the text. The total number of phenyl rings counted from the NMR spectrum at each added concentration of C6-PTC is shown in black and fit to a line with forced intercept at (0,0); the fit line has a slope of 1.1. This result shows that, when we assume that each C6-PTC displaces 2 oleate molecules, we account for all of the added C6-PTC molecules as either bound C6-PTC, or a freely diffusing degradation product. The Supporting Information contains this plot for the QDs with $R = 1.9$ nm, for which the fit line has a slope of 1.3, as well as for QDs with $R = 2.5$ nm treated with TEA-C6-PTC, for which the fit line has a slope of 1.71

Figure 3.3. A) A plot of ΔR vs. the number of bound C6-PTCs (as measured by the number of displaced $\text{Cd}(\text{oleate})_2$ ligands in the NMR spectra) on CdS QDs with $R = 1.9$ nm (blue) and $R = 2.5$ nm (red). The solid lines represent the simultaneous fits to eq 5 for each size, where N_{sites} is fixed at the maximum theoretical number of bound ligands, $\Delta r_k = Ck\Delta r_0$, and $Ck \geq 1$. The dashed lines are linear fits to the data with a forced intercept at (0,0). B) Simulated response of ΔR vs. number of bound C6-PTCs on CdS QDs with $R = 1.9$ nm, calculated using a 3D spherical potential well model (schematic shown in inset) where increased surface coverage of the delocalizing ligand corresponds to a lower average barrier height (which ranges from 0 to 2.3 eV) for the excitonic hole. C) Simulated response of ΔR to the surface coverage, θ , of delocalizing ligand for spheres with radii of 1.1 and 3.2 nm. We show the average (points) and range over five trials (error bars) for each size. Inset: Simulated response of ΔR to θ for a sphere with a radius of 1.1 nm, where the delocalizing ligands are either placed maximally far apart on the sphere's surface (hollow circles) or in a Janus particle-like configuration with maximal adjacency (solid circles), for barrier heights of 0 eV (black) and 0.6 eV (blue). From these plots, it is evident that a greater number of adjacent ligand interactions on the surface of the sphere results in a greater ΔR74

Figure 3.4. Hollow circles: Plots of the calculated values of Δr_0 – the contribution to ΔR per isolated ($k = 0$) delocalizing ligand – for barrier heights of 0 (black), 0.6 (red), and 1.2 (green) eV vs. bandgap (E_g) of the QD coated entirely by native insulating ligands. Solid turquoise circles: Plots of the measured values of Δr_0 for $R = 1.9$ nm ($E_g = 3.0$ eV) and $R = 2.5$ nm ($E_g = 2.8$ eV). The error bas

arise from the fits of the dataset ΔR vs. (no. of bound C6-PTC) $\pm \delta$ (no. of bound C6-PTC), respectively, in Figure 3.3A.81

Figure 3.5. We plot ΔR as a function of bound C6-PTCs per QD for CdS QDs with $R=2.5$ nm. We used C6-PTC with two different counterions: DIPEA (black) and TEA (red). In the plot, we observe that the counterion of C6-PTC does not significantly affect the shape of the ΔR vs. bound C6-PTCs curve.....84

Figure 3.6. Plots of the total number of phenyl rings per QD (from C6-PTC and its degradation products) in each sample, measured by NMR, vs. the number of phenyl rings per QD added to each sample, for a mixture of C6-PTC and 2.5 nm CdS QDs (A, with TEA as the counterion) and 1.9 nm CdS QDs (B, with DIPEA as the counterion).89

Figure 3.7. The vinyl regions of the NMR spectra of CdS QDs with $R = 2.5$ mixed with 0-800 molar equivalents of C6-PTC. The spectra were acquired at six time points after the initial mixing of C6-PTC with CdS QDs. These spectra show that C6-PTC, once bound to the QD surface, remains bound over the course of over 62 hours.....90

Figure 3.8. To calculate ΔR from the confinement energies from the spherical potential well model, we fit a calibration curve to calculated confinement energy for the non-delocalizing potential wells vs. radius. The resulting calibration curve is described by eq 3.7, which was used to calculate a radius for different surface coverages of delocalizing ligands. We subtracted the radius for a surface coverage of zero from this radius to obtain ΔR91

Figure 3.9. Plot of ΔR vs. equivalents of C6-PTC added to CdS QDs with $R = 2.5$, at a series of time points during the ligand exchange. We obtained these data from the same samples used to collect the NMR spectra shown in Figure 3.7. This plot shows that the bathochromic shift upon ligand exchange with C6-PTC stays fairly constant over time, which further implies that once bound, C6-PTC does not desorb from the QD surface.....91

Figure 3.10. Plot of ΔR , calculated using a simple three-dimensional particle-in-a-spherical potential well model, vs. the number of bound delocalizing ligands for a 2.5-nm core radius. A similar plot for a core with a 1.9-nm radius is shown in the main text, Figure 3.3B.92

Figure 3.11. We calculated adjacency number, k , by tracking the number of neighboring delocalizing ligands for each bound delocalizing ligand in our 3D pseudopotential model. We plot the average adjacency, k_{avg} , of the bound delocalizing ligands as a function of surface coverage for several core sizes. Ligands placed as close together as possible are solid circles, and ligands placed maximally far apart are hollow circles. We see that, at surface coverages ≤ 0.2 , adjacency is zero for the minimally adjacent case; it then increases rapidly to reach an average adjacency of ~ 692

Figure 3.12. Linear fits of the calculated ΔR from the pseudopotential model vs. the number of bound delocalizing ligands for the zero adjacency case ($\theta \leq 0.2$, open circles, Figure 3.11), where ligands are placed maximally far apart on the surface. The slope of each line corresponds to Δr_0 . We report the slopes and fit errors in Table 3.1.93

Figure 3.13. TEM images of oleate-capped (A, B) and C6-PTC-capped (C, D) CdS QDs. The oleate-capped CdS QDs (measured from 14 QDs) measure 3.7 ± 0.4 nm in diameter and the C6-PTC capped CdS (measured from 12 QDs) measure 3.6 ± 0.3 nm in diameter from ImageJ analysis.94

Figure 3.14. Adjacency distribution of ligands from simulation of $R = 3.2$ nm sphere with 515 surface sites for surface coverages ranging from 0.2 – 0.8. The solid lines are guides to the eye. Inset: Schematic representation of a section of the QD surface, showing the individual surface sites as circles. Open circles represent empty binding sites, and filled circles represent filled binding sites. Each site has 6 nearest-neighbor sites. The bound ligand outlined in red has two adjacent ligands ($k = 2$).....95

Figure 3.15. Plots of calculated ΔR (from our pseudopotential model) *vs.* delocalizing ligand surface coverage, showing five random trials of delocalizing ligand placement on the surface of a spherical potential well with four different radii. The points and error bars show the average and range, respectively, of the calculated ΔR values for a given arrangement of delocalizing ligands (that impose a barrier height of 0 eV) on the surface. It is evident that smaller sphere sizes show a much greater variation in ΔR at a given surface coverage. This phenomenon is due to different degrees of ligand adjacency, which has a greater impact on small spheres because each bound ligand takes up a greater fraction of the total surface area.96

Figure 3.16. The aromatic region of ^1H NMR spectra of A) 4-hexylaniline, B) TEA-C6-PTC, and C) DIPEA-C6-PTC in d_6 -benzene. The vertical lines are guides to the eye, and highlight the peaks assigned to 4-hexylaniline (blue), 4-hexylphenylisothiocyanate (ITC, green), d_6 -benzene (purple), and C6-PTC (red).97

Figure 3.17. Full NMR spectra of ~ 717 molar equivalents of C6-PTC mixed with A) 2.5 nm CdS QDs with DIPEA as the counterion B) 2.5 nm CdS QDs with TEA as the counterion, and C) 1.9 nm CdS QDs with DIPEA as the counterion. These spectra possess a complex aliphatic region, easily interpretable vinyl region, and multiple aromatic peaks which we assign to the degradation products of C6-PTC. Further NMR details are discussed below, in Figures 3.18-3.21.98

Figure 3.18. The vinyl region of the NMR spectra shown in Figure 3.17 (at all concentrations of C6-PTC), for A) 2.5 nm QDs with TEA as the counterion and B) 1.9 nm CdS with DIPEA as the counterion. The corresponding NMR spectra for 2.5 nm CdS QDs with DIPEA as the counterion are shown in the main text, Figure 2A.99

Figure 3.19. Plots showing the conservation of phenyl rings per QD (similar to Figure 3.2B) for alternate stoichiometries of the C6-PTC-for-oleate exchange. A) and B) show a one-to-one displacement of C6-PTC for oleic acid, and the case where one C6-PTC displaces an average of 1.5 oleates, respectively, for 1.9 nm CdS QDs with DIPEA counterion. C) and D) show the same for 2.5 nm CdS QDs with TEA counterion, and E) and F) show the corresponding plots for 2.5 nm CdS QDs with DIPEA counterion. 100

Figure 3.20. Peak assignments for the ^1H NMR spectra of samples of C6-PTC mixed with 2.5 nm CdS QDs with DIPEA as the counterion (the same samples depicted in Figure 3.17A and Figure 2A in the main text). Here, we show A) the aromatic region, B) the downfield aliphatic region from 2-3.5 ppm, and C) the upfield aliphatic region from 0.5-2 ppm. 101

Figure 3.21. ^1H NMR signals of the A) TEA ethylene protons and B) DIPEA $(\text{CH}_3)_2\text{CH}$ - (isopropyl) proton for the free counterion, free C6-PTC, and C6-PTC + QDs showing the broadening of the counterion protons upon addition of QDs, which indicates adsorption of the counterion to the QD surface..... 102

Figure 3.22. A) Absorption spectra of CdS QDs with 200 and 800 added equivalents of unsubstituted aniline (AN), phenylisothiocyanate (ITC), and N, N'-diphenylthiourea (TU). Only 800 equivalents of TU induces a detectable bathochromic shift of the spectrum. The inset shows a zoom-in of the excitonic peak; the spectra of the blank and TU samples are solid lines, whereas the other samples are dashed lines. B) The vinyl region of the spectra of CdS QDs (black), and mixtures of CdS QDs with 800 equivalents of aniline (AN, blue), phenylisothiocyanate (ITC, yellow), and N,N'-diphenylthiourea (TU, green). Only TU displaces oleate from the CdS QD surface when it is added..... 102

Figure 3.23. A) The vinyl region of ^1H NMR spectra of CdS QDs with 0-800 equivalents of N,N'-bis(4-hexylphenyl)thiourea (TU), showing partial oleate displacement. Inset: Plot of displaced oleate (OA) per QD *vs.* the measured TU per QD (as measured by direct integration of the TU NMR peaks), fit to a Langmuir-type function. B) Aromatic region of the NMR sequential NMR spectra of CdS QDs with 0-800 equivalents of N,N'-bis(4-hexylphenyl)thiourea (TU), showing moderate broadening and shifting of one of the aromatic peaks relative to free TU with no QDs (gray trace). There is some free TU present with QDs, but much of it is bound..... 103

Figure 3.24. Plot of ΔR *vs.* C6-PTC surface coverage for CdS QDs with $R = 1.9$ nm (blue) and $R = 2.5$ nm (red). We show the fit to our model with a solid line, a quadratic function with a dashed line, and a linear function with a dotted line. 105

Figure 3.25. A) Calculated ΔR *vs.* fractional surface coverage of delocalizing ligand with a barrier height of 0 eV. The solid circles are data points where the delocalizing ligands have been placed in a Janus particle-like configuration with maximum adjacency, and the hollow circles are points where the delocalizing ligands are placed maximally far apart on the surface, with minimal adjacency. It is clear that, at a surface coverage, delocalizing ligands with more adjacency result in a greater ΔR , even though their distribution is less isotropic. B),C) are schematic images of what maximal (B) and minimal (C) adjacency looks like at a delocalizing ligand surface coverage of 30% (marked on A as a red line), where the native ligands are blue and the delocalizing ligands are red. Although the minimal adjacency case (C) is more isotropic, it has a smaller ΔR (hollow spheres) than the maximal adjacency case (B). 105

Figure 4.1. Schematic showing the film deposition technique used in this study. QDs in hexanes were pipetted over a float glass slide submerged in acetonitrile (ACN). Due to the immiscibility of hexanes and ACN, the QDs self-assemble into a single monolayer at the air-solvent interface. 115

Figure 4.2. A) The bathochromic shift of the first excitonic peak of PbS QDs upon exchange with CH_3 -PTC, in a QD film composed of one to three QD monolayers. We quantify the bathochromic shift using the parameter ΔR , the apparent increase in excitonic radius of the QDs, which we obtain from empirically derived sizing curves.⁴ B) A plot of the measured conductivity (in the dark) of CH_3 -PTC-treated PbS QD films as a function of the film thickness in monolayers. Each data point

corresponds to a single measurement on a section of QD film (some films had multiple measurements taken from different areas). 116

Figure 4.3. Current vs. voltage curves for PbS QD films treated with mixtures of benzoic acid (BA) and CH₃-PTC. Where there is less than 100% CH₃-PTC, the remainder of the ligand mixture is composed of BA (for example, 25% CH₃-PTC films were exchanged with a 1:3 mixture of CH₃-PTC:BA. We treated each QD film with approximately 1000 molar equivalents of ligand per QD. The black traces correspond to measurements taken in the dark, and the green traces correspond to measurements taken under 532-nm illumination. The insets show the same data zoomed in to show the y-axis range. From these figures, we observe hysteresis at low CH₃-PTC concentration, with a “turn-on” of conductivity that occurs between 25% and 75% CH₃-PTC. From 75% to 100% CH₃-PTC, we observe an order of magnitude increase in conductivity. 117

Figure 4.4. SEM images of PbS QD films exchanged with A) 4-methylphenyldithiocarbamate (CH₃-PTC) or B) benzoic acid (BA). We observe no major structural or packing differences between these two films; both have approximately hexagonally close-packed QDs with many cracks and defects present. 118

Figure 4.5. SEM image of a 2-ML PbS QD film treated with PTC. This image reveals large cracks and heterogeneities present in the film, which is the likely culprit of our reproducibility problems and lower than expected conductivity of PTC-treated PbS QD films. 120

Figure 4.6. Current vs. voltage curves for spin-coated PbS QD films treated with A) BA and B) CH₃-PTC. The black traces correspond to measurements taken in the dark, and the green traces correspond to measurements taken under 532-nm illumination. The maximum current for CH₃-PTC-treated films is ~2 nA, and the corresponding maximum current for BA-treated PbS QD films is ~20 pA. 121

Figure 4.7. Schematic of the proposed future electrode fabrication and deposition process. First, a PDMS stamp is poured onto a smooth silicon wafer and cured using half of the typical amount of crosslinking agent. Once cured, the PDMS stamp is removed from the silicon wafer, and gold electrodes are deposited by thermal evaporation through a prefabricated shadow mask. Finally, the stamp is pressed onto the substrate to transfer the electrodes onto the surface of the QD film. 122

Figure 4.8. Our electrochemical measurement setup. A) Schematic of the PbS QD film on top of a float glass substrate. We used conformal electrodes fabricated from a eutectic of gallium and indium (EGaIn) templated by PDMS. We applied a potential across these electrodes and measured the resulting current across the film, for PbS QD films treated with different ligands. B) Top and C) bottom views of the EGaIn electrodes on top of a QD film. Adapted from McPhail *et al.*⁶ 124

Figure 5.1. Schematic of the QD-linker-ZnPc conjugates employed in this study and photoinduced hT scheme. The QD is selectively excited at 430 nm, and subsequently transfers a hole to the ZnPc. We refer to these complexes as “CdS-NCS₂-ZnPc” and “CdS-SH-ZnPc” in the text. 131

Figure 5.2. Ground state absorption spectra of the CdS QDs (black), ZnPc (blue), a mixture of CdS QDs with 250 molar equivalents of ZnPc (navy), ZnPc with 50-150 molar equivalents of pyr-SH (teal-light green), CdS-SH-ZnPc (lime green), ZnPc with 50-150 molar equivalents of pyr-NHCS₂ (violet-maroon), and CdS-NHCS₂-ZnPc (red). Spectra have been vertically offset for clarity. 132

Figure 5.3. A) Normalized ground state absorption spectra for CdS QDs exchanged with 50-200 equivalents of pyr-NCS₂ (shades of red) and pyr-SH (shades of blue). B) Plot of ΔR , the apparent increase in excitonic radius, as a function of added ligand (pyr-NCS₂ or pyr-SH). The points and error bars correspond to the average and standard deviation, respectively, of three identically prepared samples of oleate-capped CdS QDs exchanged with one of these ligands. For the same quantity of ligand added to the CdS QDs, the pyr-NCS₂ delocalizes the QD exciton to a greater degree than pyr-SH. To obtain these ΔR values, we took the average first excitonic peak of six blank CdS QD samples, and used this peak position as R_{init} . The value of ΔR is equal to $R - R_{\text{init}}$, where R is calculated from λ_{abs} using the calibration curves from Yu *et al.*⁴ 133

Figure 5.4. A) Full TA spectra of the CdS-NHCS₂-ZnPc complex from 1-2000 ps after excitation at 420 nm. The bleach at 606 nm corresponds to direct absorption of the ZnPc Q-band. The peak at 500 nm appears to correspond to the oxidized form of ZnPc, ZnPc^{•+}. The large absorption below 450 nm is from the excitation at 420 nm. B) Spectroelectrochemistry of ZnPc in DCM, with an applied potential of + 0.8 V vs. Ag (pseudoreference). The gradient from black to red shows an increase in time (0-75 minutes). Over time, the Soret and Q-band of neutral ZnPc (325 and 680 nm, respectively) decrease, and we observe the appearance of a peak at 500 nm, which corresponds to the radical cation of ZnPc.³ 134

LIST OF SCHEMES

| | |
|--|-----|
| Scheme 2.1. The anionic ligand phenyldithiocarbamate (PTC). It is added to dispersions of CdSe QDs as an ammonium salt. | 31 |
| Scheme 2.2. Schematic representation of a cross-section of a CdS QD capped with oleate ligands in both bridging (gray) and chelating (blue) binding modes. Red circles represent cadmium ions and yellow circles represent sulfur ions. Although this 2D slice of the QD is not charge balanced, in 3D, the oleate ligands (with a 1- charge) balance the excess Cd ²⁺ ions over the entire surface of the QD. | 46 |
| Scheme 4.1. The chemical structures of 4-methylphenyldithiocarbamate (CH ₃ -PTC) and benzoic acid (BA), the two QD ligands investigated in this study. | 109 |

LIST OF TABLES

| | |
|---|-----|
| Table 2.1. Time Constants for Decay of the PL, PL/PL ₀ and k _r /k _{r0} of CdSe QDs (R = 2.5 nm) upon Treatment with NH ₄ ⁺ PTC ⁻ and cadmium acetate..... | 45 |
| Table 2.2. Number of Free and Bound Oleates within Samples of Oleate-Coated CdS QDs. | 53 |
| Table 3.1. Values of Δr ₀ , Calculated from the Linear Fits of the Zero-Adjacency Case in the Minimal Adjacency Plots where θ ≤ 0.2 (Figure 3.12)..... | 106 |
| Table 3.2. Experimental values of Δr _k from fits of Figure 3A to eq 5 and 6 in the main text. | 106 |
| Table 3.3. Values of ΔR for CdS QDs with R = 1.9 nm, Measured Before and After NMR Analysis. | 106 |
| Table 4.1. Field-Effect Measurements of the Electrical Properties of Colloidal QD Films..... | 112 |
| Table 4.2. Measurements of Photo-electrical Properties of Colloidal QD Films. | 114 |

1 INTRODUCTION

Adapted from: Harris, R.D.*; Bettis Homan, S.* et al. Electronic Processes within Quantum Dot-Molecule Complexes. *Chem. Rev.* **2016**, *116* (21), pp 12865–12919.

1.1 Chapter Summary

A quantum dot (QD) is a single crystal of semiconductor with an electronic wavefunction that is quantum-confined in all three dimensions. This chapter introduces the physical and optoelectronic properties of colloidal QDs, and some of their potential applications. We describe the importance of the QD ligand shell in determining a QD's properties; research on interactions of ligands with colloidal QDs has revealed that ligands determine not only the excited state dynamics of the QD but also, in some cases, its ground state electronic structure. Specifically, we discuss the measurement of the electronic structure of colloidal QDs and the influence of their surface chemistry, in particular, exciton-delocalizing ligands, on their electronic energies. We also describe the analytical techniques used to characterize (both qualitatively and quantitatively) the QD ligand shell. This chapter concludes with an outline of the topics covered in this dissertation.

1.2 What are Quantum Dots?

A quantum dot (QD) is a single crystal of semiconductor with an electronic wavefunction that is quantum-confined in all three dimensions. Quantum confinement for QDs is defined in terms of its excitonic states. An exciton (electron-hole pair) in a bulk semiconductor has a characteristic delocalization length, quantified through the “Bohr radius” parameter, which depends on the material's band structure.⁷⁻⁹ The Bohr radius for a semiconductor (in contrast to its definition for

hydrogenic systems) is the most-probable distance between the electron and hole within the exciton. The exciton becomes quantum-confined when one or more spatial dimensions of the semiconductor crystal are on the order of or smaller than this natural delocalization radius. The energies for quantum-confined excitons (at least the kinetic, or “confinement” energies) are discretized approximately according to the version of a simple particle-in-a-box potential model that is appropriate for the shape of the crystal in the confined dimension(s). The source of quantum confinement for a QD, which if spherical has states with the energies that approximate those dictated by the boundary conditions of a particle in a spherical potential well, is the sharp dielectric interface between the single crystalline core of the QD and its surrounding environment. This interface amounts to a tunneling barrier for the excitonic charge carriers (electron and hole) that, for sharp dielectric contrast, is effectively infinitely high. As a result, QDs have a dependence of their band gaps on their size, which leads to size-tunable optoelectronic properties and makes them desirable for applications in display and lighting technology, biological imaging, photocatalysis, and quantum computing. Modifications to this QD core-environment interface, by changing the molecules that are coordinated to the QD’s surface or by depositing a shell of inorganic semiconductor with a different bandgap, change the height and shape of the potential barrier (changes in height have been modeled more extensively than changes in shape) and therefore the degree of tunneling of the electron and hole wavefunctions into the interfacial region.

Is the electronic structure of a quantum dot special? Does it lead to photophysical and chemical processes and electronic dynamics and energy dissipation pathways that are not observed in bulk semiconductor systems or in purely molecular systems? The answer is, of course, “yes”, for two major reasons: (i) the electrons within QDs are quantum-confined, as described above, and (ii) the high surface-area-to-volume ratio of QDs demands that a large fraction, sometimes the majority, of the

atoms in the QD directly interface their environment. The latter reason is the defining characteristic of all nanostructures, semiconductor or other. Perhaps a more subtle point is that, for QDs, the quantum confinement amplifies the influence of the environment on the properties of the nanocrystal because the local environment shapes the dielectric interface that determines the boundary conditions for the wavefunction. The core-environment interaction of a colloidal QD is therefore important in determining not only the excited state dynamics of the QD (the processes that occur out of equilibrium) but also the ground state electronic structure of the QD.

1.3 The Importance of QD Surface Chemistry.

When particles are reduced in size to the nanoscale, the surface area to volume ratio increases rapidly. This increase in surface area relative to volume occurs because surface area scales as r^2 whereas volume scales as r^3 (**Figure 1.1**). The large number of surface atoms with

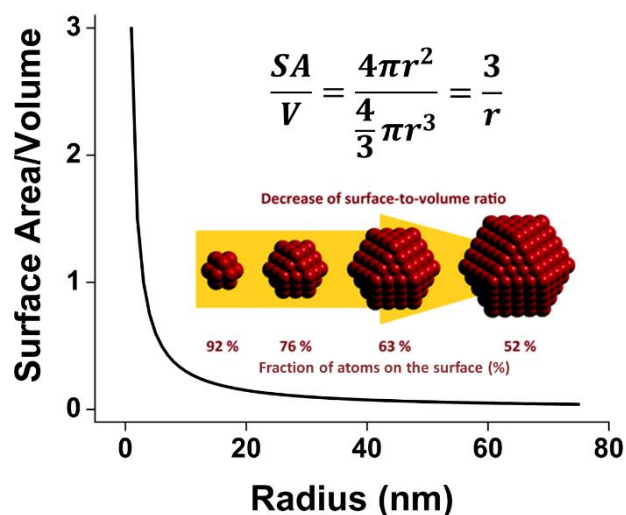


Figure 1.1. A Plot of the surface area to volume ratio (SA/V) of a sphere as a function of radius. As the radius increases, the SA/V decreases rapidly, then levels off after ~ 10 nm. **Inset:** Pictographic representation of nanoparticles with increasing size, showing that as size increases, the fraction of atoms on the nanoparticle surface decreases. Adapted from ref ⁵

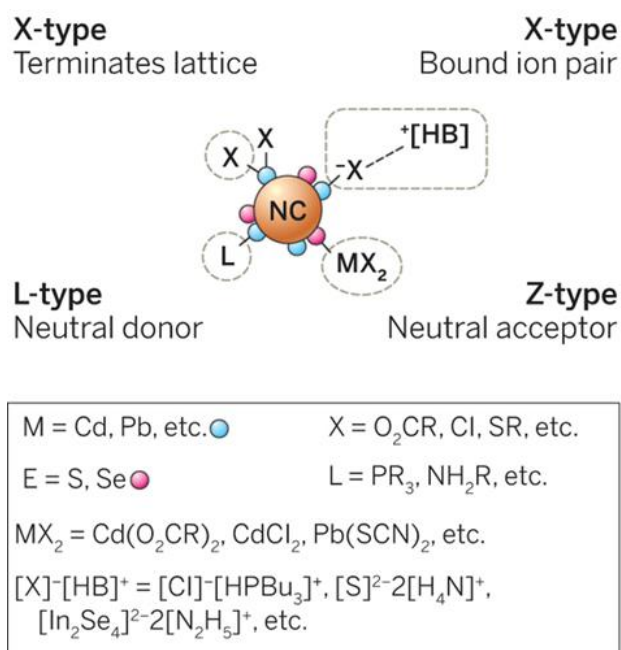


Figure 1.2. A schematic of the types of surface ligands on colloidal nanocrystals (NCs). Adapted from ref. ¹

insufficient coordination requires surface ligands to passivate those dangling bonds. There exist a plethora of potential surface ligands, but we can broadly define them as one of three main types, as characterized by Owen and coworkers (**Figure 1.2**)^{1,10}:

(i) L-type ligands, which are two-electron donors that form dative bonds with neutral metal surface sites, such as amines, phosphines, and thiols;

(ii) X-type ligands, which are anionic one-electron donors that form normal covalent or ionic bonds with cationic surface sites, such as carboxylates, phosphonates, thiolates, and halides;

(iii) Z-type ligands, which are comprised of two-electron acceptors, which bind to neutral surface sites, such as cadmium oleate and lead chloride.

Chemical functionalization of the QD surface is a powerful and versatile strategy to tune the electronic structure (i.e., energies and spatial distributions of core and surface states) of colloidal QDs because the surface ligands control (i) the degree of surface enrichment of cations or anions,^{1,10-19} (ii) the degree of coordination of surface ions (how electron-rich or electron-poor they are),²⁰⁻²⁵ (iii) in some cases, the magnitude of the confinement energy of excitonic charge carriers,²⁶⁻³³ and (iv) the crystal structure and the size of QDs, when those ligands are present as surfactant in the reaction mixture.³⁴⁻³⁷ Common protocols to prepare colloidal QDs^{11-12,38-45} produce QDs terminated with aliphatic organic molecules (such as alkyl-carboxylates, -phosphonates, or -amines). Depending on the particular application of the QDs, these ligands can be replaced post-synthetically with a large variety of organic molecules,^{10,18,46-48} in order to tune the electronic structure of the nanoscale interface, and, in some cases, the electronic structure of the QD's core.

1.4 The Role of Molecules in the Electronic Structure of Colloidal QDs.

When QDs are coated with insulating “native” ligands (their ligands as-synthesized, typically aliphatic carboxylates, phosphonates, or amines), the probability density for excitonic carriers (electron

and hole) outside of the relatively high-dielectric semiconductor core is negligible.⁴⁹⁻⁵¹ These native ligands impose a high energetic barrier to charge transfer processes, which hinders the use of QDs in applications where they are used to convert photons into other forms of energy, such as solar electricity generation or photocatalysis. Exchange of these native ligands for less insulating ligands – that is, organic ligands with orbitals that are of the correct energy and symmetry to mix with the delocalized orbitals of the QD core – decreases the energetic barrier for tunneling of excitonic carriers into the organic/inorganic interfacial region of the colloid. The basic characteristic of these “exciton delocalizing” ligands are: (i) anchoring groups that bind strongly to the QD surface, and (ii) frontier orbitals that align well energetically, and match symmetry-wise, with states at or near the VB- or CB-edge of the bulk semiconductor equivalent of the QD (for the reasoning behind this requirement, please see refs ⁵²⁻⁵⁴). When these requirements are met, one or both excitonic charge carriers has a pathway for delocalization into QD/ligand interfacial states, formed upon ligand binding, and a sometimes drastic decrease in the excitonic energy results.

The Weiss group has studied a class of molecules – phenyldithiocarbamate (hereafter referred to as PTC) and its *para*-substituted derivatives – that decreases the confinement energy of the exciton *via* what we propose to be delocalization of the excitonic hole into mixed QD/PTC states. We have observed a decrease in, for instance, the optical band gap of small CdS QDs of up to 970 meV, and substantial bathochromic shifts in the absorption spectra CdSe and PbS QDs.^{26,52,55} The interfacial states have contributions from the highest occupied molecular orbitals (HOMOs) of PTC, the under-passivated Cd²⁺ surface site to which the dithiocarbamate binds, and the valence band states of the QD, which are composed predominantly of chalcogenide p-orbitals. It is the mixing of the ligand states with the QD VB states that provides orbital density for hole delocalization.

There is evidence that the exciton delocalization effect is greater for more strongly confined excitons (i.e., smaller particles).⁵⁵ Sardar and coworkers, for example, treated ultrasmall CdSe nanocrystals (diameters ranging from 1.6 to 2.0 nm) with PTC, and observed a decrease in the optical band gap of up to 610 meV *via* what they propose is hole delocalization.⁵⁶

We and others^{28,31,57-68} have also observed exciton delocalization in metal chalcogenide QDs upon their treatment with thiol (or other chalcogenol) ligands, rather than dithiocarbamate ligands. Due in part to a smaller density of energetically accessible sulfur states, thiolates do not shift the absorption spectra of the QDs as much as do dithiocarbamates.

1.5 Characterization of QD Surface Chemistry by NMR.

The accurate characterization of QD surfaces presents an interesting analytical challenge. Firstly, these measurements usually have to be in the ensemble. Single QD studies have been performed, but these analyses do not characterize the surface chemistry, focusing instead on the QDs' photophysical properties. The rigorous investigation of QD surface chemistry demands the use of analytical techniques capable of characterizing the QD surface in the solution phase. Nuclear magnetic resonance (NMR) is an excellent choice because it is nondestructive, can differentiate between free and bound ligands, can identify and quantify these ligands, and allows for the observation of ligand exchange *in situ*.

The slow motion of nanoparticles (and molecules bound to them) in solution increases the rotational correlation time of the bound molecules, which causes broadening of their resonances in NMR.^{69,70,71,72,73} **Figure 1.3** shows the structure and assigned NMR spectra of free oleic acid (**Figure 1.3A**) and oleate-coated CdSe QDs (**Figure 1.3B**). Oleic acid, which is capable of self-exchange due to the lability of the carboxylate-metal bond,² and which is also relatively long and flexible, has broadened but still clearly observable NMR signals when bound to QDs. The full width at half-

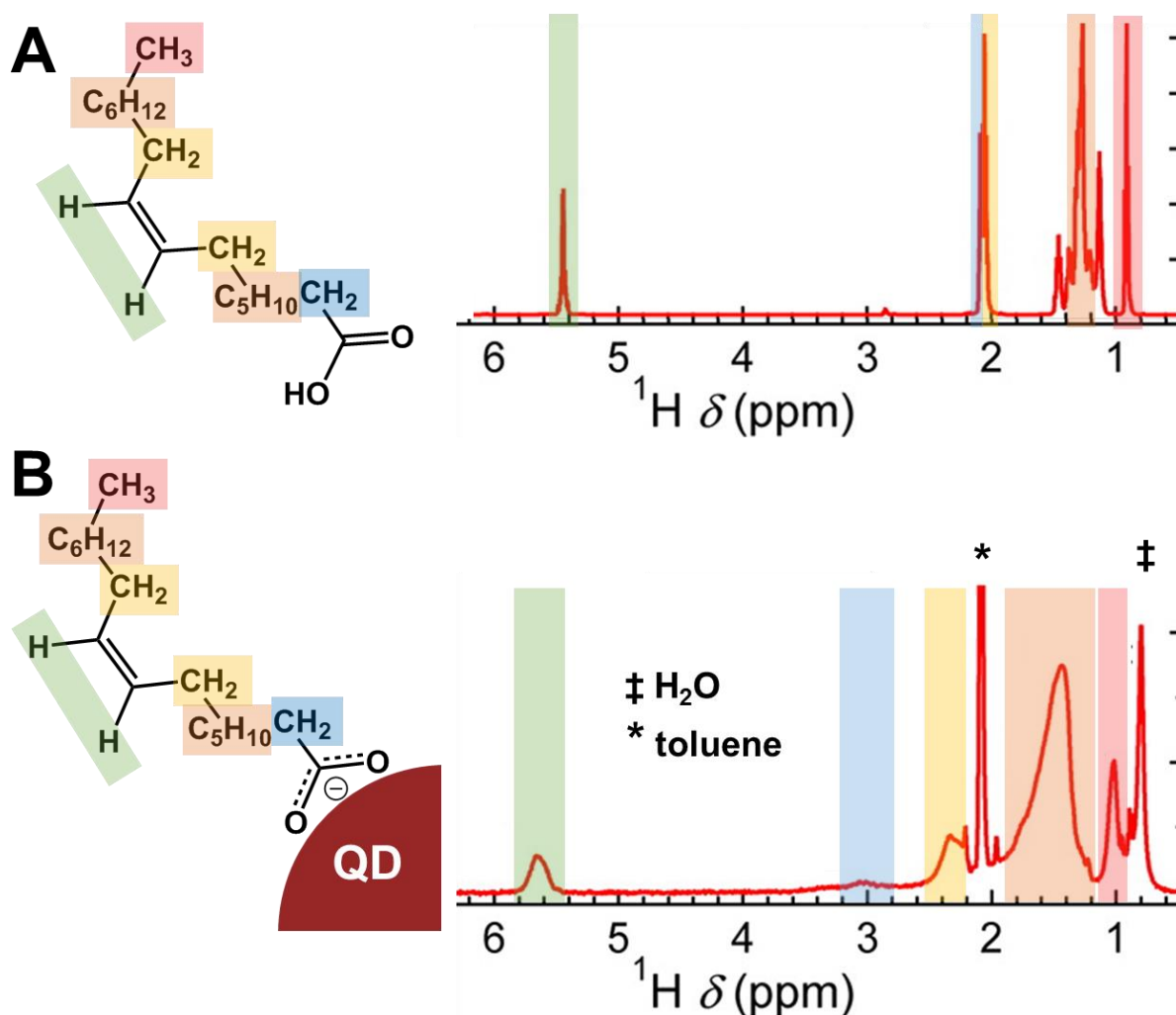


Figure 1.3. The structure and corresponding 1D ^1H NMR spectra of A) free oleic acid and B) oleate-capped CdSe QDs. The NMR spectrum of free oleic acid has sharp, well-resolved proton signals. These signals are broadened in the NMR spectrum of oleate-capped CdSe QDs due to the restriction of motion for molecules bound to the surface of a (comparatively) large nanoparticle. This broadening is analogous to the broadening that occurs in the NMR of solids. NMR spectra adapted from ref. ²

maximum (fwhm) of an NMR signal is inversely proportional to the spin-spin relaxation time, T_2 (eq 2.1).

$$fwhm = \frac{1}{\pi T_2} \quad (2.1)$$

Some ligands, such as aromatic dithiocarbamates, bind very strongly to metal-enriched QD surfaces,⁷¹ and possess a short, rigid structure, which causes their NMR signals to disappear entirely

when these ligands are bound to QDs.^{74,75,76} We discuss specific NMR strategies for quantitative characterization of QD ligand shells in Chapters 2 and 3.

1.6 Dissertation Outline.

This dissertation aims to quantitatively describe the relationship between surface chemistry of QDs and their photoluminescence and quantum confinement, and explores avenues to improve conductivity of QD films and the yield and rate of hole transfer to a molecular acceptor using hole-delocalizing ligands. Chapter 2 discusses the utilization of solution nuclear magnetic resonance (NMR) spectroscopy for QD surface chemistry characterization, and the relationship between QD surface chemistry and photoluminescence. Chapter 3 describes a quantitative NMR method to determine the number of bound exciton-delocalizing ligands on the surface of CdS QDs, and its relationship to the degree of confinement relaxation; it also describes the discovery of cooperative interligand effects on exciton delocalization. Chapter 4 investigates the effect of exciton-delocalizing ligands on the conductivity of lead sulfide QD films. Chapter 5 studies the improvement in hole transfer yield and rate from a photoexcited CdS QD to a zinc phthalocyanine (ZnPc) using an exciton-delocalizing molecular linker, N-4-pyridinylcarbamodithioate. This dissertation concludes with a summary of what has been learned, as well as potential future research directions.

2 USING NUCLEAR MAGNETIC RESONANCE TO CORRELATE THE SURFACE CHEMISTRY OF QUANTUM DOTS WITH THEIR PHOTOLUMINESCENCE

Adapted from:

1. Jin, S.; Harris, R.D., *et al.* Enhanced Rate of Radiative Decay in CdSe Quantum Dots upon Adsorption of an Exciton-Delocalizing Ligand. *Nano Lett.*, 2014, *14* (9), pp 5323-5328.
2. Nepomnyashchii, A.B.; Harris, R.D.; Weiss, E.A. The Composition and Permeability of Oleate Adlayers of CdS Quantum Dots upon Dilution to Photoluminescence-Relevant Concentrations. *Anal. Chem.* **2016**, *88* (6), pp 3310-3316.

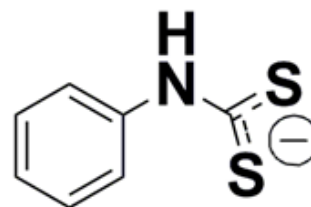
2.1 Chapter Summary

This chapter describes the utilization of solution nuclear magnetic resonance (NMR) to characterize the surface chemistry of colloidal nanocrystals (quantum dots, QDs), and the correlation of QD surface chemistry with their photoluminescence. First, we describe the correlation of the surface coverage of an exciton-delocalizing ligand, phenyldithiocarbamate, with the photoluminescence of CdSe QDs. Next, we describe the relationship between surface coverage of cadmium oleate and the photoluminescence of CdS QDs in progressively dilute concentrations. Finally, we summarize the common methods used in the Weiss group to quantitatively describe the

QD surface chemistry with NMR. Chapter 3 of this dissertation describes in detail one of these methods and the consequences of ligand packing on the QD surface.

2.2 Correlation of the Surface Chemistry of QDs with Photoluminescence Enhancement.

2.2.1. Introduction. This section describes an enhancement of the photoluminescence quantum yield (PL QY) of colloidal CdSe quantum dots (QDs) upon replacement of the native alkylphosphonate ligands of the QDs with an exciton-delocalizing ligand, phenyldithiocarbamate (PTC), **Scheme 2.1**. Our previous work showed that replacement of the insulating native ligands of metal-chalcogenide QDs (including alkylphosphonates and oleate) with PTC ligands results in a dramatic decrease in optical band gap of the QDs by, in the case of CdS QDs, up to 1 eV and in the case of CdSe QDs, up to 220 meV, and a concomitant shift in the PL spectrum, without broadening of either spectrum.^{26,52,55} We have determined, through several mechanistic studies, that the decrease in bandgap is primarily due to stabilization of the excitonic state by delocalization of the excitonic hole into newly available interfacial states formed upon binding of PTC ligands to Cd²⁺ or Pb²⁺ on the QD surface.^{26,52,55} This hole delocalization is potentially advantageous for extraction of excitonic carriers by molecular redox partners,⁷⁷⁻⁸⁰ and increased mobility of charge carriers within solid-state arrays of QDs,⁸¹⁻⁸⁵ for photovoltaic, photocatalytic, and chemical and biological sensing applications. Here we show that manipulation of the shapes of strongly confined excitonic wavefunctions within these nanostructures impacts not only the energies, but also the oscillator strength of absorptive and emissive transitions, and therefore the PL lifetimes and quantum yields. We identify, account for, and minimize the nonradiative pathways for exciton decay introduced by treatment of CdSe QDs with PTC, namely charge transfer to unbound PTC molecules. We show that delocalization of the



Scheme 2.1. The anionic ligand phenyldithiocarbamate (PTC). It is added to dispersions of CdSe QDs as an ammonium salt.

wavefunction of the strongly confined exciton of these QDs by less than 10% increases the PL QY by more than a factor of two by increasing the integrated extinction of the first excitonic transition. Adsorption of phenyldithiocarbamates therefore simultaneously provides greater electronic access to the QD's exciton (for the purpose of, for example, charge extraction) and enhances the strength of absorptive and emissive transitions of the QD.

We study the relationship between exciton delocalization and PL QY using ensembles of CdSe QDs with a first excitonic absorption peak at 539 nm, which corresponds to a radius of the QD core of 1.42 nm.⁴ The excitonic hole in a CdSe QD of this size is strongly confined, so it is maximally sensitive to the delocalizing effects of PTC.⁵⁵ We synthesize the ammonium salt of PTC (NH_4^+ -PTC⁻), a white powder, from carbon disulfide and aniline using a previously published procedure.²⁶ The primary native ligands (ligands on as-synthesized QDs) are octylphosphonates (OPA).⁸⁶⁻⁸⁷ To replace OPA with PTC, we add ~0.2 mg of NH_4^+ -PTC⁻ powder to 2 mL of a 1 μM dispersion of QDs in CH_2Cl_2 . NH_4^+ -PTC⁻ is only marginally soluble in CH_2Cl_2 , so we accelerate the ligand exchange by sonicating the mixture for different amounts of time ranging from 1 h to 12 h. Longer sonication times result in more uptake of the NH_4^+ -PTC⁻ powder into the dispersion and greater surface coverage of PTC on the QD (all control experiments in this study involve the same degree of sonication of the samples). Before acquiring optical spectra of the QDs, we pass the samples through a 0.45 μm filter to remove undissolved NH_4^+ -PTC⁻.

2.2.2. Results and Discussion. Figure 2.2 shows the absorption spectra, normalized to the height of the first excitonic absorption peak, of CdSe QDs in CH_2Cl_2 , and the same QDs in CH_2Cl_2 treated with PTC for increasing amounts of time. The first excitonic peak shifts to lower energy as the ligand exchange time increases, saturating by 12 hours of exchange. For each spectrum within the series

shown in **Figure 2.2**, we use a pre-constructed calibration curve of the energy of the first excitonic transition vs. the physical radius, R , of the core of the CdSe QD⁴ to calculate the apparent increase in excitonic radius of the QDs upon treatment with PTC (the physical size of the QD core does not increase^{26,55}). We denote this

apparent change in excitonic radius “ ΔR ”.^{26,52,55}

The inset to **Figure 2.2** is a plot of ΔR vs. ligand exchange time.

Upon treatment with NH_4^+ -PTC⁻ for any of the ligand exchange times shown in **Figure 2.2**, the PL of the QDs is quenched by more than 95%. The potential quenchers present in the

system are: (i) PTC adsorbed to QD by chelating or bridging Cd^{2+} , the two most stable binding motifs⁸⁸, (ii) PTC freely diffusing or weakly adsorbed to the QD in monodentate geometry (such PTC is probably in rapid exchange on and off the surface), and (iii) the degradation products of PTC: aniline, phenylisothiocyanate, and diphenylthiourea, which is the condensation product of aniline and phenylisothiocyanate. The value of ΔR for QDs treated with PTC for a given length of time is indefinitely stable; we therefore know that none of these degradation products is capable of displacing PTC from the QD surface and that, once adsorbed to the QD, PTC itself does not degrade. Furthermore, none of the degradation products, when added intentionally to dispersions of CdSe QDs, causes a bathochromic shift of the absorption spectrum.

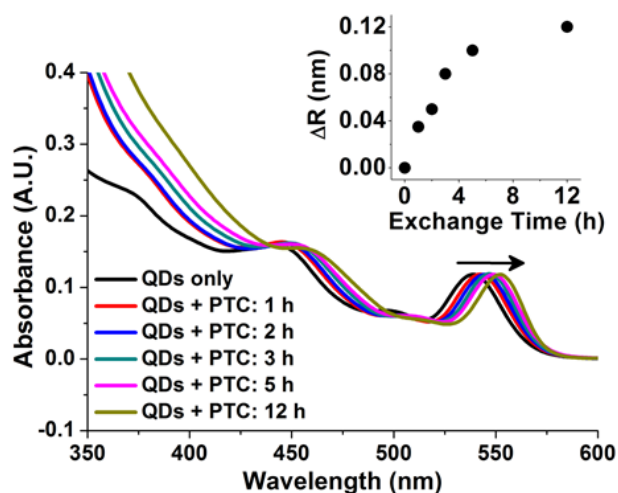


Figure 2.1. Absorption spectra of CdSe QDs with radius $R=1.42$ nm in CH_2Cl_2 , and the same QDs treated with PTC for increasing amounts of time, which leads to increasing surface coverage of PTC on the QD. Spectra are scaled such that they have their first excitonic peaks have the same height.

Inset: A plot of the apparent increase in excitonic radius, ΔR , for the QDs upon ligand exchange of native phosphonates for PTC, as a function of the ligand exchange time. The text describes the ligand exchange procedure and the calculation of ΔR from the absorption spectra in this figure.

This degree of PL quenching of the QDs due to, presumably, charge transfer to one or more of these species⁸⁹⁻⁹² obscures the relationship that we are aiming to determine – that between the PL and the degree of exciton delocalization – so eliminating or mitigating the efficacy of these nonradiative pathways is important for this study. We noticed that, although the PL of QDs was quenched immediately after exposure to $\text{NH}_4^+\text{-PTC}^-$, the PL of all samples recovers (to various degrees, depending on how much PTC was added) over longer timescales of 24-48 hours. According to ^1H NMR and ground state absorption spectra of the samples, this recovery is correlated with the degradation of unbound PTC and formation of the degradation products (see **Figure 2.3**). As we noted previously, ΔR is constant throughout this degradation and PL recovery process, so it is unbound PTC, and not PTC contributing to exciton delocalization, that acts as the PL quencher. Based on the frontier orbital energies of the QD and PTC, the probable mechanism of quenching is hole transfer to PTC.⁹² This non-adiabatic quenching process is distinct from the adiabatic delocalization of the excitonic hole into interfacial states formed by bound PTC.

In order to confirm our suspicion that free or weakly associated PTC molecules are primarily responsible for PL quenching of PTC-treated QDs, and to remove this quenching pathway, we added cadmium acetate (in a MeOH co-solvent) to the samples of QDs; MeOH is necessary to promote adequate dispersion of cadmium acetate in CH_2Cl_2 , and all control experiments include addition of the same amount of MeOH as the experiments with added cadmium acetate. The purpose of adding excess cadmium ions is to precipitate the PL-quenching free PTC molecules from solution,⁸⁸ and thereby remove them faster and more completely than if they were to naturally chemically degrade over tens of hours. **Figure 2.4** shows the white precipitate that forms within seconds of mixing $\text{NH}_4^+\text{-PTC}^-$ with cadmium acetate (in the absence of QDs), in CH_2Cl_2 with a MeOH co-solvent. NMR spectroscopy confirms that $\text{NH}_4^+\text{-PTC}^-$ is removed from solution upon precipitation, and that the

precipitate is a molecule that is structurally very similar to cadmium *bis*-(phenyldithiocarbamate), probably the commonly formed Cd-dithiocarbamate clusters (**Figure 2.4**).⁸⁸

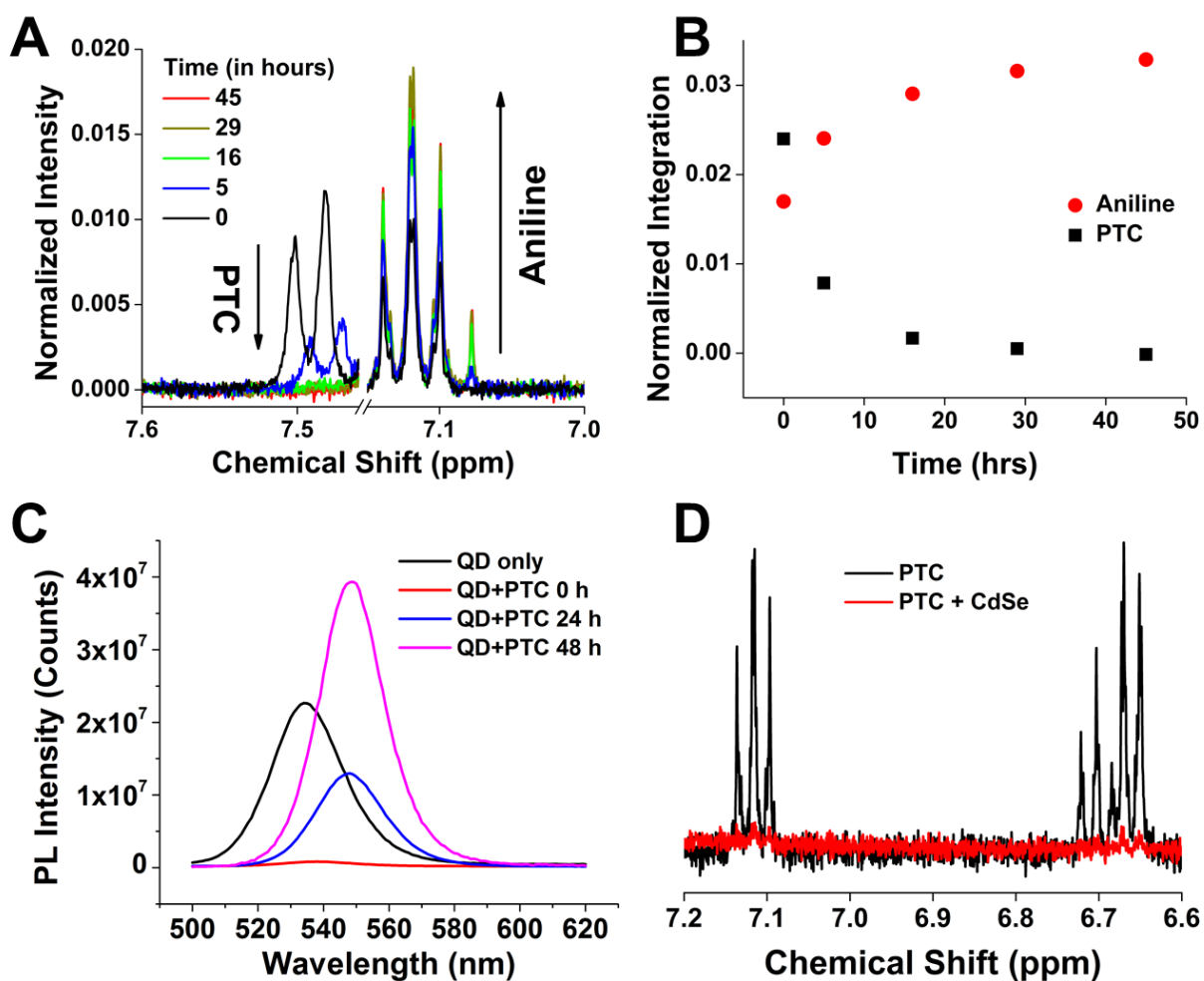


Figure 2.2. **A)** ¹H NMR spectra of PTC in CD₂Cl₂ at 0, 5, 16, 29, and 45 h. The PTC peaks decrease noticeably until they are undetectable after 16 h. The peaks attributable to aniline, a degradation product of PTC, increase continuously over the measured time period. Only one set of PTC peaks is shown for clarity; we believe that these peaks shift as PTC degrades because degradation proceeds, at least in part, through protonation of PTC by ammonium. Release of ammonia changes the pH of the solution. **B)** Relative normalized integrations of 2H peaks for aniline (red circles) and PTC (black squares) showing the increase of aniline and decrease of PTC in solution over time relative to the residual solvent peak. **C)** Emission spectra of CdSe QDs (R = 1.31 nm) before and after treated with PTC to achieve a ΔR = 0.1 nm at 0, 24 and 48 h. Recovery and eventual enhancement of the CdSe QD PL over time corresponds to the degradation of excess PTC. **D)** ¹H NMR spectra of a solution of NH₄-PTC in d₄-methanol added to either 0.8 mL CD₂Cl₂ or 0.8 mL (black) or to 0.8 mL of CdSe QDs in CD₂Cl₂, after stirring for 10 min., to show the disappearance of NMR signals from PTC protons upon adsorption to the surfaces of QDs.

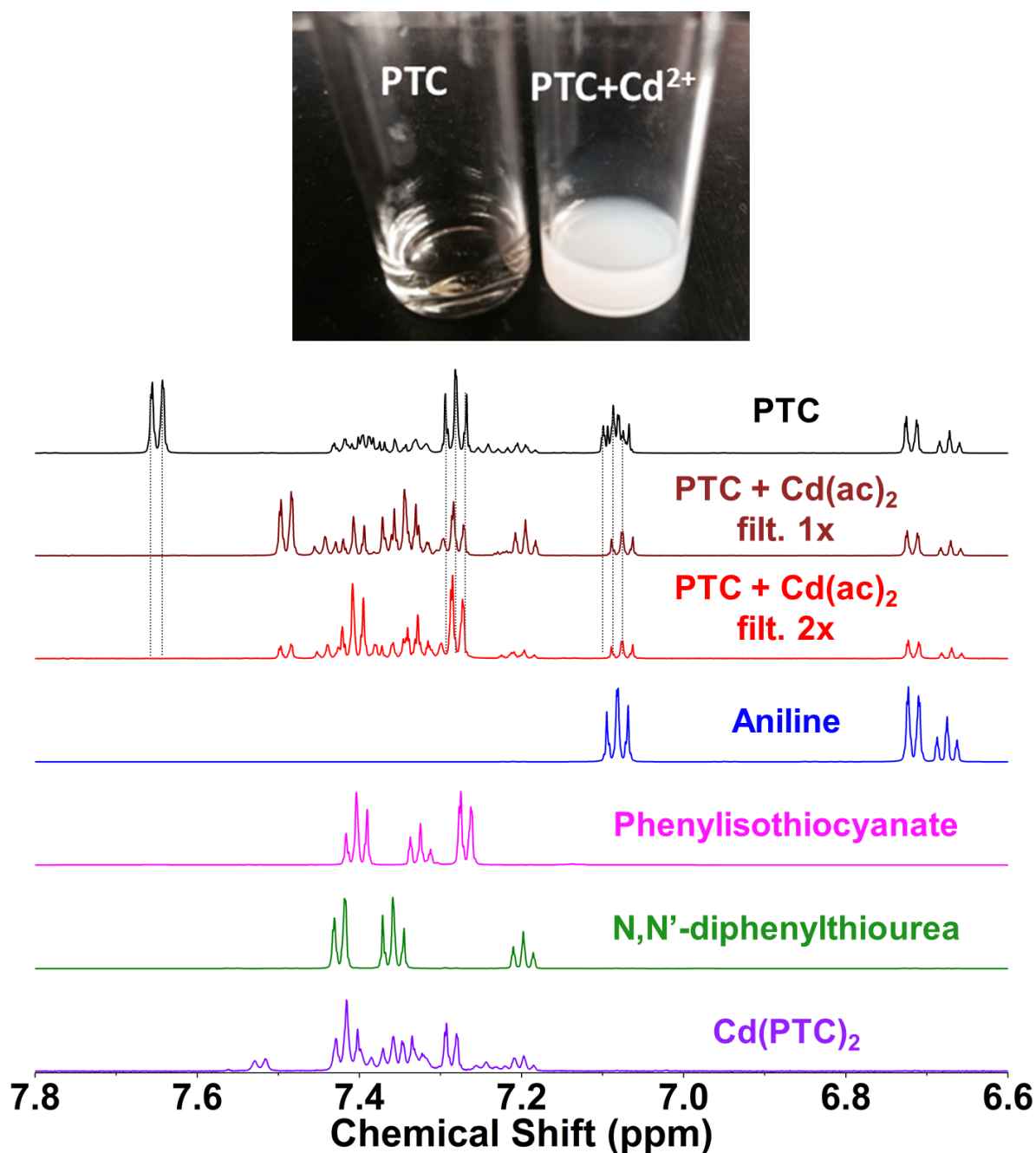


Figure 2.3. (Top) Photograph showing the formation of a white precipitate (cadmium bis(phenyldithiocabamate) $\text{Cd}(\text{PTC})_2$) upon addition of cadmium acetate ($\text{Cd}(\text{ac})_2$) to a solution of PTC in methanol and CH_2Cl_2 co-solvent. (Bottom) ^1H NMR spectra (in CD_3OD) of PTC and PTC + $\text{Cd}(\text{ac})_2$ after one and two filtrations. Upon addition of $\text{Cd}(\text{ac})_2$, the NMR signals due to free PTC disappear entirely. This is demonstrated by the disappearance of the doublet at 7.65 ppm, the overlaid triplets at 7.12 ppm resolving to a single triplet attributed to aniline, and the disappearance of the triplet at 7.28 reappearing as a doublet attributable to either phenylisothiocyanate or the $\text{Cd}(\text{PTC})_2$ complex. We also include spectra of $\text{Cd}(\text{PTC})_2$, as well as aniline, phenylisothiocyanate, and N,N'-diphenylthiourea, the degradation products of PTC.

Based on the effective precipitation of free PTC by Cd^{2+} , we added (i) 50 μl methanol, and (ii) 1.5 mg of cadmium acetate solid (in that order) to 2-mL samples of QDs (in CH_2Cl_2) that had been pre-treated with PTC for various lengths of time and therefore exhibit a range of ΔR values. We then sonicated the mixtures for 2 h, and monitored the change in the PL spectra of the QDs. During the sonication process, cadmium *bis*-(phenyldithiocarbamate) precipitated, and the absorbance of the sample at wavelengths shorter than 400 nm – the region where PTC absorbs – significantly decreased (see **Figure 2.8** in the Supporting Information). We passed the mixtures through a 0.45- μm filter to remove the precipitates before characterizing the samples.

Figure 2.5A shows the emission spectra of (i) a QD sample treated only with MeOH (QY = 2% vs. Rhodamine B), (ii) an identical QD sample treated with only MeOH and cadmium acetate (no PTC), (iii) an identical QD sample treated with only PTC (no cadmium acetate or MeOH) for enough time to induce a ΔR of 0.05 nm, and (iv) a set of QD samples treated first with PTC to achieve a series of ΔR values, and then with MeOH and cadmium acetate. The same amount of MeOH and cadmium acetate was added to all PTC-treated QD samples, and all samples underwent the same sonication and filtering treatment no matter what was added to the QDs. All of these spectra are acquired with an excitation wavelength 460 nm, and, importantly, all spectra are scaled to account for the samples' respective optical densities at 460 nm (shown in **Figure 2.7** of the Supporting Information). We therefore know that any change in PL intensity shown in these spectra is due to a difference in the number of emitted photons per absorbed photon, not the number of absorbed photons. Analysis of

the spectra in **Figure 2.5A**, along with the absorption spectra of the samples, yields the following conclusions:

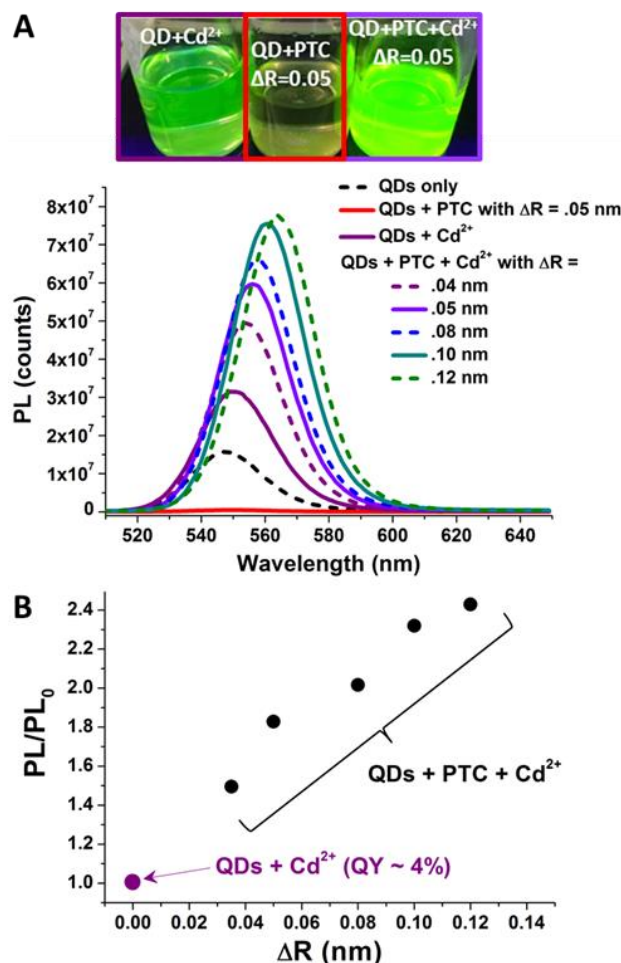


Figure 2.4. A) Emission spectra of a sample of CdSe QDs with no further treatment (“QDs only”), a sample of CdSe QDs treated with cadmium acetate (“QDs + Cd²⁺”), a sample of CdSe QDs treated with PTC to achieve $\Delta R = 0.05$ nm (“QDs + PTC with $\Delta R = .05$ nm”), and a set of samples of CdSe QDs treated first with PTC to achieve a series of ΔR values, and then with the same amount of cadmium acetate (“QDs + PTC + Cd²⁺”). All samples are in CH₂Cl₂ and are excited at 460 nm, and their photoluminescence intensities (PL) are scaled by their absorbances at 460 nm. Also shown on top of the spectra are photographs of three of the samples (as labeled) showing the quenching of PL by PTC, and the recovery of the PL of PTC-treated QDs by addition of cadmium acetate. Addition of cadmium acetate to the PTC-treated sample with $\Delta R = 0.05$ increases the PL intensity of the sample by a factor of 1.9, after accounting for the increase in absorption intensity. **B)** A plot of PL/PL_0 – the PL intensity of the sample of QDs treated with PTC and cadmium acetate divided by the PL intensity of the sample of QDs treated with cadmium acetate but with no added PTC – as a function of ΔR .

(i) Treatment of QDs with PTC-only completely quenches the PL of the sample, and treatment of the QDs with cadmium acetate-only increases the integrated PL intensity of the sample by a factor of two, presumably by passivating any under-coordinated selenium ions on the QD surface and thereby decreasing the number of sites for non-radiative trapping of the hole.⁹³ The addition of cadmium acetate to PTC-treated samples allows the PL of the QDs to recover to an integrated intensity that is *higher* – a factor of 1.9 higher in the case of PTC-treated QDs with $\Delta R = 0.05$, for example – than that of the sample of QDs treated only with cadmium acetate and no PTC (see also the photograph of these samples in **Figure 2.5A**). This result indicates that, once the number of non-radiative pathways is reduced by passivation and precipitation of free PTC, adsorption of PTC itself additionally increases the PL of the QDs. **Figure 2.9** in the Supporting Information shows that, upon adding cadmium acetate to PTC-treated QDs with $\Delta R = 0.05$ nm, the PL of QDs recovers to its saturated value within 2 h.

(ii) The enhancement of the PL intensity due to PTC is clearly correlated with the value of ΔR for each sample. **Figure 2.5B** shows a plot of PL/PL_0 vs. ΔR , where “PL” is the integrated PL intensity of the sample of PTC-treated QDs with added cadmium acetate, and “ PL_0 ” is the integrated PL intensity of the sample of QDs treated only with cadmium acetate but with no added PTC. This plot indicates that the presence of adsorbed PTC – and not freely diffusing PTC, its degradation products, or cadmium acetate – is associated with the enhancement of PL of the sample.

(iii) For PTC-treated QDs with all values of ΔR , the treatment with cadmium acetate results in a 2-to-4 nm bathochromic shift of the PL peak (and the absorption peak) in addition to that caused by adsorption of PTC alone. We observe a similar magnitude of bathochromic shift upon treatment with cadmium acetate for QDs without PTC ligands (see **Figure 2.10** in the Supporting Information), and this shift is probably due to formation of patches of a CdSe shell at sites where Cd^{2+} passivates

undercoordinated Se on the surface of the QD.⁹³ We see no evidence – in the form of a shift of the QD absorption to higher energy – of displacement of adsorbed PTC ligands by Cd²⁺.

2.2.3. Conclusions. In summary, we have demonstrated that displacement of insulating native ligands on the surfaces of CdSe QDs by exciton-delocalizing phenyldithiocarbamate ligands enhances the photoluminescence quantum yield of the QDs. This effect could only be identified once the non-radiative exciton decay pathways introduced by treatment of the QDs with PTC were eliminated by addition of cadmium salt, which precipitates PL-quenching free (or weakly adsorbed) PTC molecules and passivates the surfaces of the QDs. More theoretical work, and possibly experiments that determine the dependence of the PL enhancement on magnetic field or temperature, are needed to determine the role of transitions from states within the exciton fine structure in the observed transition intensity, and whether an increase in the number of oscillators participating in the transition or an increase in the magnitude of the matrix elements for formerly disallowed transitions (or both) is responsible for the increase in the magnitude of this matrix element upon adsorption of PTC.

2.2.4. Supporting Information.

EXPERIMENTAL METHODS:

Synthesis and Purification of CdSe QDs. We combined 90% technical grade trioctylphosphine oxide (TOPO, 7.76 g, 20.08 mmol), hexadecylamine (HDA, 7.76 g, 24.12 mmol), and cadmium stearate (CdSt₂, 0.448 g, 0.660 mmol) in a dry 100-mL three-neck round bottom flask and heated the mixture, with stirring, to 150 °C for 1 hour. Nitrogen flowed through one arm of the flask over the solution. This step serves to remove any water in the reaction mixture. The flask was sealed and heated to 330 °C under positive nitrogen flow. After the CdSt₂ completely dissolved, we rapidly injected trioctylphosphine selenide (TOPSe, 4 mL of 1 M solution in TOP, prepared and stored in a glovebox), and then cooled to room temperature under ambient conditions. The QDs were precipitated in

methanol and centrifuged at 3500 RPM for five minutes. We dispersed the resultant QD pellet in a minimal amount of hexanes (~10 mL), centrifuged for five minutes, and extracted the colored supernatant, which sat in the dark overnight while excess ligands precipitated. We again centrifuged the QD dispersion, separated the hexanes portion from the solid white pellet, and precipitated the QDs again by addition of acetone. We discarded the supernatant, dispersed the resulting pellet in a minimal amount of hexanes (~10 mL), and precipitated the QDs by addition of acetone a final time. The colored pellet was dispersed in ~20 mL of dichloromethane. The native ligand on the final QD product is octylphosphonate (OPA).

Synthesis of Ammonium Phenylthiocarbamate (PTC). We synthesized ammonium phenylthiocarbamate ($\text{NH}_4^+\text{-PTC}^-$) by adding two equivalents of carbon-disulfide (1.9 mL, 32 mmol) drop-wise to one equivalent of aniline (1.5 mL, 16 mmol) in a rapidly stirring suspension of 10-mL of 28-30% ammonium hydroxide at 0 °C, and stirred overnight. We washed the resulting white powder with hexanes and chloroform and dried under N_2 for 1 h.

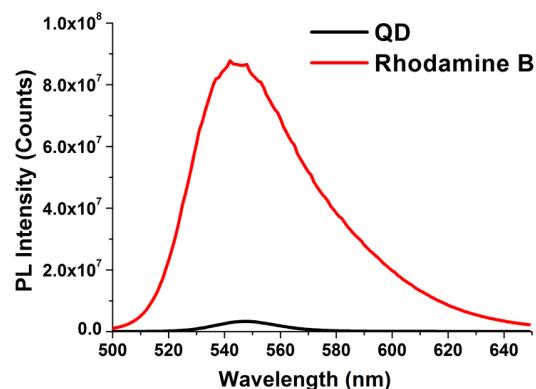


Figure 2.5. Emission spectra of Rhodamine B in CH_2Cl_2 and CdSe QDs in CH_2Cl_2 with 50 μl MeOH. All samples are excited at 460 nm, and their photoluminescence intensities (PL) are scaled by their absorbance at 460 nm. The quantum yield (QY) of the QDs is calculated to be $\sim 2\%$ relative to Rhodamine B.

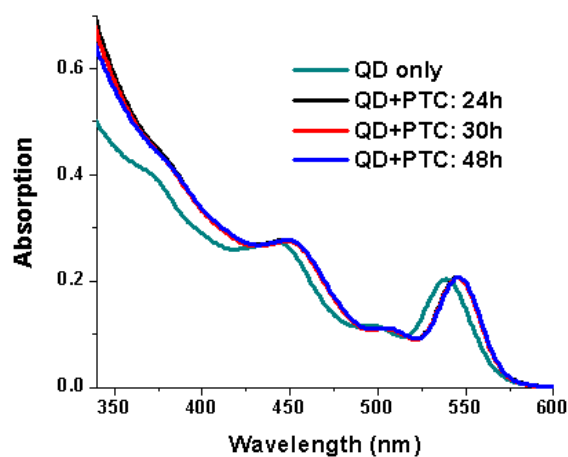


Figure 2.6. Ground state absorption spectra of CdSe QDs ($R=1.42$ nm) (no PTC) and QDs at 24 h, 30 h and 48 h after treated with PTC to achieve a $\Delta R = 0.07$ nm. The first excitonic absorption peak of the QDs treated with PTC is almost unchanged, which indicates a stable ΔR over at least 48 h.

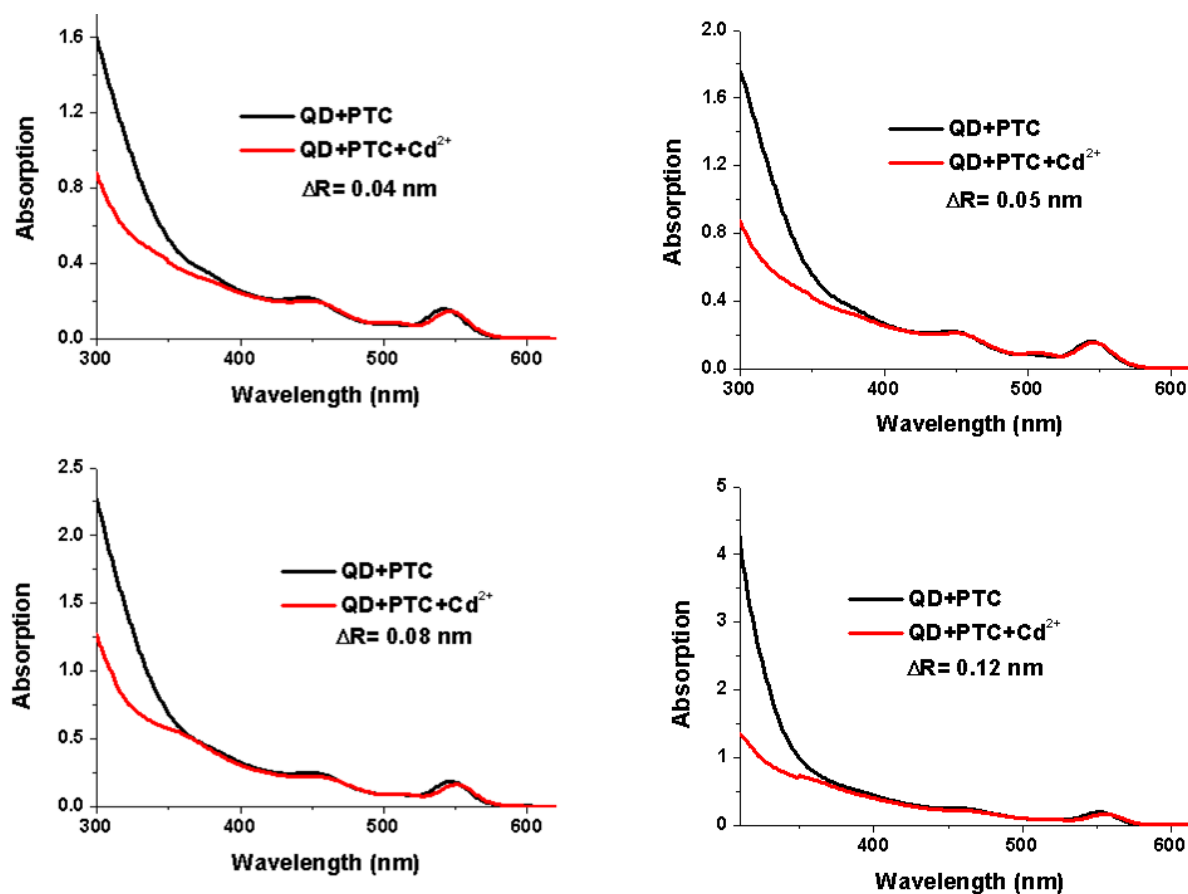


Figure 2.7. Ground state absorption spectra of PTC-treated QDs with a series of ΔR values before (“QD+PTC”) and after (“QD+PTC+Cd²⁺”) the treatment with cadmium acetate. The absorbance of the sample at wavelengths shorter than 400 nm – the region where PTC absorbs – significantly decreases due to the formation of cadmium *bis*-(phenyldithiocarbamate) precipitates. The addition of cadmium acetate also results in a 2-to-4 nm bathochromic shift.

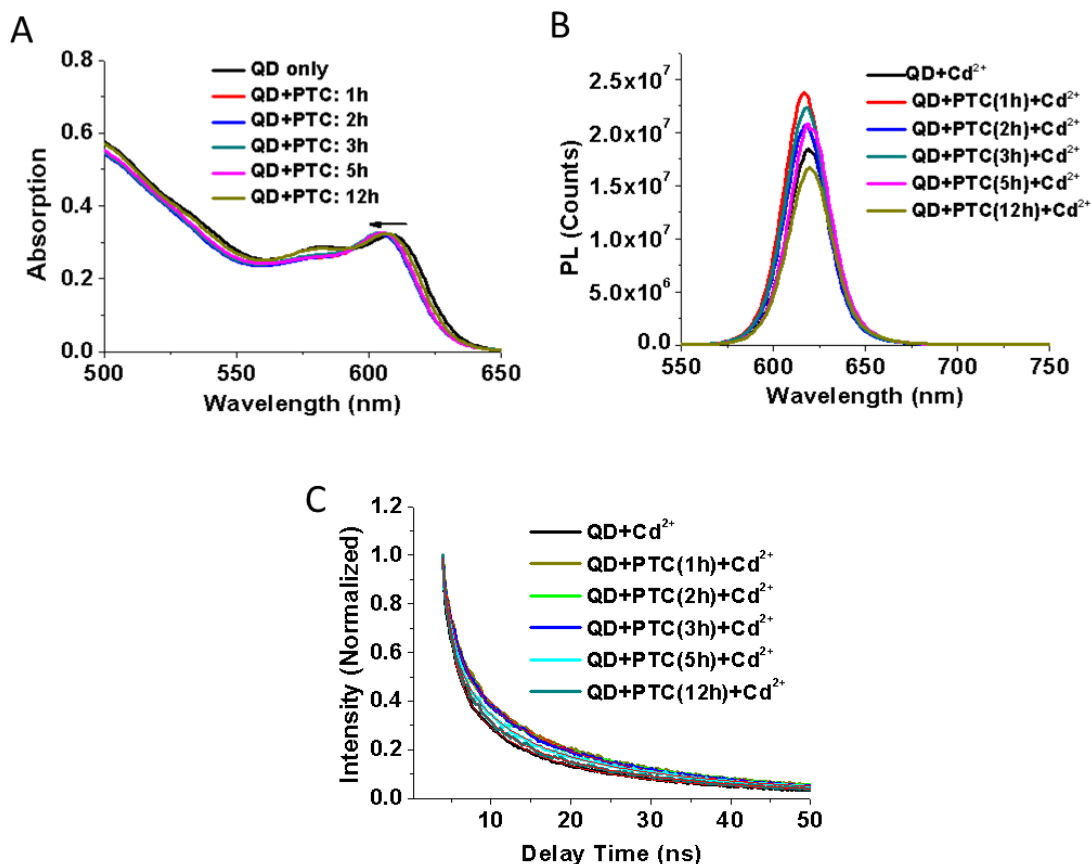


Figure 2.8. A) Absorption spectra of CdSe QDs with a radius $R=2.5$ nm in CH_2Cl_2 , and the same QDs treated with PTC for increasing amounts of time. B) Emission spectra of a sample of CdSe QDs ($R=2.5$ nm) treated with cadmium acetate (“QDs + Cd^{2+} ”) and a set of samples of CdSe QDs treated first with PTC with increasing amount of time, and then with the same amount of cadmium acetate (“QDs + PTC (1~12 h) + Cd^{2+} ”). All samples are in CH_2Cl_2 and are excited at 460 nm, and their photoluminescence intensities (PL) are scaled by their absorbances at 460 nm. We observe a small (~ 3 -4 nm) blue-shift of the absorbance and PL spectra of these samples due to etching of their surfaces by PTC. This blue-shift is apparent for these samples, and not for the samples of smaller QDs, since $\Delta R = 0$, but the etching may also occur in the samples of smaller QDs and lead to a systematic underestimating of ΔR . C) PL decay curves of the same set of samples shown in B). Black solid lines are the best fits of the decay curves to a multi-exponential function with the fitting parameters listed in Table 2.1.

Table 2.1. Time Constants for Decay of the PL, PL/PL₀ and k_r/k_{r0} of CdSe QDs (R = 2.5 nm) upon Treatment with NH₄⁺PTC⁻ and cadmium acetate.

| Sample | τ_1/ns (A ₁) | τ_2/ns (A ₂) | τ_3/ns (A ₃) | τ_s/ns | PL/PL ₀ | k _r /k _{r0} |
|--------------------------------|--------------------------------------|--------------------------------------|--------------------------------------|--------------------|--------------------|---------------------------------|
| QDs+Cd ²⁺ (no PTC) | 27.1 (.15) | 7.1 (.32) | 1.3 (.53) | 18.0 | 1 | n/a |
| QD+PTC (1h) +Cd ²⁺ | 26.6 (.26) | 6.9 (.36) | 1.3 (.38) | 20.4 | 1.23 | 1.09 |
| QD+PTC (2h) +Cd ²⁺ | 26.4 (.25) | 6.5 (.35) | 1.1 (.40) | 20.4 | 1.08 | 0.95 |
| QD+PTC (3h) +Cd ²⁺ | 1.6 (.46) | 9.3 (.36) | 29.3 (.18) | 20.5 | 1.18 | 1.04 |
| QD+PTC (5h) +Cd ²⁺ | 1.2 (.43) | 6.1 (.34) | 26.5 (.23) | 20.1 | 1.09 | 0.97 |
| QD+PTC (12h) +Cd ²⁺ | 1.3 (.51) | 7.1 (.31) | 26.7 (.17) | 18.7 | 0.92 | 0.88 |

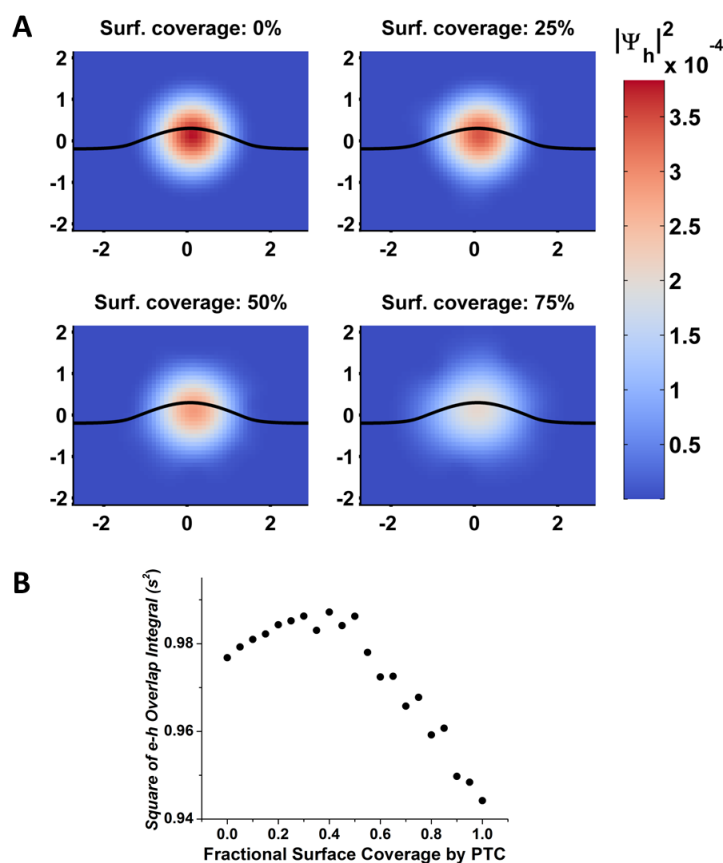
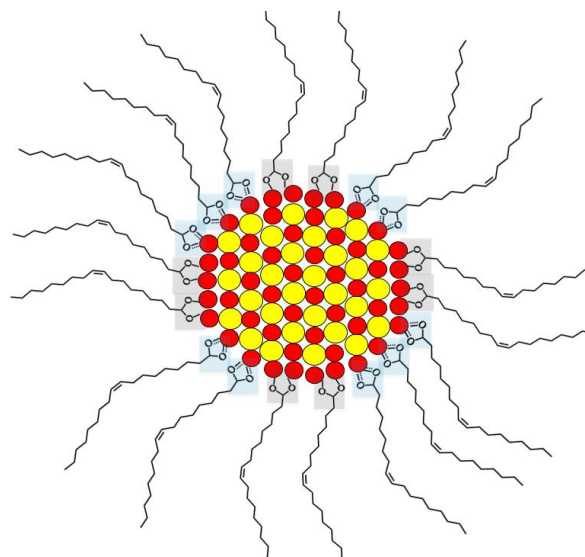


Figure 2.9. A) A two-dimensional slice of the three-dimensional hole wavefunction, taken through the center of the nanoparticle. The probability density is plotted against the x and y coordinate for four different ligand surface coverages. The electron wavefunction has spherical symmetry and is sketched as a radial slice (black curve). **B)** The square of the overlap integral between the hole and electron wavefunctions versus the fractional ligand surface coverage. The overlap increases to a maximum at 50% surface coverage, then decreases.

2.3 The Composition and Permeability of Oleate Adlayers of CdS QDs upon Dilution to Photoluminescence-Relevant Concentrations.

2.3.1. Introduction. This section describes the investigation of the effects of dilution, from concentrations typically used for proton nuclear magnetic resonance (^1H NMR)^{12,94-95} analysis to concentrations typically used for photoluminescence (PL) experiments,⁹⁶⁻⁹⁷ on the surface structure and photophysical properties of oleate-capped cadmium sulfide quantum dots (CdS QDs) (**Scheme 2.2**). CdS QDs are easily



Scheme 2.2. Schematic representation of a cross-section of a CdS QD capped with oleate ligands in both bridging (gray) and chelating (blue) binding modes. Red circles represent cadmium ions and yellow circles represent sulfur ions. Although this 2D slice of the QD is not charge balanced, in 3D, the oleate ligands (with a 1- charge) balance the excess Cd^{2+} ions over the entire surface of the QD.

synthesized with a variety of surface chemistries, have high reduction and oxidation potentials, and are useful for both fundamental photophysical studies^{85,98} and for applications such as redox photocatalysis.⁹⁹⁻¹⁰¹

The most common method for preparing dispersions of high-quality CdS QDs is “hot-injection synthesis” (addition of elemental sulfur to CdO at temperatures > 250 °C) with oleic acid as the primary surfactant and the final, post-purification ligand coating.¹¹⁻¹² The long hydrocarbon chain provides a large steric barrier to particle aggregation, and the carboxylic acid head group binds to cadmium ions on the QD surface.^{12,40-41,94,102-104} The size, shape, and degree of cation enrichment of metal sulfide QDs are influenced by the injection temperature, the amount of oleic acid added, and

the preparation conditions for the sulfur precursor.¹⁰⁵ The PL spectra of well-passivated cation-enriched QDs are dominated by “band-edge emission”, radiative recombination of the excitonic electron with the excitonic hole, whereas the PL spectra of sulfur-enriched QDs show a greater contribution from lower-energy “trap emission”, recombination of the excitonic electron with a surface- or lattice-trapped hole.^{11-12,106}

Key factors in determining the PL quantum yield and the ratio of band-edge to trap emission is the degree of electronic passivation of lattice-terminating ions, since these ions, if left under-coordinated, are thermodynamic traps for excitonic charge carriers.^{13-14,107-110} It is therefore crucial, in analyzing the photophysical properties of a QD, to quantitatively characterize its surface chemistry, in order to estimate the density of potential electronic defects. NMR is a very useful tool for this purpose. Correlation of the composition of the ligand shell by NMR with PL energies, intensities, or lifetimes is often, however, problematic because in order to avoid reabsorption and other non-linear behaviors, PL spectra should be acquired on samples of cadmium chalcogenide QDs that are in a concentration range from nanomolar to single micromolar,^{11,111} whereas NMR investigations of the same systems are usually performed at concentrations from tens to hundreds of micromolar (in QDs) to achieve a usable level of signal to noise with a minimal number of scans.^{2,10,12,94,112-116} Given that the composition and density of the ligand shell of a solution-phase QD depends on the absolute concentration of the QDs, due to the dynamic equilibrium of most surface-adsorbed molecules,⁹⁶ the datasets acquired from these two types of experiments on the same sample (at different concentrations) may or may not be comparable.

Here, we acquire NMR and PL data on the same samples, and same concentrations, of oleate-coated CdS QDs, which are prepared at concentrations ranging from NMR-relevant to PL-relevant, in three different solvents. We use these data to probe the relationship between surface chemistry and

emissive properties of the QDs, and conclude that dilution induces desorption of “z-type” cadmium oleate molecules and clusters^{10,15,97,117-118} (as opposed to breaking the cadmium-oleate bond). We find that the surface coverage of these cadmium oleate ligands does not affect the pathways for excitonic decay in the QD, and therefore does not affect the PL spectrum or yield, but does influence the redox activity of the QDs with respect to a small-molecule charge transfer partner.¹²⁻¹³ These results indicate that, for oleate-coated CdS QDs, we can correlate PL data acquired at low sample concentrations with NMR data acquired at high concentrations to aid in the interpretation of both datasets, but that the absolute concentration of the QDs must be taken into account when reporting the yield of charge transfer with a molecular adsorbate.

2.3.2. The Effect of Dilution on the Surface Chemistry of Oleate-Capped CdS QDs. **Figure 2.10** shows the vinyl proton regions of the ¹H NMR spectra of (i) free oleic acid (“free OAc”), (ii) a synthesized sample of cadmium oleate, which is actually a combination of Cd(oleate)₂ and oleic acid and which we denote “Cd-OA”, and (iii) oleate-capped CdS QDs (“CdS-OA QDs”) in three solvents, C₆D₆, C₆D₁₂ and CDCl₃. Oleate has a spectrally isolated ¹H NMR signal from its two vinyl protons, which makes oleate-capped CdS QDs an ideal system for NMR studies.^{10,94,113,119} The QD samples are 10 μM, 1 μM, and 0.1 μM in each solvent. Given the high sensitivity of the instrument used, the purity of the solvent was the major limiting factor in obtaining reliable measurements at lower concentrations, and spectra of 10 nM samples were mostly indistinguishable from the baseline (**Figure 2.11**). We know from previous work^{12,116} that there are several hundred total oleate molecules per QD within samples prepared with our procedure, so in order to cover the range of possible concentrations of ligand in the QD samples, we show spectra of 200 μM and 2 mM free OAc and Cd-OA.

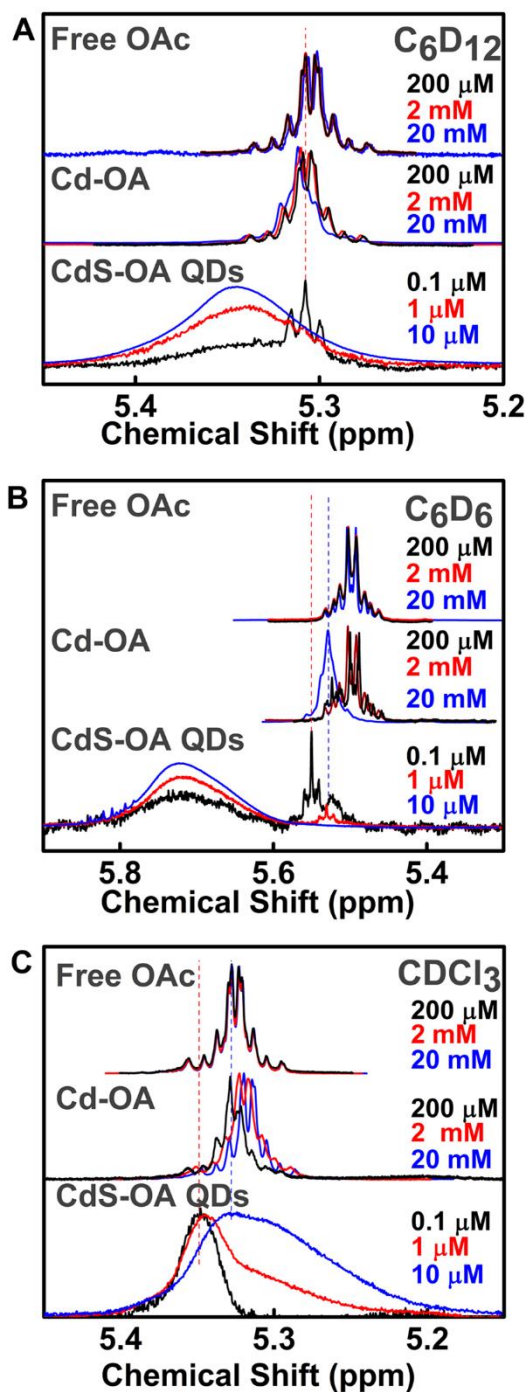


Figure 2.10. The vinyl proton region of the NMR spectra of oleate-capped QDs (“CdS-OA QDs”); a mixture of Cd(oleate)₂, oleic acid, and CdO (“Cd-OA”); and free oleic acid (“Free OAc”) in (A) C_6D_6 , (B) C_6D_{12} , (C) $CDCl_3$. The legends indicate the sample concentrations. The vertical lines are guides to the eye. The y -axes are intensity in arbitrary units. Note that the x -axes are not the same for each figure panel.

In C_6D_6 (**Figure 2.11A**), the spectrum of Cd-OA has overlapping features of oleic acid (the upfield multiplet that overlaps with the free OAc spectrum) and cadmium oleate. The spectrum of the QD sample evolves upon dilution from a single, asymmetric broad peak at $10\ \mu\text{M}$ to a broad peak and a sharper, upfield multiplet that roughly aligns with the cadmium oleate feature at $1\ \mu\text{M}$, to a broad peak plus a set of multiplets, one of which aligns with the cadmium oleate feature and one of which is

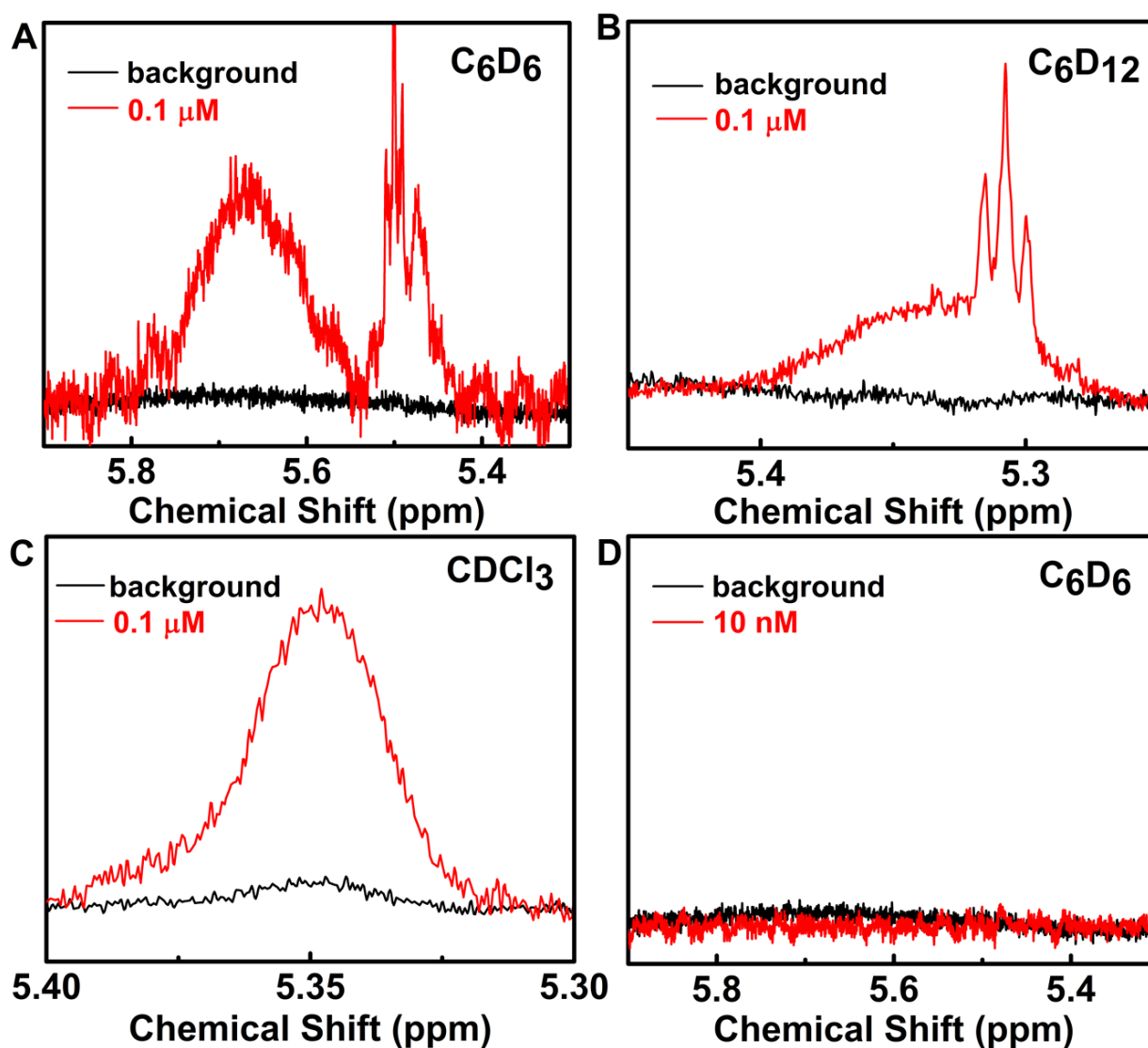


Figure 2.11. A), B), C) Comparison between ^1H NMR signal from oleate-capped CdS QDs ($0.1\ \mu\text{M}$) and the background in C_6D_6 , C_6D_{12} and $CDCl_3$. D) Comparison between ^1H NMR signal from oleate-capped CdS QDs ($10\ \text{nM}$) and the background in C_6D_6 .

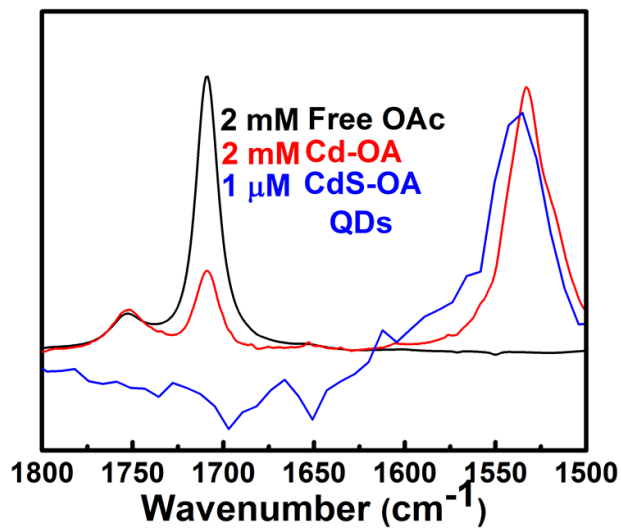


Figure 2.12. FTIR spectra for 1 μM oleate-capped QDs (“CdS-OA QDs”, blue), 2 mM cadmium oleate with oleic acid impurity (“Cd-OA”, red), and 2 mM oleic acid (“Free OAc”, black), in C_6D_6 . The y -axis is intensity in arbitrary units. The peak at 1709 cm^{-1} corresponds to the C=O stretching mode of the carbonyl group in oleic acid. The peak at 1750 cm^{-1} is its side-band. The peak at $\sim 1530\text{ cm}^{-1}$ corresponds to the O-C-O stretching modes of bridging and chelating carboxylates within cadmium-bound oleate. Resolution of the measurement is 2 cm^{-1} for Cd-OA and oleic acid and 8 cm^{-1} for CdS-OA QDs.

further downfield, at $0.1\ \mu\text{M}$. We acquired an FTIR spectrum of the $1\ \mu\text{M}$ QD sample in C_6D_6 (see **Figure 2.12**). There is no detectable oleic acid (only deprotonated oleate) in this FTIR spectrum; we can therefore assign the broad peak at $\sim 5.72\text{ PPM}$ in the NMR spectra in **Figure 2.10A** to oleate bound to the surface of the QD, and the sharp multiplet at $\sim 5.53\text{ PPM}$ in the spectra of the $1\ \mu\text{M}$ and $0.1\ \mu\text{M}$ samples to desorbed cadmium oleate complexes (so-called “z-type ligands”).^{10,15,97,117-118} The sharp feature at 5.55 ppm probably corresponds to desorbed Cd_xOA_y clusters; we have detected analogous clusters in samples of oleate-coated PbS QDs.¹²⁰

The broadening of the vinyl resonance for bound oleate is caused by the restricted rotation of the ligand and chemical heterogeneity of the QD surface.^{2,94,120}

In C_6D_{12} (**Figure 2.10B**), dilution of the QD sample produces a desorbed species with a spectrum that matches that of either cadmium oleate or free oleic acid, which are not readily distinguishable. In CDCl_3 (**Figure 2.10C**), the spectrum of the QDs includes broad signals from desorbed ligands, probably due to fast exchange of oleate between free and bound states in this solvent. There is also

the possibility of exchange between the vinyl protons of oleate and the chloroform proton.² The FTIR spectra of the QDs in C_6D_{12} and $CDCl_3$ do not allow us to conclusively assign the desorbed species to cadmium oleate or oleic acid, due to the overlap between signals of the solvent and sample; however, based on the fact that cadmium oleate is the desorbing species in C_6D_6 , and that desorption of oleate as oleic acid has been shown to require excess oleic acid (or some other protonating species) in organic solution,² we conclude that dilution of the QDs results in desorption of cadmium oleate (and Cd_xOa_y complexes) in all solvents.

Desorption of cadmium oleate from the surfaces of the QDs is reversible; upon re-concentrating QD samples from $1 \mu M$ to $10 \mu M$, we observe that the vinyl signal broadens and shifts to its “bound” position and linewidth (see **Figure 2.13**).

We determine the ratio of free to bound oleate molecules for each sample in C_6D_6 and C_6D_{12} by integrating the vinyl signals in their respective NMR spectra and comparing these integrations to ferrocene, an internal standard, **Table 2.2**. We do not attempt this quantitative analysis for the samples in $CDCl_3$, where the integration is complicated by the overlapping signals from free and bound states in fast exchange.⁹⁴ **Table 2.2** shows that, in C_6D_6 and C_6D_{12} , diluting the $10 \mu M$ sample to $1 \mu M$ induces only minor changes the composition of the QD’s ligand shell, but further dilution to $0.1 \mu M$ induces desorption of $\sim 25\%$ of the oleate ligands in C_6D_6 , and $\sim 40\%$ of the oleate ligands in C_6D_{12} . There is no detectable precipitation or agglomeration of the QDs upon dilution.

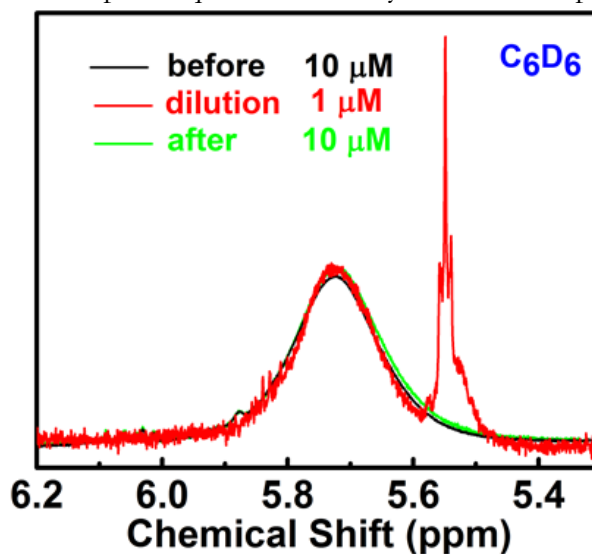


Figure 2.13. 1H NMR spectra of oleate-capped CdS QDs at $10 \mu M$ (black line), after dilution to $1 \mu M$ (red line) and after re-concentrating to $10 \mu M$ (green line).

Table 2.2. Number of Free and Bound Oleates within Samples of Oleate-Coated CdS QDs.

| Concentration of CdS-OA QD Sample | Solvent | Bound oleate ^a | Free oleate ^{a,b} |
|-----------------------------------|--------------------------------|---------------------------|----------------------------|
| 10 μM | C ₆ D ₆ | 210 \pm 30 | 0 |
| 1 μM | C ₆ D ₆ | 201 \pm 30 | 12 \pm 8 |
| 0.1 μM | C ₆ D ₆ | 150 \pm 30 | 64 \pm 10 |
| 10 μM | C ₆ D ₁₂ | 210 \pm 20 | 0 |
| 1 μM | C ₆ D ₁₂ | 204 \pm 40 | 6 \pm 4 |
| 0.1 μM | C ₆ D ₁₂ | 125 \pm 30 | 94 \pm 20 |

^a The error bars are derived from five measurements on separately prepared samples from the same batch of QDs ; ^b “Free” oleate is in the form of freely diffusing cadmium oleate (Cd(oleate)₂) molecules and Cd_xOA_y complexes.

2.3.3. The Photophysical Effects of Dilution. The ground state absorption spectra of 0.1 - 1 μM CdS QDs (the concentration range usable for PL measurements) in C₆D₆, C₆D₁₂ and CDCl₃ include a first excitonic peak at 420 nm (**Figure 2.14**), which corresponds to a radius of 2.0 nm. We also observe two distinct higher-energy excitonic peaks. We do not observe any hypsochromic shift due, for example, to surface etching of the QDs upon dilution in any of the solvents we studied. Dilution does not affect the solubility of the QDs, so the intensity of the absorption peak scales linearly with concentration of the sample.

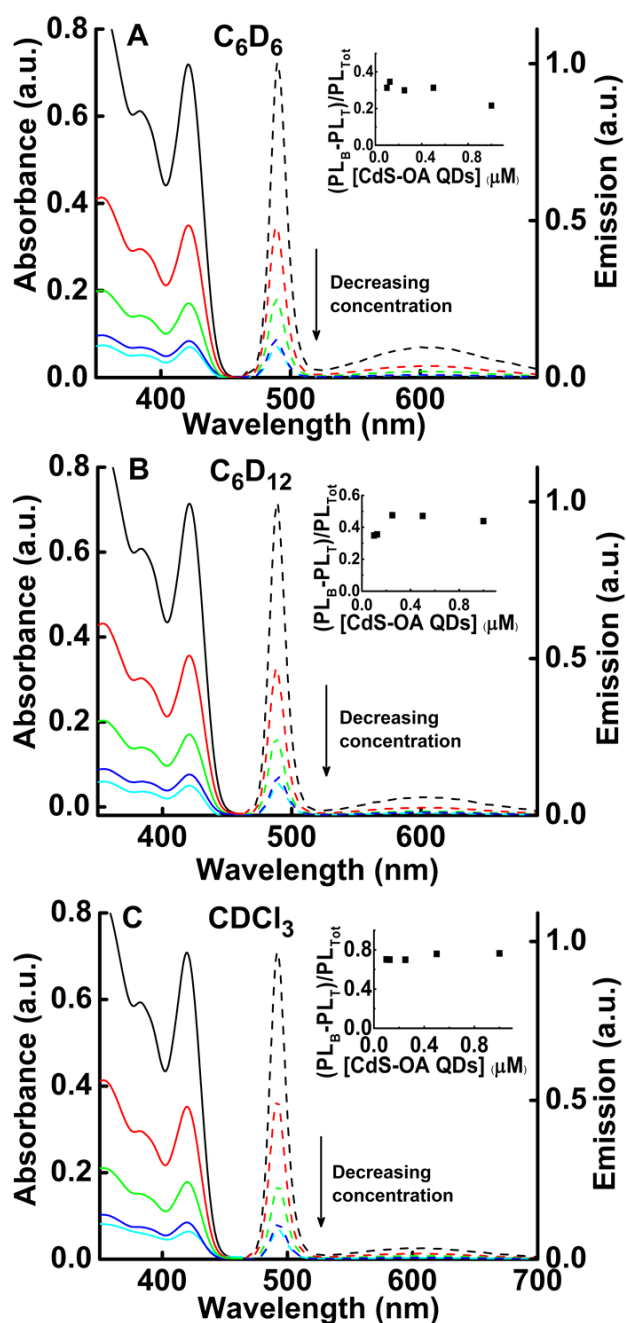


Figure 2.14. Ground state absorption (solid, left axis) and emission (dashed, right axis) spectra for oleate-capped CdS QDs in (A) C_6D_6 , (B) C_6D_{12} and (C) $CDCl_3$. The sample concentrations are 1 μM (black), 0.5 μM (red), 0.25 μM (green), 0.125 μM (blue), and 0.1 μM (cyan). **Insets:** plots of the difference between the integrated band-edge PL (centered at 490 nm) and the integrated “trap emission”, centered at 605 nm (scaled by the total PL intensity), vs. the concentration of the sample.

The PL spectrum of the QDs peaks at 435 nm due to emission from the band-edge exciton, and

also contains a second, broader peak at 605 nm due to emission from recombination of an excitonic electron with a trapped hole (we refer to this PL as “trap emission”).¹² The energies of these emission features are constant with solvent and concentration (**Figure 2.14**). The relative PL quantum yield (defined as the integrated intensity of the total PL spectrum of the sample scaled by the absorbance at the excitation wavelength, 390 nm) does not change with dilution of the samples from 1 μM to 0.1 μM . Furthermore, there is only a very minor (apparently random) dependence of the ratio of the intensities of band-edge emission (PL_B) to trap emission (PL_T) upon dilution for any of the three solvents. In the insets to **Figure 2.14**, we plot the difference between PL_B and PL_T , scaled by the total emission intensity, for each solvent; this quantity displays no trend with increasing concentration of the sample. We therefore conclude that desorption of 25% – 40% of the oleate ligands, which is what occurs upon dilution of the QDs from 1 μM to 0.1 μM (according to **Table 2.2**), neither increases nor decreases the yield of trapping of excitonic electrons or holes, relative to the yield of radiative recombination. This result implies that the cadmium oleate molecules and complexes that desorb are not involved in electronic passivation of either cadmium or sulfur on the QD surface.

Importantly, since (i) the composition of the ligand shell of the QDs is very similar at 10 μM and 1 μM (**Table 2.2**), and (ii) ligand desorption upon dilution from 1 μM to 0.1 μM does not affect the photophysical properties of the QDs (at least those related to the PL, **Figure 2.14**), we conclude that, at least for oleate-capped CdS QDs, the set of radiative and non-radiative exciton decay pathways reflected in the PL spectra acquired on low-concentration samples will be the same set of pathways utilized (with the same probabilities) by the exciton within QD samples at higher concentrations (10 μM QDs or 1 - 10 mM ligands), where NMR is more practical.^{12,72,116,121}

We note that the ratio of band edge emission to trap emission is larger for QDs in CDCl_3 than for QDs in C_6D_6 or C_6D_{12} ; given that the surface coverage of cadmium oleate does not appear to affect this ratio, this trend is probably due to passivation of the surface by CDCl_3 .¹²²

2.3.4. The Effects of Dilution on the Permeability of the Ligand Shell to a Small Molecule.

Finally, we monitored the PL spectra of the QDs in the concentration range of 0.1-1 μM with and without the addition of *p*-benzoquinone (BQ), a known photo-oxidant of cadmium chalcogenide QDs, in CDCl_3 (Figure 2.15A). We know, from extensive previous work on QD-BQ, QD-viologen, and QD-aminoferrocene systems,^{96,116,123} that the yield of photoinduced electron transfer from the QD to a small molecule – whether adsorbed statically or transiently on the QD surface – is directly related to the density and permeability of the ligand shell of the QD to the molecule.

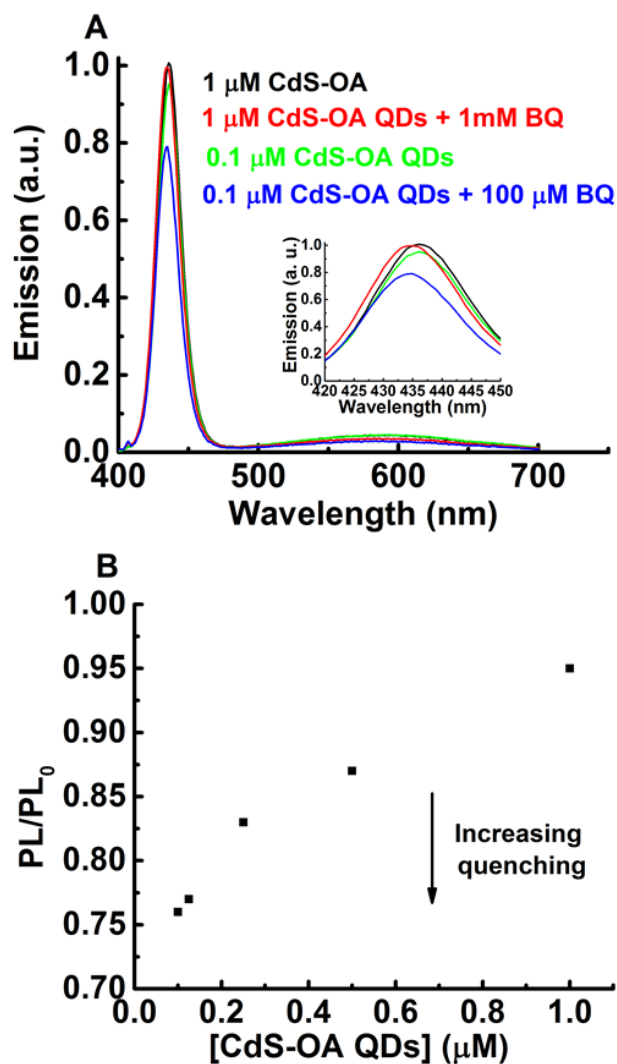


Figure 2.15. **A)** Photoluminescence (PL) spectra of oleate-capped CdS QDs in CDCl_3 with and without 1000 equivalents of *p*-benzoquinone (BQ) added. The PL spectra are scaled in intensity by their absorbance at the excitation wavelength, 390 nm, and plotted relative to the intensity of the band-edge emission peak of the 1 μM CdS QD sample with no added BQ (black curve). *Inset:* A magnified version of the band-edge PL peak of A, which shifts to higher energy upon addition of BQ due to mild etching of the QD surface. **B)** Plot of PL/PL_0 , the fraction of QDs that are still emissive after addition of 1000 equivalents of BQ, vs. the absolute concentration of QDs.

Figure 2.15B shows explicitly that, for a given molar ratio of QDs to BQ (here, 1:1000), there is more pronounced quenching of the QDs' PL as the absolute concentration of the QDs decreases (**Figure 2.15B**). There exists, therefore, a direct correlation between quenching efficiency of a small-molecule redox partner and the absolute concentration of the QDs *via* the permeability of their protective ligand layers. We have also observed this correlation in the case of CdS QD-viologen complexes,⁹⁶ but did not directly measure ligand coverage as a function of concentration in that study.

2.3.5. Conclusions. Upon dilution of oleate-capped CdS QDs from NMR-relevant concentrations (10 μM) to photoluminescence-relevant concentrations (0.1 μM), oleate ligands, in the form of cadmium oleate and Cd_xOA_y clusters, desorb. Changes in the ligand coverage by 30% - 40% do not impact the solubility, extinction coefficient, absorption or PL linewidths, relative partitioning between band-edge and "trapped" exciton emission, or total PL quantum yield. Desorption of surface ligands as a result of dilution of the QDs does, however, make the QDs more redox-active with respect to small molecule charge-transfer partners, because less dense organic adlayers allow a greater number of molecular quenchers to permeate the ligand shell and achieve charge transfer-active adsorption geometries on the QD surface.

This study shows that, for systems like oleate-capped CdS QDs, which have weakly-bound "z-type" neutral ligands, one can dilute samples without changing the pathways available for excitonic decay, and therefore can correlate PL data acquired at low sample concentrations with NMR data acquired at high concentrations. When a molecular quencher is present, however, the absolute concentration of the sample determines the vulnerability of the QDs to adsorption of the quencher and subsequent photo-oxidation or -reduction. We suspect that the weakly bound cadmium oleate molecules and clusters that survive the purification process, but desorb upon dilution, are part of a disordered, polymeric network of excess cadmium ions and charge-balancing oleate ligands that bridge

them on the surface of the QD, similar to the cadmium phosphonate network that results in high degrees of cadmium enrichment for CdSe QDs synthesized with reagent-grade trioctylphosphine oxide as the coordinating solvent.^{13,124} Examples of systems where photophysical properties will probably be more sensitive to the absolute concentration of the QDs are (i) QDs dispersed in water or other very polar solvents, where a charged ligand could desorb without the accompanying metal cation, (ii) chalcogenide-terminated QDs, where weakly bound surface chalcogenides serve as hole traps when adsorbed to the QD and leave under-passivated metal ions to serve as electron traps upon desorption, or (iii) QDs with more stoichiometric ratios of metal to chalcogenide, where ligands are typically neutral and datively bound (e.g., amines), and therefore easily desorb to leave under-passivated metal ions.

2.3.6. Experimental Methods. All chemicals were used as-received from Sigma-Aldrich, VWR or Alfa Aesar. Deuterated solvents (99.96% C₆D₆, 99.6% C₆D₁₂, and 99.96% CDCl₃) were used for all absorbance, NMR, FTIR, and photoluminescence experiments.

Synthesis and Purification of Oleate-Capped CdS Quantum Dots (QDs). To synthesize CdS QDs with $R = 2.0$ nm, we used a procedure modified from Peterson, *et al.*¹² We combined 90% technical grade octadecene (14.0 ml, 43.88 mmol), 90% technical grade oleic acid (4.4 ml, 13.9 mmol) and 99.99% cadmium oxide (0.360 g, 2.80 mmol) in a clean, dry three-neck flask. We cycled the mixture two times between heating at 120 °C under nitrogen flow and drying under vacuum at 100 °C to remove water from the system and avoid extensive water bumping while heating to higher temperatures, and then heated the mixture to 260 °C until a clear solution formed. We prepared our sulfur precursor by dissolving elemental sulfur in octadecene at 120 °C, and injected this solution into the cadmium precursor mixture. The QDs were grown for three minutes at 250 °C.

To purify the samples, we (i) added a 1:1 (v:v) mixture of methanol and chloroform to the QDs and centrifuged the mixture at 3500 rpm for 5 minutes, (ii) decanted the top layer, which contained the QDs, and discarded the bottom layer, and (iii) precipitated the QDs with acetone, centrifuged, and redispersed in chloroform. Three cycles of precipitation with acetone, centrifugation, and redispersion were performed to ensure that all excess unbound ligands were removed. The final purified QD pellet was redispersed in hexane. Prior to each experiment, we dried the QDs completely using a rotary evaporator, and then redispersed them in the deuterated solvent of interest.

Synthesis and Purification of Cadmium Oleate (Cd-OA). cadmium oleate was prepared according to a previously published procedure.¹¹³ Cadmium oxide (0.207 g, 8.07 mmol) was added to oleic acid (2.04 ml, 32.2 mmol) in a three-neck flask. This mixture was evacuated twice at 100 °C, and then heated to 190 °C under N₂ until the solution turned clear. We cooled the resulting solution to room temperature, and washed the product three times with acetone to remove unreacted oleic acid. It is very difficult to achieve complete purity for Cd(oleate)₂, as it decomposes rapidly into CdO and free oleic acid.^{113,120} We estimate, from FTIR spectroscopy in C₆D₆ (see **Figure 2.13**), that the amount of oleic acid impurity in cadmium oleate samples is 20 – 40%. We denote the as-synthesized product “Cd-OA”.

Nuclear Magnetic Resonance (NMR) Measurements. We obtained ¹H NMR spectra for all samples using an Agilent DD2 600 MHz spectrometer and glass NMR tubes from Wilmad. We varied the concentration of QDs from 10 nM to 10 μM, and varied the concentrations of Cd-OA and free oleic acid control samples from 0.2 to 2 mM. We increased the number of NMR scans from 32 for higher concentration samples to 1024 for lower concentration samples. We cleaned the NMR tubes prior to analysis by soaking them in aqua regia overnight to remove trace organic and metal impurities, followed by triple-rinsing with water, isopropanol, acetone, and finally chloroform. We used a

ferrocene integration standard, and the solvent peaks for cyclohexane, benzene, and chloroform as ppm standards.

Fourier Transform Infrared (FTIR) Spectroscopy. We collected FTIR spectra with a Thermo Nicolet Nexus 870 spectrophotometer in transmission mode, using a resolution of 2 cm^{-1} for the cadmium oleate and oleic acid samples, and 8 cm^{-1} for our experiment with $1\text{ }\mu\text{M}$ QDs, because the higher resolution scans introduced a high level of noise. The IR cell comprised two $38.5\text{ mm} \times 19.5\text{ mm} \times 4\text{ mm}$ KCl plates with a mercury amalgam spacer, and was cleaned with chloroform before use.

Ground State Absorption Measurements. We performed UV-visible-NIR ground state absorption experiments with samples in a 1-cm path length quartz cuvette using a Varian Cary 5000 spectrometer. We baselined our spectra with the corresponding neat solvents.

Photoluminescence (PL) Measurements. We collected PL spectra with samples in a 1-cm path length quartz cuvette on a Fluorolog-3 spectrofluorometer, using a front-face geometry configuration, with excitation and emission slit widths of 5 nm. We carried out the QD quenching experiments with added *p*-benzoquinone in CDCl_3 .

2.4 Summary of Methods for Quantitative Characterization of QD Surface Chemistry.

The Weiss group utilizes a number of different NMR techniques to characterize the surface chemistry of QDs. We describe these methods below.

2.4.1. Direct measurement of spectrally resolved signals due to bound and free species. Species bound to the QD surface with sufficient length, lability, and degrees of rotational freedom may be observed directly as broadened signals in the NMR spectrum. Depending upon the chemical nature of the ligand and the solvent, the signal due to the bound species may or may not be spectrally resolved from that of the free, unbound species. Direct integration of spectrally resolved bound and free ligand NMR signals is the simplest and most straightforward method of characterizing the chemistry of the

QD surface. The Weiss group has utilized this method to quantify the amount of perfluorodecanethiol (PFDT) bound to PbS QDs in d_6 -benzene. Using ^{19}F NMR, Weinberg *et al.* examined the signal from the terminal $-\text{CF}_3$ group and integrated the broad and sharp signals (corresponding to bound plus free PFDT) centered at -81.3 ppm. They compared this integral to that of the broad signal alone to obtain the fraction of PFDT that is bound, and multiplied this fraction by the number of equivalents of PFDT added to determine the number of bound PFDT ligands per QD.¹²⁵

2.4.2. Measurement of bound species using signal subtraction. Some species bound to QDs, such as aromatic thiols, are short and rigid, and bind so strongly to the surface of the QD, that their signals become broadened into the baseline of the NMR spectrum. In the case of these short, rigid ligands, the number of bound species can be calculated by comparing the signal from ligands and QDs to the signal of ligands alone, and subtracting the difference. Amin *et al.* and Aruda *et al.* both used this method to calculate the number of substituted thiophenols on CdSe QDs. Amin *et al.* calculated the number of 4-methylthiophenols ($\text{CH}_3\text{-TP}$) bound per QD by subtracting the number of free $\text{CH}_3\text{-TP}$ per QD within the mixture from the number of $\text{CH}_3\text{-TP}$ per QD that was added, as determined from the signals at 7.08 and 7.20 ppm within a spectrum of a QD-free standard sample.¹²⁶ Aruda *et al.* used this same method for a variety of para-substituted thiophenols.¹²⁷

Lian *et al.* also used a signal subtraction method to determine the number of 4-phenothiazin-10-yl-dithiocarbamate (PTC-PTZ) ligands bound to CdS QDs. They compared the aromatic proton intensity of the same amount of added PTC-PTZ with and without QDs. They accounted for the fact that, in the absence of QDs, PTC-PTZ degrades exclusively to its aniline derivative, but in the presence of QDs, unbound PTC-PTZ also forms phenothiazine-phenyl-thiourea (PTZ-Ph-TU). These degradation products do not bind, or bind only weakly, to the QD and do not displace bound PTC-PTZ.¹²⁸ All of the aromatic signals in mixtures of PTC-PTZ with QDs correspond to freely diffusing

or weakly binding degradation products of PTC-PTZ; the signals from bound PTC-PTZ are not detectable. They then calculated the number of bound PTC-PTZ per QD, λ , using **eq 2.3**:

$$\lambda = \frac{18}{a} \times \frac{(I_A - I_B) \times M_{IS}}{I_{IS} \times M_{QD}} \quad (2.3)$$

where I_A and I_B are the integrated ^1H NMR intensities of all of the aromatic proton signals in a sample of PTC-PTZ alone and in a mixture of PTC-PTZ with QDs, respectively. I_{IS} is the intensity of the signal from an internal standard hexamethylcyclotrisiloxane. M_{QD} and M_{IS} are the number of moles of QDs and the number of moles of internal standard, respectively, in the sample. The prefactor “18/a” accounts for the fact that the internal standard molecule has 18 protons, and the number of aromatic protons in the integrated region is a.¹²⁹

2.4.3. Measurement of displaced native ligands to determine the number of bound species.

Another method of determining the surface coverages of ligands that are too broad to see directly by NMR is to utilize the signal from displaced native ligand as a proxy for the number of bound ligands. Since the NMR signals of free species are sharp, and sometimes at a different chemical shift from those of bound species, this method is an indirect, but useful way to determine the number of bound ligands, particularly in cases where these ligands degrade when not bound to the QD surface. The most common ligand to be displaced is oleic acid (OA, oleate), usually in the form of cadmium or lead complexes, $M(\text{OA})_2$ or $M_x\text{OA}_y$. Oleate has a very convenient NMR signal that arises from its two vinyl protons between 5-6 ppm, which is well-separated from competing aromatic or aliphatic proton signals. In benzene and toluene, bound and free oleate are well-resolved enough to be integrated separately.^{71,111} Weinberg *et al.* corroborated their results from direct integration of the ^{19}F NMR signal by observing the amount of native oleate displaced by PFDT, where each bound PFDT molecule displaced an average of two oleate molecules in the complexed form described above.¹²⁵

Lian *et al.* also used the signal from displaced oleate to determine the quantity of bound ligands covalently attached to the hole acceptor phenothiazine. To estimate the number of bound PTC-PTZ per QD using displaced oleate, they integrated the NMR signals of freely diffusing oleic acid (OA) ($\delta = 5.5$ ppm, sharp) as well as the signals from bound oleate ($\delta = 5.7$ ppm, broad). The increase in free OA and the decrease in bound OA signal indicates that addition of PTC-PTZ displaces oleate ligands from the QD surface. Using the ratio of one PTC-PTZ bound per two oleates displaced, they were able to estimate the number of bound PTC-PTZs per QD.¹²⁹

Finally, Harris *et al.* used displaced oleate to determine the number of bound 4-hexylphenyldithiocarbamate molecules bound to CdS QDs, which is described in detail in Chapter 3 of this dissertation.¹²⁸

3 ROLE OF INTERLIGAND COUPLING IN DETERMINING THE INTERFACIAL ELECTRONIC STRUCTURE OF CDS QUANTUM DOTS

Adapted from: Harris, R.D.; Amin, V.A.; Lau, B.; Weiss, E.A. Role of Interligand Coupling in Determining the Interfacial Electronic Structure of Colloidal CdS Quantum Dots, *ACS Nano*, **2016**, *10* (1), 1395-1403.

3.1 Chapter Summary

Displacement of cadmium oleate ($\text{Cd}(\text{oleate})_2$) ligands for the exciton-delocalizing ligand 4-hexylphenyldithiocarbamate (C6-PTC) on the surfaces of CdS quantum dots (QDs) causes a decrease in the band gap (E_g) of the QD of ~ 100 meV for QDs with a radius of 1.9 nm and ~ 50 meV for QDs with a radius of 2.5 nm. The primary mechanism of this decrease in bandgap, deduced in previous work, is a decrease in the confinement barrier for the excitonic hole. The increase in apparent excitonic radius of the QD that corresponds to this decrease in E_g is denoted ΔR . The dependence of ΔR on the surface coverage of C6-PTC, measured by ^1H nuclear magnetic resonance (NMR) spectroscopy, appears to be non-linear. Calculations of the excitonic energy of a CdS QD upon displacement of native insulating ligands with exciton delocalizing ligands using a 3D spherical potential well model show that this response includes the contributions to ΔR from both isolated, bound C6-PTC ligands and from groups of adjacent C6-PTC ligands. Fits to the experimental plots of ΔR vs. surface coverage

of C6-PTC with a statistical model that includes the probability of formation of clusters of bound C6-PTC on the QD surface allow for the extraction of the height of the confinement barrier presented by a single, isolated C6-PTC molecule to the excitonic hole. This barrier height is less than 0.6 eV for QDs with a radius of 1.9 nm and between 0.6 and 1.2 eV for QDs with a radius of 2.5 nm.

3.2 Introduction

There exist several examples of photophysical processes in colloidal semiconductor nanocrystals (quantum dots, QDs) that depend not only on the chemical structures and geometries of their surface ligands, molecular adsorbents, or surface states, but also on the surface coverage of these species. For instance, the probability of electron or hole transfer from the excitonic state of a QD to a proximate molecular acceptor or surface trap depends linearly on the surface density of thermodynamically accessible acceptors or traps.¹³⁰⁻¹³³ Given recent advances in the precise preparation¹³⁴⁻¹³⁵ and quantitative characterization^{71,111} of the surface chemistry of QDs, it is now reasonable to synthetically or post-synthetically tune this surface density and therefore chemically control the optical and electronic properties of QDs. Here, we introduce a new synthetic “knob” by which we can exert this chemical control by demonstrating the dependence of the optical bandgap of a CdS QD on both the surface coverage and *spatial distribution* of an exciton-delocalizing ligand, 4-hexylphenyldithiocarbamate (C6-PTC), **Figure 3.1A**. Ligand “patchiness” on the surface of nanoparticles has been useful for self-assembly and targeted drug delivery;¹³⁶⁻¹³⁸ this study, however, is the first to examine the effect of the degree of adjacency of functional ligands on the electronic spectra of nanoparticles.

Dithiocarbamates, upon binding to the surfaces of cation-enriched metal chalcogenide QDs, cause a large bathochromic shift in the first excitonic absorption of the QDs (up to 1 eV for phenyldithiocarbamate on very small CdS QDs)⁵⁵ while enhancing the oscillator strength of this transition,¹³⁹ and preserving the linewidth of the absorption and photoluminescence peaks.²⁶ We have

presented evidence, in previous publications,^{26,52,55} that this decrease in the optical bandgap is due primarily to stabilization of the first excitonic state through adiabatic delocalization of the excitonic hole into resonant or near-resonant interfacial states of mixed QD-ligand character that form in the ground state of the QD-dithiocarbamate complex. This mechanism is supported by high-level density functional theory calculations performed by a separate group.¹⁴⁰ The primary motivation for discovering (and, ultimately, predicting the structures of) organic ligands like dithiocarbamates that couple electronically to the QD core is that dissociation of excitons at the interfaces of QDs with surrounding redox centers (*e.g.*, other QDs, electrodes, or organic molecules) is typically an efficiency-limiting step in photovoltaic, photocatalytic, and optical sensing systems based on QDs, especially when the carrier being extracted is the hole, which, in cadmium chalcogenides, is the “heavier” (in terms of effective mass), more localized carrier.¹⁴¹⁻¹⁴² The native ligands that serve as an effective surfactant in the synthesis of high-quality colloidal QDs are highly electronically insulating and therefore further inhibit exciton dissociation. Post-synthetic displacement of these native ligands with delocalizing ligands using simple ligand exchange procedures provides a mechanism for charge carrier or exciton extraction from the QD, without sacrificing the narrow linewidth and high oscillator strength of excitonic transitions associated with quantum confinement, or the chemical and electronic passivation afforded by organic adlayers.¹⁴³⁻¹⁴⁷

In this work, we use ¹H nuclear magnetic resonance (NMR) spectroscopy to determine the surface coverage of the delocalizing ligand C6-PTC on CdS QDs and correlate this surface coverage with the average exciton delocalization radius for QDs within the ensemble (a parameter we denote “ ΔR ”). We find – in some experimental data and in simulations of this data using a three-dimensional, multi-step particle-in-a-sphere potential – a nonlinear response of ΔR to surface coverage of C6-PTC that, according to the simulations, corresponds to a cooperative effect among adjacent delocalizing ligands.

We propose a statistical model to fit the simulated and experimental data that allows us to deconvolute the contributions of isolated C6-PTC molecules from the contributions of clusters of C6-PTC molecules, and to extract the magnitude of the tunneling barrier presented by each isolated C6-PTC molecule to the excitonic hole, a fundamental property of the interfacial electronic structure.

In separate work, we measured and modeled the response of ΔR of CdSe QDs to the surface coverage of another class of delocalizing ligand, thiophenolates.¹²⁶⁻¹²⁷ The interesting non-linear response of ΔR to surface coverage and the influence of ligand adjacency that we observe here is not, however, apparent in that system because (i) thiolates have a smaller density of sulfur states into which the hole delocalizes than do dithiocarbamates, and (ii) for reasons detailed in our previous work,¹²⁶⁻¹²⁷ the achievable surface coverages of thiophenolates on CdSe QDs are smaller than the achievable surface coverages of phenyldithiocarbamates on CdS QDs. We therefore achieve a smaller degree of delocalization in the CdSe-thiolate system than in the CdS-dithiocarbamate system, and never access the non-linear regime of ΔR vs. surface coverage.

3.3 Results and Discussion

3.3.1 Quantification of Exciton Delocalization and the Surface Coverage of C6-PTC on CdS

QDs. We treated the QDs with the ammonium salt of C6-PTC in benzene, **Figure 3.1A**, and monitored the position of the QDs' first excitonic peak by ground state absorption spectroscopy. We used C6-PTC, rather than unsubstituted PTC (which we have used previously)^{26,52,55} because (i) it is soluble in benzene, and (ii) the hexyl chain provides enough of a steric barrier to prevent aggregation of the CdS QDs after exchange, so we can achieve higher coverages of C6-PTC than other derivatives of PTC while keeping the QDs dispersed. In order to determine the apparent change in excitonic radius, ΔR , upon adsorption of C6-PTC for each QD/C6-PTC mixture, we converted the position of the first excitonic peak of the QDs from λ_{abs} to excitonic radius R using experimentally derived

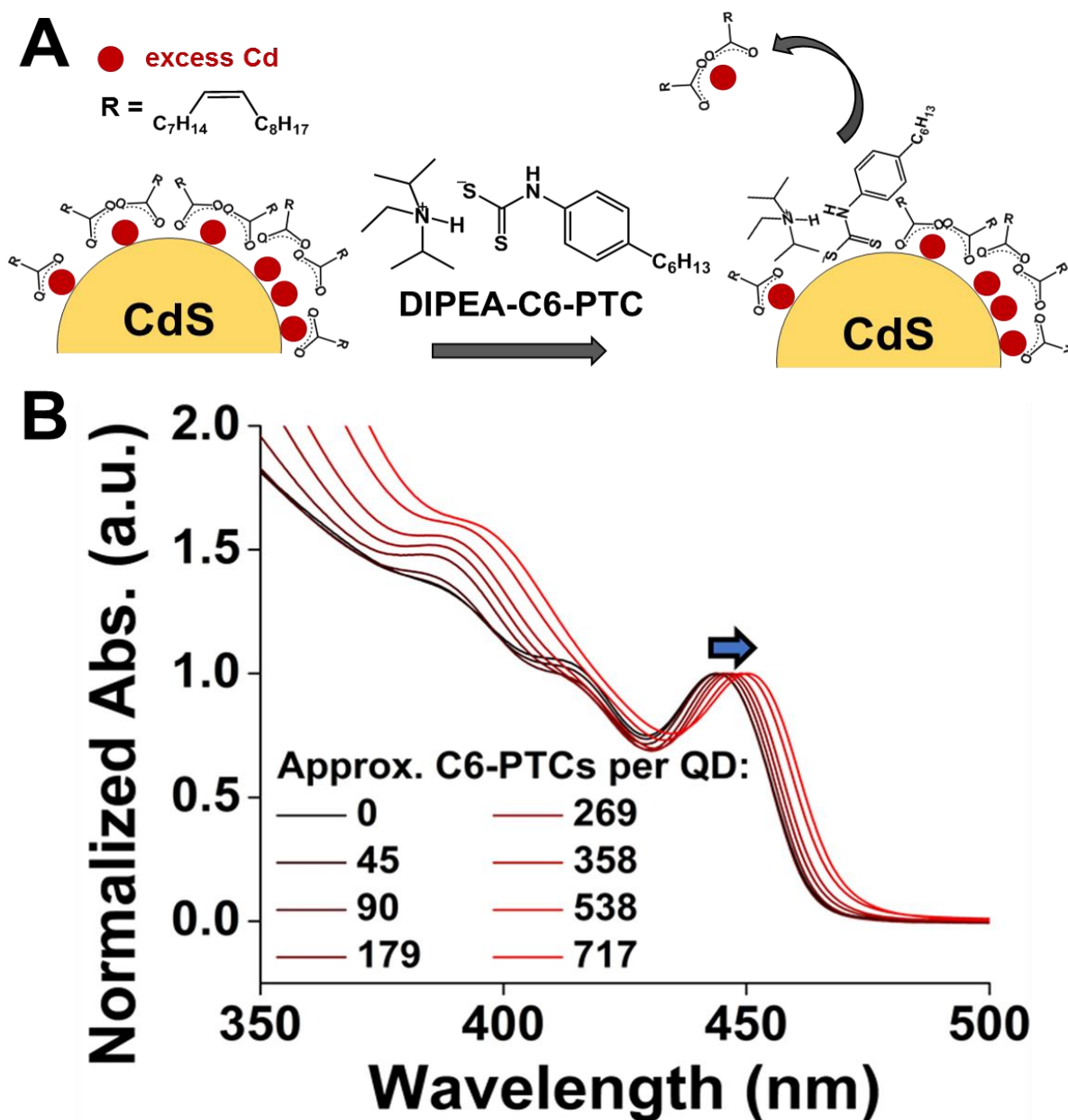


Figure 3.1. A) Schematic of the ligand exchange process, where each C6-PTC, added as either the DIPEA salt (shown) or the TEA salt (not shown), displaces, on average, one cadmium oleate complex (two oleate ligands) in order to bind to the core of the QD. The text explains how we determine the stoichiometry of the ligand exchange. **B)** Ground state absorption spectra of CdS QDs ($R = 2.5$ nm) treated with increasing (black to red) molar equivalents of C6-PTC (0 – 717); the spectra are normalized to the height of the lowest-energy excitonic peak. We use the magnitude of the bathochromic shift of this peak and experimentally determined calibration curves of the size of the QD core vs. its bandgap to calculate the parameter ΔR , the apparent increase in excitonic radius upon ligand exchange, at each surface coverage of C6-PTC.

calibration curves from Yu *et al.*⁴ During the ligand exchange, the physical size of the QD core remains constant (see the Supporting Information), so the change in λ_{abs} reflects a change in the apparent size of the exciton. **Figure 3.1B** shows the ground state absorption spectra for a series of samples of CdS QDs, with physical radius $R = 2.5$ nm, treated with increasing amounts of C6-PTC. The first excitonic absorption peak shifts to lower energy (*i.e.*, ΔR increases) as more C6-PTC is added.

The direct quantification of QD-bound C6-PTC is challenging in part because the aromatic signals from C6-PTCs are broadened sufficiently to be indistinguishable from the baseline noise when the ligand is bound to a QD.^{71,74,111,148} This degree of broadening is attributable to the rigidity of the phenyl ring portion of the molecule and its close proximity to the QD surface, the irreversible nature of its binding to the QD surface (in contrast to weakly binding anilines), and the large rotational correlation times of nanoparticles (and molecules bound to them) in solution.^{71,73,149-152} Over the course of the ligand exchange, unbound C6-PTC degrades quantitatively into products that we detail below; we therefore cannot calculate the number of bound C6-PTC by subtracting the number of NMR-observable unbound C6-PTC from the number of added C6-PTC, as we have done previously with thiophenols.¹²⁶⁻¹²⁷ Our use of CdS QDs, which are commonly synthesized with an oleate capping layer, instead of CdSe QDs, which are most commonly synthesized with an alkylphosphonate layer,¹⁵³ is motivated by the fact that oleate ligands retain some rotational motion even when adsorbed to the surface of the QD, and have a spectrally isolated signal from vinyl protons.^{150,154-157} We can therefore observe and quantify signal from both free and bound forms of oleate in mixtures with QDs, and, once we know the stoichiometry of the ligand exchange, use it to infer the surface coverage of C6-PTC. This procedure would be exceedingly difficult with an alkylphosphonate layer due to the overlap of its aliphatic signals with those from C6-PTC, and is only possible for the CdSe QD-thiophenolate

system mentioned above¹²⁶ because we can quantify the coverage of thiophenolate directly from its NMR signals.

Figure 3.2A shows the vinyl region of the ¹H NMR spectra of several samples of oleate-coated CdS QDs (R = 2.5 nm, in d6-benzene) treated with increasing amounts of added C6-PTC. The Supporting Information contains the same set of spectra for the QDs with R = 1.9 nm. These spectra include well-resolved signals corresponding to free oleate ($\delta \sim 5.50$ ppm, narrow) and bound oleate ($\delta = 5.60$ - 5.82 ppm, broad). In **Figure 3.2A**, as the concentration of added C6-PTC increases, the signal for bound oleate decreases in intensity, and the signal for free oleate increases in intensity and sharpens. The change in chemical shift and linewidth of these peaks during the C6-PTC titration indicates that the oleate molecules are in dynamic exchange between free and bound states.¹⁵⁴ The signals are well-resolved enough, however, to use their respective integrals, relative to an internal ferrocene standard, to estimate the number of (mostly) free and (mostly) bound oleate in the sample, and therefore the number of oleate ligands displaced at each point in the C6-PTC titration.

¹H NMR spectra of samples of oleate-coated CdS QDs treated with C6-PTC also contain signals from 4-hexylaniline ($\delta = 6.38$ and 6.97 ppm, both doublets), 4-hexylphenylisothiocyanate ($\delta = 6.64$ ppm, quartet), and 4,4'-dihexyl-N,N'-diphenylthiourea ($\delta = 6.90$ and 7.10 ppm, both doublets), into which unbound C6-PTC degrades during the ligand exchange. Independent control experiments show that none of these degradation products itself produces a bathochromic shift in the absorption spectrum of CdS QDs, and that, once the C6-PTC is bound to the QD, it does not desorb or degrade to these molecules (see the Supporting Information, **Figures 3.7, 3.8**).

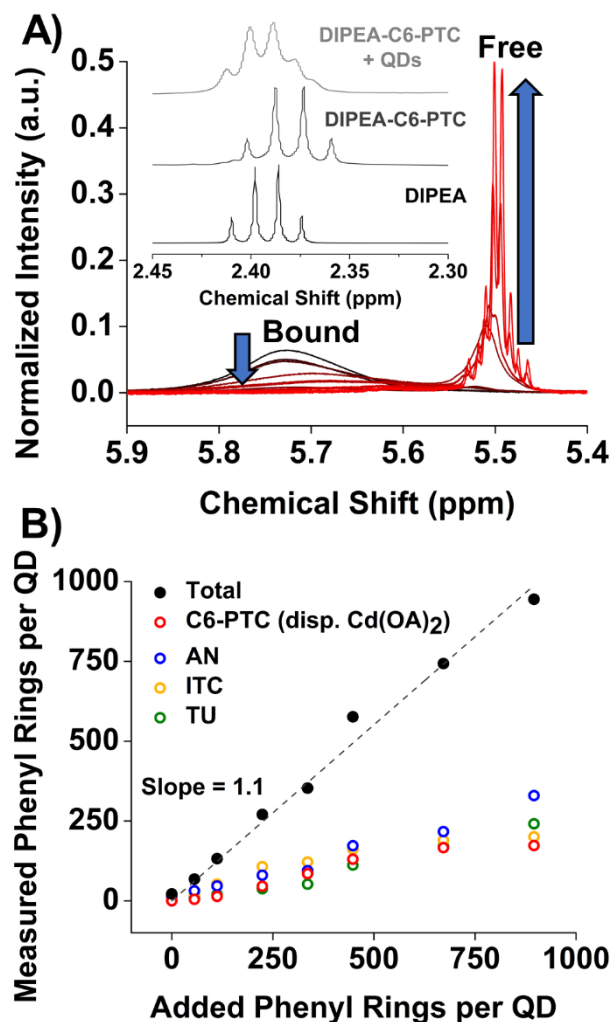


Figure 3.2. A) The vinyl proton region within ^1H NMR spectra of the oleate-coated CdS QDs ($R = 2.5$ nm) when treated with various concentrations of C6-PTC (increasing [C6-PTC] from black to red), in d_6 -benzene. The spectra are normalized to the height of a ferrocene internal standard (see Supporting Information for the full NMR spectra for these QDs and for the QDs with radii of 1.9 nm). *Inset:* NMR spectra of free DIPEA, DIPEA-C6-PTC, and CdS QDs with ~ 538 equivalents of DIPEA-C6-PTC. The peak shown is from the ethylene protons of the ethyl group. **B)** The number of C6-PTC molecules and its degradation products – 4-hexylaniline (AN), 4-hexylphenylisothiocyanate (ITC), and N,N' -bis(4-hexylphenyl)thiourea (TU) – in each sample of C6-PTC-treated CdS QDs ($R = 2.5$ nm), counted by NMR as described in the text. The total number of phenyl rings counted from the NMR spectrum at each added concentration of C6-PTC is shown in black and fit to a line with forced intercept at (0,0); the fit line has a slope of 1.1. This result shows that, when we assume that each C6-PTC displaces 2 oleate molecules, we account for all of the added C6-PTC molecules as either bound C6-PTC, or a freely diffusing degradation product. The Supporting Information contains this plot for the QDs with $R = 1.9$ nm, for which the fit line has a slope of 1.3, as well as for QDs with $R = 2.5$ nm treated with TEA-C6-PTC, for which the fit line has a slope of 1.

In order to infer the number of bound C6-PTC ligands per QD from the number of displaced oleate molecules per QD, we need to know the stoichiometry of the ligand exchange. We plot in **Figure 3.2B** the number of each of C6-PTC's degradation products per QD – measured directly by integrating their respective NMR signals – for a series of samples with different concentrations of added C6-PTC. The Supporting Information contains the data used in the quantification of each species. We do not observe any free (unbound) C6-PTC at the time of analysis because, over the course of the ligand exchange (16-24 hours), unbound C6-PTC degrades quantitatively. We estimated the number of bound C6-PTC's per QD (red hollow symbols in **Figure 3.2B**) from the number of displaced oleate molecules using eq 3.1. In eq 3.1, I_{free} is the integrated free oleate

$$N_{bound} = \frac{(I_{free} - I_{free,0}) - I_{free,TU}}{2} \quad (3.1)$$

signal in the spectrum of the QDs treated with C6-PTC, $I_{free,0}$ is the integrated free oleate signal in the spectrum of QDs with no added C6-PTC, and $I_{free,TU}$ is the estimated number of oleates displaced by the thiourea degradation product, which we determine using a separate, direct titration of the QDs with thiourea (see the Supporting Information). The value of “2” in the denominator of eq 1 means that each C6-PTC and each TU displaces two oleates – presumably in the form of the neutral species, $Cd(oleate)_2$. When we make this assumption about the stoichiometry of the ligand exchange, the slope of the linear fit to the black diamond symbols, which represent the sums of the number of all degradation products per QD plus the number of bound C6-PTCs per QD, is 1.1 (with a fixed y-intercept of zero); this slope of ~ 1 means that we have accounted for every added C6-PTC molecule as either a degradation product or a displaced oleate. If instead we calculate the number of bound C6-PTC by assuming that each C6-PTC or TU displaces an average of 1 or 1.5 oleate molecules (and therefore use a denominator of either 1 or 1.5 in eq 1), the slopes of the fit-lines are 1.3 and 1.2,

respectively, indicating that we measure more molecules than we added. We therefore deduce that the stoichiometry of the ligand exchange is one bound C6-PTC to (at least) two displaced oleates, and we count the number of bound C6-PTC per QD using eq 1.

Displacement of a so-called “z-type” ligand (like Cd(oleate)₂) has been seen previously in treatment of carboxylate-terminated metal chalcogenide nanocrystals by Lewis bases.^{118,158-159} This mechanism for ligand exchange explains why (i) C6-PTC does not bind to CdSe or CdS QDs that are not cadmium enriched (see the Supporting Information of Frederick *et al.*⁵⁵), and (ii) the NMR signals of protons belonging to the ammonium counterions of C6-PTC broaden upon addition of QDs (**Figure 3.2A, inset** and the Supporting Information). This broadening indicates that adsorption of the ammonium counterions, along with the C6-PTC, to the QD surface upon displacement of a neutral Cd(oleate)₂ balances the charge in the ligand exchange.

3.3.2. The Response of ΔR to the Surface Coverage of C6-PTC Ligands. Figure 3.3A is a plot of ΔR versus the average number of bound C6-PTC molecules per QD, determined with eq 1, for two sizes of QD cores ($R = 1.9$ and 2.5 nm). All of the data for a given size of QDs were collected on a single synthetic batch. The plot for $R = 1.9$ nm appears to be non-linear, even when considering the uncertainty, which is dominated by the error in our measurement of the number of bound ligands per QD, as explained in the Supporting Information. The Supporting Information also contains a comparison of linear and quadratic fits to these plots, and associated R^2 values.

To aid in our interpretation of these plots, and to determine their quantum-mechanically predicted shape under ideal conditions, we modeled the dependence of ΔR on the number of bound C6-PTC ligands using a simple three-dimensional particle-in-a-spherical potential well model. We assume, in applying this model, that the dominant contribution to exciton delocalization by C6-PTC is a decrease in the confinement energy of the excitonic hole (as opposed to the electron), although the model itself

can be adapted to apply to either or both carriers. We have presented evidence for this hole-specific delocalization in a previous publication,⁵⁵ and this mechanism is supported by high-level DFT calculations.¹⁴⁰ To calculate ΔR at each surface coverage of C6-PTC, we compute the confinement energy of the excitonic hole (with its known effective mass within CdS) in a three-dimensional, core/shell/shell spherical potential well (**Figure 3.3B, inset**).

In the core of the spherical potential well, which represents the nanocrystalline core of the QD, the potential energy is set to 0 eV. In the outer shell, which represents the solvent and the insulating portions of the ligands, the potential energy is set to 3.6 eV, the difference in energy between the top of the CdS valence band and the HOMO of benzene, our solvent.¹⁶⁰ The inner shell represents the interfacial region between the QD core and the ligands; this region primarily determines the

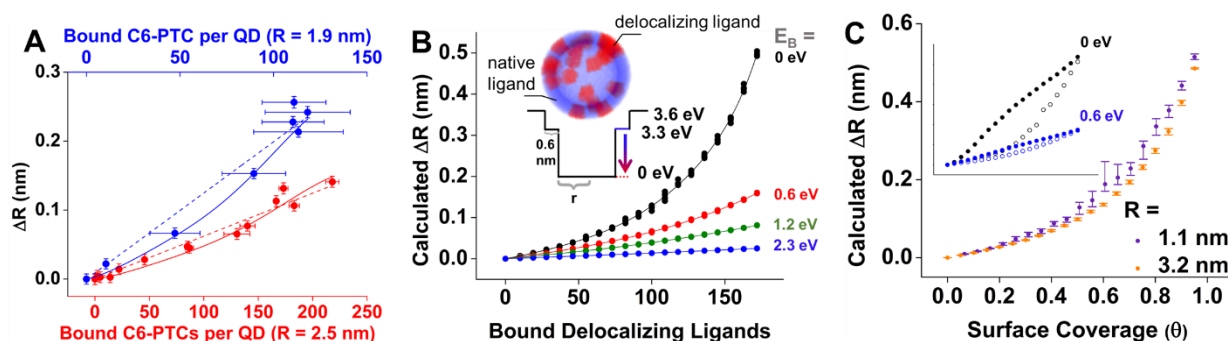


Figure 3.3. **A)** A plot of ΔR vs. the number of bound C6-PTCs (as measured by the number of displaced Cd(oleate)₂ ligands in the NMR spectra) on CdS QDs with $R = 1.9$ nm (blue) and $R = 2.5$ nm (red). The solid lines represent the simultaneous fits to eq 5 for each size, where N_{sites} is fixed at the maximum theoretical number of bound ligands, $\Delta r_k = C_k \Delta r_0$, and $C_k \geq 1$. The dashed lines are linear fits to the data with a forced intercept at (0,0). **B)** Simulated response of ΔR vs. number of bound C6-PTCs on CdS QDs with $R = 1.9$ nm, calculated using a 3D spherical potential well model (schematic shown in **inset**) where increased surface coverage of the delocalizing ligand corresponds to a lower average barrier height (which ranges from 0 to 2.3 eV) for the excitonic hole. **C)** Simulated response of ΔR to the surface coverage, θ , of delocalizing ligand for spheres with radii of 1.1 and 3.2 nm. We show the average (points) and range over five trials (error bars) for each size. **Inset:** Simulated response of ΔR to θ for a sphere with a radius of 1.1 nm, where the delocalizing ligands are either placed maximally far apart on the sphere's surface (hollow circles) or in a Janus particle-like configuration with maximal adjacency (solid circles), for barrier heights of 0 eV (black) and 0.6 eV (blue). From these plots, it is evident that a greater number of adjacent ligand interactions on the surface of the sphere results in a greater ΔR .

confinement energy of the excitonic charge carriers. We divide this region into equal radial volumes with a surface density of 4 nm^{-2} and a thickness in the radial direction of 0.6 nm, based on an estimate of the surface footprints and volume of the HOMO, respectively, of both the insulating native ligands (oleate) and the delocalizing ligands (C6-PTC).¹²⁶ We set the potential energy to 3.3 eV in each region occupied by a native oleate ligand, and to be between 0 and 2.3 eV in each region occupied by C6-PTC. These values represent the limits of large-mixing and zero-mixing, respectively, at the QD-ligand interface. The Supporting Information details the selection of appropriate solvent, native ligand, and delocalizing ligand potentials. We simulate the exchange of a single native ligand for a delocalizing ligand by decreasing the potential energy in a randomly chosen ligand volume appropriately. We repeat this process until 95% of the native ligand potentials have been set to the delocalizing ligand potential (we stop at 95% purely for computational convenience, see the Supporting Information), and record the exciton energy as a function of surface coverage during the course of the exchange. We then convert these energies to values of ΔR using the known relationship between the size and the energy of excitons in CdS QDs coated in insulating ligands (see the Supporting Information).⁴

Figure 3.3B is a plot of ΔR , calculated with this method, versus the number of bound delocalizing ligands with barrier heights between 0 and 2.3 eV, for a sphere with a 1.9-nm radius. The Supporting Information contains a similar plot for a sphere with radius 2.5 nm. The placement of C6-PTC ligands during the simulated exchange is random, so we plot three to five trials – each representing a spatial arrangement of ligands on the QD surface – for each surface coverage. Note that, as the barrier height presented by C6-PTC decreases, (i) the dependence of ΔR on the surface coverage of C6-PTC becomes more non-linear and (ii) the sensitivity of ΔR to the arrangement of C6-PTC ligands on the surface of the QD, as indicated by the trial-to-trial variation in the simulated curves, increases. These simulations also indicate that the apparent non-linear shape of the experimental plots in **Figure 3.3A**

is quantum mechanically predicted for small barrier heights. We note that, for $R = 1.9$ nm (which is the core size used to simulate the data in **Figure 3.3B**) the non-linearity is most apparent when plotting ΔR over the full range of surface coverages. Our inability to achieve a coverage of greater than ~ 110 C6-PTC ligands per QD (without particle precipitation) for this size of QD may account for the subtlety of the curvature in our experimental dataset. We explain the fits to the data in **Figure 3.3B** below.

3.3.3. The Contribution of Ligand Adjacency to Exciton Delocalization. To determine the physical origin of the response of ΔR to the surface coverage of a delocalizing ligand, we simulate the dependence of ΔR on the spatial arrangement of delocalizing ligands on the QD surface for a very small ($R = 1.1$ nm) and very large ($R = 3.2$ nm) QD core. **Figure 3.3C** shows the results of the simulation for these two radii and a barrier height presented by the delocalizing ligand of 0 eV. The calculated values of ΔR are plotted with respect to surface coverage (θ , the fractional number of bound delocalizing ligands relative to total surface sites) so that we can more easily compare the responses for different core radii. The points and error bars correspond to the average and the range of ΔR , respectively, for three to five trials of the simulation.

From **Figure 3.3C**, we see that: i) any trial-to-trial variation in ΔR for a given core radius that exists is greatest at moderate ($\theta = 0.4 - 0.8$) surface coverage, ii) the trial-to-trial variation in ΔR for a given value of θ increases as R decreases, and iii) at a given surface coverage, the average value of ΔR is always higher for smaller R . These trials differ only in the spatial distribution of delocalizing ligands, so these observations point to the degree of adjacency of delocalizing ligands as the source of variation in ΔR for a given surface coverage. At low surface coverages, delocalizing ligands are likely to have zero nearest neighbors, and at 95% surface coverage, virtually every ligand is surrounded by

nearest neighbors; therefore, at low and high surface coverages, trial-to-trial variation in ligand adjacency is low, as is trial-to-trial variation in ΔR . Most of the scatter in the simulated plots then occurs at intermediate surface coverages. The increased variation (and overall ΔR) for small spheres is due to the fact that the ligand footprint is held constant in the simulation, so each ligand takes up a greater fraction of the surface area, and changes in its adjacency result in larger variations in ΔR .

We then compare the response of ΔR to increasing surface coverage of delocalizing ligands for a simulation in which the number of nearest-neighbors for each delocalizing ligand is maximized (in a Janus particle-like configuration)¹³⁴ to that for a simulation in which the number of nearest-neighbors is minimized, **Figure 3.3C, inset**. These plots demonstrate explicitly that, at a given surface coverage, a greater number of adjacent ligands leads to a greater value of ΔR . Furthermore, the more constant the average adjacency is with increasing surface coverage, the more linear the response of ΔR (see the Supporting Information, **Figure 3.11**). For instance, in the simulations where we have enforced minimal adjacency (open symbols), at low surface coverages ($\theta < 0.2$), each bound delocalizing ligand has zero adjacent delocalizing ligands, and the relationship between ΔR and θ is approximately linear. In a simulation like this one where the excitonic energy depends only on the confinement energies of the carriers (and not the Coulomb potential), a linear dependence of ΔR on θ is predicted in the regime where each bound delocalizing ligand has zero adjacent delocalizing ligands, because adding a delocalizing ligand is equivalent to changing the effective size of the QD by a fraction of a monolayer (i.e., the delocalizing volume of each ligand can be spread over the entire surface of the QD). Once the ligands begin to bind next to each other and create “joint” potential wells, one can no longer consider the potential presented to the excitonic hole to be a simple linear average of the potentials of each isolated ligand. The average number of adjacent interactions increases rapidly with surface coverage at $\sim\theta = 0.5$, and so does ΔR , due to the formation of larger potential wells as ligands cluster.

The sensitivity of ΔR to the degree of adjacency decreases as the barrier height presented by the delocalizing ligand increases (compare the plot for a barrier height of 0 eV, black, to that for a barrier height of 0.6 eV, blue).

An interesting question is whether the dependence of ΔR on surface coverage is related to a transition from an anisotropic distribution of delocalized ligands at low coverage to a more isotropic distribution (monolayer coverage, or a “shell” of ligands) at higher coverage. The plots in **Figure 3.3C, inset**, also address this question. In the Supporting Information, we highlight a particular surface coverage on these plots, $\sim 30\%$, where maximizing the inter-ligand distance has resulted in a near-isotropic distribution of delocalizing ligands with zero adjacency, and where minimizing the inter-ligand distance has resulted in an anisotropic distribution with maximal adjacency. The value of ΔR is clearly larger for the larger-adjacency distribution, despite the fact that the zero-adjacency distribution is nearly completely isotropic. These data show that it is coupling between delocalizing ligands, and not how isotropic the delocalization is over the particle, that determines ΔR .

3.3.4. A Statistical Model for Estimating the Influence of Ligand Adjacency on Exciton Delocalization. The simulations have told us that we need to derive a model based on ligand adjacency in order to fit our experimental data in **Figure 3.3A**. We therefore classify ligands by their “adjacency number”, k . For example, a delocalizing ligand surrounded exclusively by native ligands has $k = 0$. A delocalizing ligand with two nearest-neighbor delocalizing ligands has $k = 2$. For each ligand in a hexagonally close packed system (which is what we assume here), $0 < k < 6$.

We then define ΔR at a particular number of bound delocalizing ligands per QD (N_{bound}) as a sum of contributions from ligands with $k = 0$, ligands with $k = 1$, ... ligands with $k = 6$, eq 3.2. In

$$\Delta R(N_{bound}) = \sum_{k=0}^6 [\Delta r_k * N_{bound} * P(k; 6, \theta)] \quad (3.2)$$

eq 2, Δr_0 is the value of ΔR per bound, isolated delocalizing ligand, Δr_1 is the ΔR per bound delocalizing ligand with one nearest neighbor, and so on, and $P(k; 6, \theta)$ is the probability that a bound delocalizing ligand will have k adjacent delocalizing ligands at a surface coverage of θ .

We use a binomial distribution function to define $P(k; 6, \theta)$; in doing so, we assume that the ligands are distributed randomly on the surface of the QD. A similar approach used a Poisson distribution to determine the probability of finding a neighboring peptide on the surface of a gold nanoparticle.¹⁶¹ We consider each of the six sites surrounding a bound delocalizing ligand to be a Bernoulli trial, where success means that another bound delocalizing ligand exists at that site, and the probability of success is equal to the fractional surface coverage of delocalizing ligands ($p = \theta$). Then, the probability that a particular bound ligand has k adjacent ligands $P(k; 6, \theta)$ is defined by eq 3.3, and the number of

$$P(k; 6, \theta) = \binom{6}{k} \theta^k (1 - \theta)^{6-k} \quad (3.3)$$

delocalizing ligands with a particular adjacency number, $N_{bound,k}$, is given by eq 3.4.

$$N_{bound,k} = N_{bound} * \binom{6}{k} \theta^k (1 - \theta)^{6-k} \quad (3.4)$$

Substituting eq 3 into eq 2 (and using the fact that $\theta = \frac{N_{bound}}{N_{sites}}$), we obtain eq 3.5 for the

$$\Delta R = \sum_{k=0}^6 \Delta r_k * N_{bound} * \binom{6}{k} \left(\frac{N_{bound}}{N_{sites}}\right)^k \left(1 - \frac{N_{bound}}{N_{sites}}\right)^{6-k} \quad (3.5)$$

observed value of the average delocalization radius ΔR , where $N_{sites} = 4 * 4\pi r^2$ because 4 ligands/nm² is the ligand density used in our simulation, based on the calculated ligand footprint of C6-PTC. Equation 5 describes ΔR as a function of N_{bound} , which we can measure, and fitting parameters Δr_k for $k = 0 - 6$.

To determine whether this functional form of ΔR reasonably reproduces the response of ΔR to surface coverage for these systems, we first fit the simulated plots of ΔR vs. N_{bound} for QDs with a series of core radii, and for barrier heights between 0 and 2.3 eV with eq 3.5 (**Figure 3.3B** and the Supporting Information). We constrain these fits by fixing the value of Δr_0 to the value we obtain from linear fits of plots of ΔR vs. N_{bound} for the same potentials, but where we have intentionally distributed the ligands such that $k = 0$ for the entire range of surface coverage we plot. For these linear plots, the only contribution to ΔR is the $k = 0$ term in eq 3.5 (see the Supporting Information, **Figure 3.12**). The value of Δr_0 , the variable most directly related to the height of the barrier presented by the delocalizing ligand to the excitonic hole, decreases with increasing size of the QD core, and with increasing barrier height for all core sizes, as expected, **Figure 3.4**.⁵⁵ Upon fixing the value Δr_0 to that found from fits of the linear plots, eq 5 fits well to the simulated data sets in **Figure 3.3B**. The values of $\Delta r_k, k = 1 \dots 6$ (Table 3.1) are not individually physically meaningful as they are heavily co-dependent; this co-dependency is not surprising since, according to eq 3.5, the ranges of surface coverage where ligands have a particular adjacency number have considerable overlap.

The fits to the simulated data in **Figure 3B** show that eq 3.5 reasonably reproduces the shape of the response of ΔR to surface coverage with an independently determined value of Δr_0 . We then used eq 5 to fit the experimental plots of ΔR vs. N_{bound} , **Figure 3.3A**. We cannot independently determine a value of Δr_0 for these experimental data like we did for the simulated plots, because we can never ensure that each adsorbed ligand has zero nearest neighbors; therefore, to constrain the fit we define Δr_k as fractions of Δr_0 (eq 3.6), where $C_k < 1$, and the

$$\Delta r_k = \Delta r_0 * C_k \quad (3.6)$$

values of C_k are shared across both sizes of QDs ($R = 1.9$ nm and 2.5 nm). The fits from eq 3.5 and 3.6, shown in **Figure 3.3A**, yield $\Delta r_0 = 6.0 \times 10^{-4} \pm 1.4 \times 10^{-4}$ nm for $R = 1.9$ nm, and $\Delta r_0 = 2.0 \times 10^{-4} \pm 1.0 \times 10^{-5}$ nm for $R = 2.5$ nm. We estimate the uncertainties in these values from the error bars on the data in **Figure 3.3A**, as described in the Supporting Information. By comparing these values of Δr_0 to those from fits of our simulated data at various barrier heights, **Figure 3.4**, we conclude that the barrier height presented to the excitonic hole upon mixing of the orbitals of an isolated, bound C6-PTC with those of the QD core is 0-0.6 eV for CdS QDs with $R = 1.9$ nm, and 0.6-1.2 eV for CdS QDs with $R = 2.5$ nm. The larger value of Δr_0 and the smaller apparent barrier height for smaller QDs is consistent with the dependence of the delocalization radius on the confinement energy of the excitonic hole over this range of sizes of CdS QDs.⁵⁵

3.4 Conclusions

This study reports a method for using NMR to count the number of “NMR-invisible” phenyldithiocarbamate ligands adsorbed to CdS QDs, by measuring the signal from the displaced native ligand, which we determined to be cadmium oleate. This quantification depends critically on identifying all of the degradation products of unbound C6-PTC, and on the use of d6-benzene, in which the signals from bound and free oleate are spectroscopically distinguishable. We determined the dependence of ΔR , the apparent increase in excitonic radius resulting

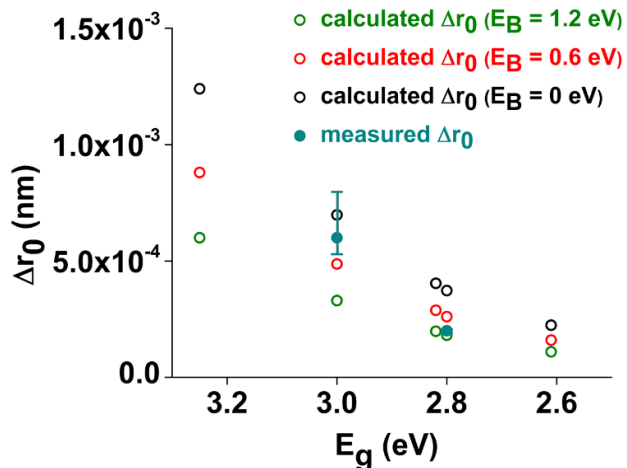


Figure 3.4. Hollow circles: Plots of the calculated values of Δr_0 – the contribution to ΔR per isolated ($k = 0$) delocalizing ligand – for barrier heights of 0 (black), 0.6 (red), and 1.2 (green) eV vs. bandgap (E_g) of the QD coated entirely by native insulating ligands. **Solid turquoise circles:** Plots of the measured values of Δr_0 for $R = 1.9$ nm ($E_g = 3.0$ eV) and $R = 2.5$ nm ($E_g = 2.8$ eV). The error bars arise from the fits of the dataset ΔR vs. (no. of bound C6-PTC) $\pm \delta$ (no. of bound C6-PTC), respectively, in Figure 3.3A.

from the electronic coupling of C6-PTC orbitals to the valence band states of the QD, on the surface coverage of C6-PTC ligands; this dependence is increasingly non-linear as the physical radius of the QD decreases. Simulations of this dependence with a three-dimensional model of an excitonic hole within a spherical potential well showed that the non-linearity is due to the enhancement of the delocalization effect with increasing degree of adjacency of delocalizing C6-PTC molecules on the QD surface. We developed a statistical model that separates the total observed ΔR into contributions from isolated, bound C6-PTC molecules and clusters of C6-PTC molecules of various size. Fits of this model to our experimental data yielded an estimate of the barrier height imposed by a single isolated C6-PTC on the excitonic hole: < 0.6 eV for CdS QDs with $R = 1.9$ nm, and $0.6 - 1.2$ eV for CdS QDs with $R = 2.5$ nm.

The influence of ligand adjacency on the measured value of ΔR resolves a longstanding puzzle in the behavior of QDs coated with derivatives of PTC. We have historically observed larger variability in ΔR from batch to batch of QDs than we expect based on variability in surface coverage of PTC. We now know that relatively small changes in ligand surface coverage and spatial distribution have a measureable effect on the value of ΔR measured for the ensemble. As a consequence, even a reduction of a few percent in the number of binding sites per QD, due to different degrees of cadmium enrichment during the growth of the particles, can result in a large decrease in ΔR .

We also learn here that the decrease in quantum confinement of excitonic carriers due to an exciton-delocalizing ligand will be more efficient in cases where the delocalizing ligands phase-segregate on the QD surface, and that bound delocalizing ligands may couple electronically with each other, in addition to coupling to the QD core. Future experiments might attempt to control exciton delocalization at fixed surface coverages by changing ligand surface arrangements from well-mixed to

highly phase-segregated (*i.e.*, Janus particles), or to synthetically modify the exciton-delocalizing ligands to encourage or inhibit nearest-neighbor interactions.

3.5 Methods

3.5.1 Synthesis and Purification of CdS Quantum Dots. We synthesized oleate-coated CdS QDs with $R = 1.9$ nm by adding 90% technical grade oleic acid (4.4 mL, 13.9 mmol), 90% technical grade octadecene (14.0 mL, 43.8 mmol), and cadmium oxide (0.360 g, 2.80 mmol) to a dry, three-neck round bottom flask, and heating the reaction mixture to 260 °C under an N_2 atmosphere with vigorous stirring. Once the solution became clear, we injected elemental sulfur (0.064 g, 2 mmol) dissolved in 4 mL of octadecene and allowed the QDs to grow for three minutes at 250 °C. In order to extract the unused cadmium precursor, we added an equal volume of a 1:1 (v:v) mixture of CH_3OH and $CHCl_3$ to the QD colloidal dispersion and centrifuged the mixture at 3500 RPM for five minutes. The cadmium precursor separated into the bottom $CH_3OH:CHCl_3$ layer, while the QDs remained in the top layer of octadecene. We decanted this top layer, precipitated the QDs by the addition of ~8 mL acetone and centrifugation, discarded the supernatant, and redispersed the QDs in hexanes. We filtered the final redispersed solution using 0.45- μm syringe filters to remove any remaining aggregated QDs.

We prepared oleate-coated CdS QDs with $R = 2.5$ nm as described above. Upon injection of the sulfur-octadecene mixture, we allowed the CdS QDs to grow for one minute at 250 °C. We then added alternating 0.5-mL aliquots of cadmium oleate and sulfur solutions, one minute apart. We monitored the QD growth after each addition by ground state absorption spectroscopy until we reached the desired size.

3.5.2. Synthesis of the Ammonium Salts of 4-hexylphenyldithiocarbamate (C6-PTC). We treated the QDs with $R = 1.9$ nm with a diisopropylethylammonium (DIPEA) salt of C6-PTC. We

treated the QDs with $R = 2.5$ nm with both a DIPEA and a triethylammonium (TEA) salt of C6-PTC to test whether the counterion influenced the response of ΔR to surface coverage (it does not; see

Figure 3.5 of the Supporting Information). We synthesized DIPEA C6-PTC by adding two

equivalents of carbon-disulfide drop-wise to one

equivalent of 4-hexylaniline in a rapidly stirring

suspension of five equivalents of

diisopropylethylamine at 0 °C, and stirring

overnight under N_2 . We washed the resulting

white powder with hexanes and dried under N_2

flow for several minutes. We prepared TEA C6-

PTC with the same procedure we used for

DIPEA C6-PTC, but using triethylamine as the

base. The Supporting Information contains 1H

and ^{13}C NMR spectra of the DIPEA and TEA

C6-PTC products.

3.5.3. Solution-phase Ligand Exchange. We added 50 to 800 molar equivalents of either 0.04 M

DIPEA C6-PTC or 0.04 M TEA C6-PTC in d_6 -benzene to 0.8 mL of 10 μM oleate-coated CdS QDs

in 99.5% d_6 -benzene in a 6 mL scintillation vial. Upon addition of C6-PTC, we stirred the samples

vigorously for 16-24 hours before acquiring NMR and ground state absorption spectra for each

sample.

3.5.4. Nuclear Magnetic Resonance (NMR) Spectroscopy. We included ferrocene (Fc) as an

internal integration standard in the CdS QD stock by adding 50 μL of 0.12 M Fc in d_6 -benzene to 20

mL of 10 μM CdS QD solution before treating the QDs with C6-PTC. We acquired 1H NMR spectra

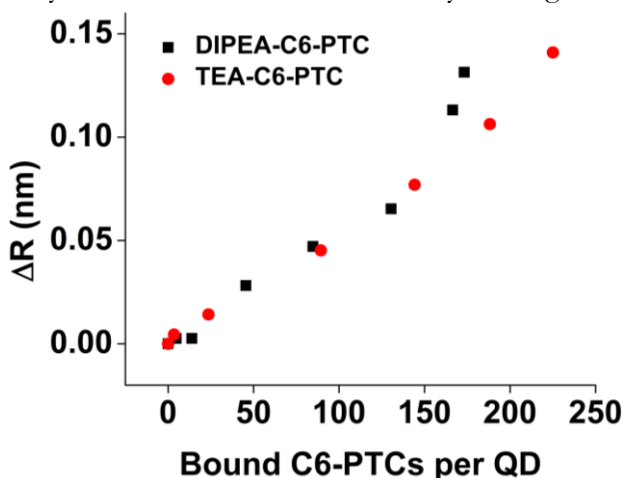


Figure 3.5. We plot ΔR as a function of bound C6-PTCs per QD for CdS QDs with $R=2.5$ nm. We used C6-PTC with two different counterions: DIPEA (black) and TEA (red). In the plot, we observe that the counterion of C6-PTC does not significantly affect the shape of the ΔR vs. bound C6-PTCs curve.

of each sample on an Agilent DD2 600 MHz spectrometer (32 scans with a relaxation delay time of 2 s). Quartz NMR tubes (Wilmad, 600 MHz frequency) were obtained from Sigma-Aldrich and used in all NMR and absorption experiments.

3.5.5. Ground State Absorption Spectroscopy. We acquired ground state absorption spectra on a Varian Cary 5000 spectrometer before and after acquisition of each ^1H NMR spectrum. To obtain each spectrum, we placed the sample (contained in an NMR tube) inside a 1-cm-pathlength quartz cuvette and stabilized the tube with a plastic pipette tip inserted in the top of the cuvette. We corrected the baselines of all spectra with neat solvent (in the same NMR tube/cuvette holder) prior to measurement. If the position of the first excitonic peak of the QDs in the sample acquired before and after the NMR spectrum differed, we report the average (in the main text) and range (in the Supporting Information) of these two measurements. The two measurements of peak position never differed by more than 1.5 nm. If the sample was too concentrated to accurately measure the position of the first excitonic peak, we diluted 100 μL of the sample into 3 mL of benzene after acquiring the NMR spectrum and before acquiring the absorption spectrum.

3.6 Supporting Information.

3.6.1 *Experimental Methods.*

Determination of Horizontal Error Bars in Figure 3.3A. The horizontal error bars in Figure 3.3A of the main text were determined from the residuals that result from fitting the plots of measured *vs.* added total phenyl rings (*i.e.*, Figure 3.2B) with a line with slope equal to exactly 1 and a fixed intercept at (0,0). We converted the residuals at each data point into a percent error for that data point, and plotted $\pm(\%error)$ as the error bars in Figure 3.3A.

Determination of Vertical Error Bars in Figure 3.3A. The vertical error bars in Figure 3.3A of the main text were determined from the half width at half maximum (HWHM) of the first excitonic peak in the

ground state absorption spectrum of each sample. These peaks did not fit well to Gaussian functions, because taking the spectra with the NMR tube distorts the shape of the peak slightly. Instead, we manually determined the HWHM for each peak using Origin's Data Reader tool. The uncertainty in ΔR ($\delta\Delta R$) is given by eq 3.7, where δR_i is the uncertainty in

$$\delta\Delta R = \sqrt{(\delta R_i)^2 + (\delta R_{PTC})^2} \quad (3.7)$$

radius for untreated QDs and δR_{PTC} is the uncertainty in radius for QDs treated with C6-PTC at each point in the titration. Since we calculate $R(E)$ for a given measured peak energy (E) using a previously determined calibration curve⁴, the uncertainty in $R(E)$ is propagated from the uncertainty in E according to eqs 3.8, 3.9.

$$\delta R_i(E_i) = \frac{dR(E)_i}{dE_i} \times \delta E_i = \frac{dR(E)_i}{dE_i} \times HWHM_i \quad (3.8)$$

$$\delta R_{PTC}(E_{PTC}) = \frac{dR(E)_{PTC}}{dE_{PTC}} \times \delta E_{PTC} = \frac{dR(E)_{PTC}}{dE_{PTC}} \times HWHM_{PTC} \quad (3.9)$$

Determination of Vertical Error Bars for Δr_0 in Figure 3.4. To obtain the error range for Δr_0 , we used $x+\delta x$ and $x-\delta x$ (shown as the limits of the error bars in Figure 3.3A, described above) as proxy x -values, and refit each of these datasets using eq 5 and 6 (fixing C_1 - C_6 to the values obtained from using the original x -values). The Δr_0 values we obtain from these fits determine the error bars for the experimental data in Figure 4.

The Direct Addition of Aniline, Phenylisothiocyanate, and N,N'-diphenylthiourea Does Not Induce Exciton Delocalization. We added each degradation product of PTC (specifically, unsubstituted PTC rather than C6-PTC) directly to CdS QDs to verify that none of these products causes a bathochromic shift in the absorption spectrum of the QDs. We added 0, 200, or 800 molar equivalents of each molecule to 10 μ M CdS QDs in d6-benzene. The samples were stirred in a 6-mL scintillation vial for \sim 17h. **Figure**

3.22 shows the ground state absorption spectra of the QDs before and after addition of these molecules.

Synthesis and Control Experiments with 1,3-bis(4-hexylphenyl)thiourea. We synthesized 1,3-bis(4-hexylphenyl)thiourea as described in the literature,¹⁶² using 4-hexylaniline as the precursor. We added 0-800 equivalents of this substituted thiourea to 10 μ M CdS QDs in d6-benzene. The samples were stirred in a 6-mL scintillation vial for \sim 17h. We took NMR spectra as described in the main text, and the ground state absorption spectra on diluted samples in a cuvette. **Figure 3.23** shows the NMR spectra of the C6-TU.

Broadening of the NMR Signals from the DIPEA and TEA Counterion upon Addition to QDs. We observe broadening of the NMR signals from the DIPEA and TEA counterion protons in the presence of QDs, which suggests that the counterion binds to the surface along with the anionic C6-PTC ligand in order to balance charge during the ligand exchange (Figure S17). This data corroborates our deduction, based on “conservation of phenyl protons”, that C6-PTC displaces Cd(oleate)₂, not oleic acid.

TEM of Oleate-capped and C6-PTC-capped CdS QDs. We obtained transmission electron microscopy images of natively-capped and exchanged CdS QDs. Representative TEM images are shown in **Figure 3.12**, and indicate that the overall size and shape of the QDs do not change upon treatment with C6-PTC.

3.6.2 *Computational Methods*

Determination of the Hole Confinement Energy with Increasing (up to 95%) Surface Coverage of Delocalizing Ligand. In order to simulate the plot of ΔR vs. the surface coverage of C6-PTC, we constructed a potential energy surface representing a ligand-coated QD centered in a 3D grid with 256 points in each dimension. Each grid point represented a cube 0.05 nm on a side. The surface included a core

region where the potential energy was set to 0 eV, and two concentric annular barrier regions to represent the core/ligand interface, and the surrounding insulating region, respectively. The core radius of the QD was set to 1.1, 1.2, 1.4, 1.9, 2.4, 2.5, or 3.2 nm, the QD core/ligand interface (potential barrier 1) extended 0.6 nm radially, and the insulating portion of the ligand shell and solvent (potential barrier 2) filled the rest of the potential cube. We set the potential at each grid point relative to the QD core potential. The potential energy was set to 3.6 eV for solvent (the energy difference between the CdS valence band-edge and the HOMO of benzene),¹⁶⁰ 3.3 eV for the core/ligand interfacial region for insulating native ligands (the energy difference between the CdS valence band-edge and the HOMO of stearate), and ranged between 0 and 2.3 eV for the core/ligand interfacial region for delocalizing C6-PTC ligands (2.3 eV being the energetic barrier imposed by a completely uncoupled C6-PTC ligand to the CdS core). We used stearate as a proxy for oleate in this calculation to ensure that the HOMO is isolated on the carboxylate head group (and not on the alkene functionality). We divided the surface of the QD into N_{sites} evenly distributed sites based on a density of 4/nm². We determined the site locations by performing a classical electrostatic simulation of N_{sites} point charges of unit charge free to move on the surface of a unit sphere. The motion of the point charges was damped so that the overall repulsive energy decreased and converged over the course of the simulations. The final coordinates of the point charges were used as unit radial vectors pointing at QD surface sites. We assigned each grid point within the ligand shell to the surface site where the dot product of the grid point's position and the site's unit vector was maximized. The eigenfunctions for a particle with an effective mass of 0.45 (corresponding to the effective mass of the hole in bulk CdSe) were calculated by an imaginary time relaxation. The range of surface coverage was selected in 20 steps (0-95%, in increments of 5%) for computational time savings, as the cluster used had 20 processors per node.

The HOMOs of stearic acid and C6-PTC were calculated by DFT using a B3LYP functional and a 6-311G(d, p) basis set. We first performed geometry optimizations of the two molecules, then performed single point energy calculations for the neutral and ionized species to get the ionization potential; the negative of the ionization potential of the HOMO energy according to Koopman's Theorem.¹²⁶

Calculation of ΔR from the Confinement Energies Produced by the 3D Pseudopotential Model. To calculate ΔR from the confinement energies from the spherical potential well model, we fit a calibration curve to the calculated confinement energy for the non-delocalizing potential wells *vs.* radius (**Figure 3.9**). The resulting calibration curve, eq 3.10, was then used to calculate a

$$R = \left(\frac{E^{-0.5}}{1.38} \right) - 0.17 \quad (3.10)$$

radius for different surface coverages (θ) of delocalizing ligands. As with the experimental measurements, $\Delta R = R_{\theta=0} - R_{\theta}$.

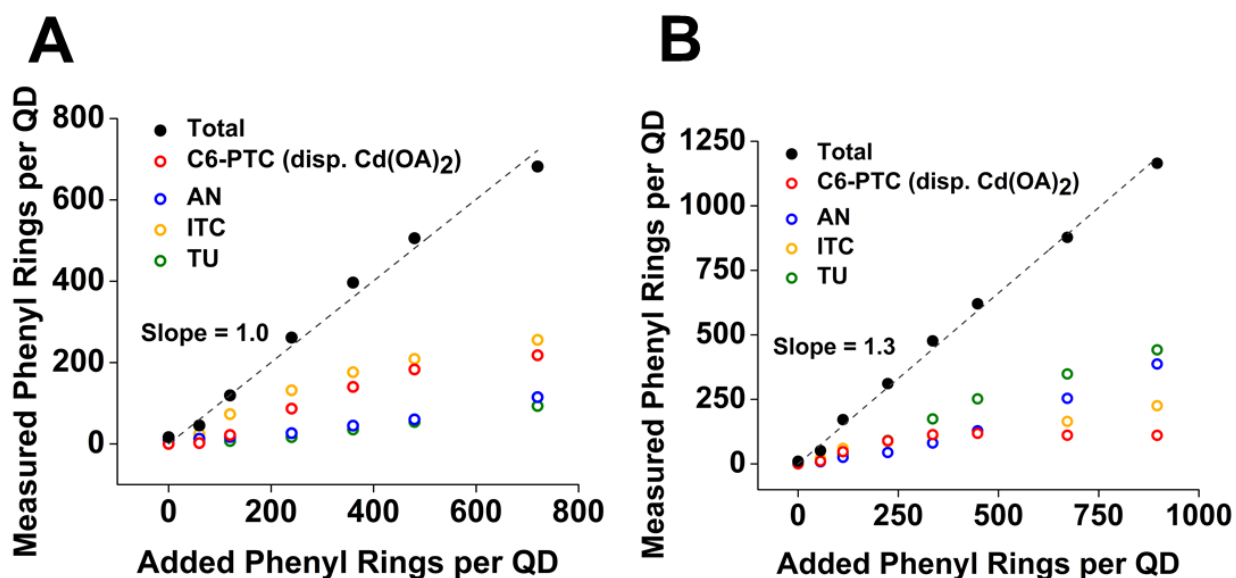


Figure 3.6. Plots of the total number of phenyl rings per QD (from C6-PTC and its degradation products) in each sample, measured by NMR, *vs.* the number of phenyl rings per QD added to each sample, for a mixture of C6-PTC and 2.5 nm CdS QDs (A, with TEA as the counterion) and 1.9 nm CdS QDs (B, with DIPEA as the counterion).

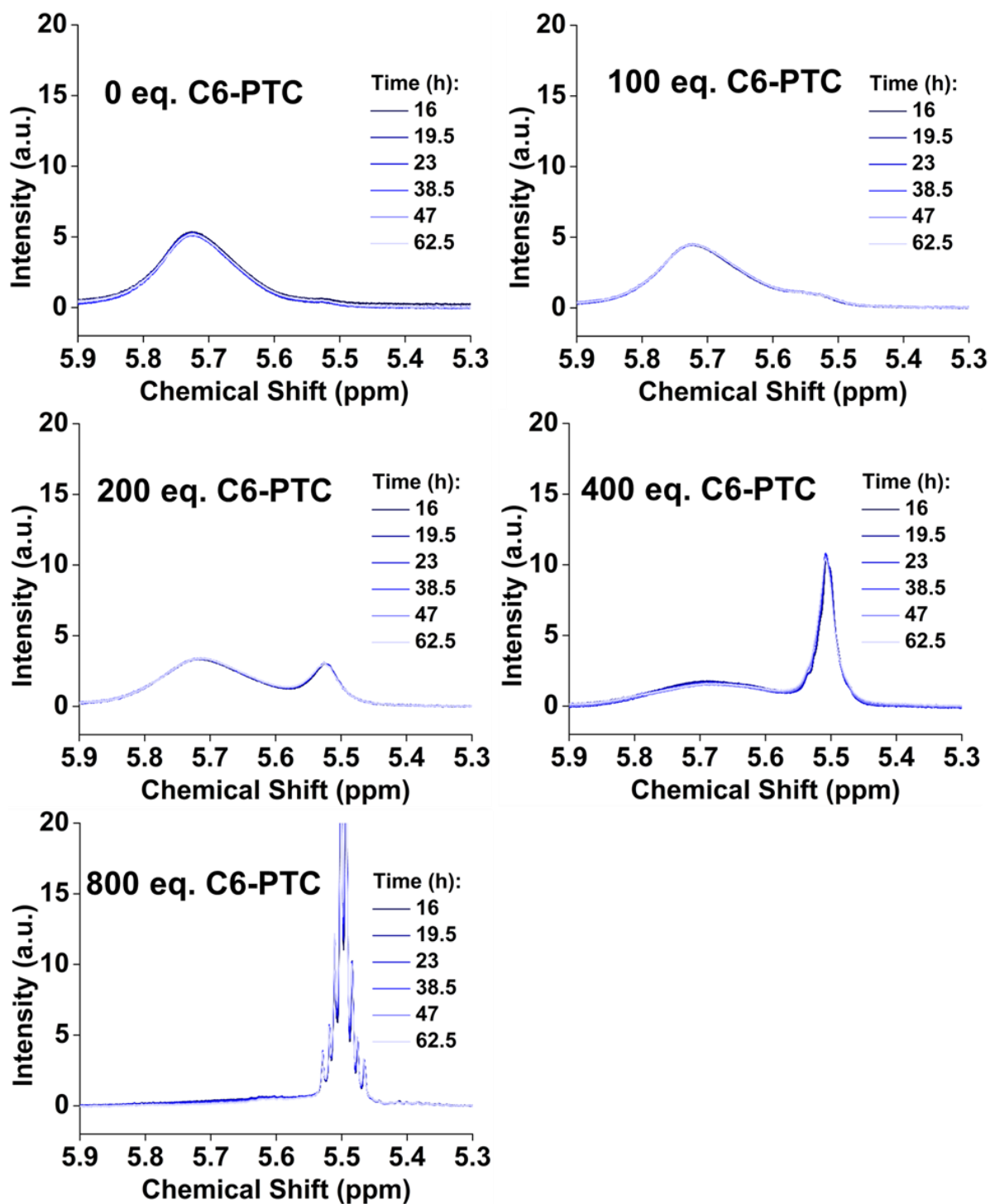


Figure 3.7. The vinyl regions of the NMR spectra of CdS QDs with $R = 2.5$ mixed with 0-800 molar equivalents of C6-PTC. The spectra were acquired at six time points after the initial mixing of C6-PTC with CdS QDs. These spectra show that C6-PTC, once bound to the QD surface, remains bound over the course of over 62 hours.

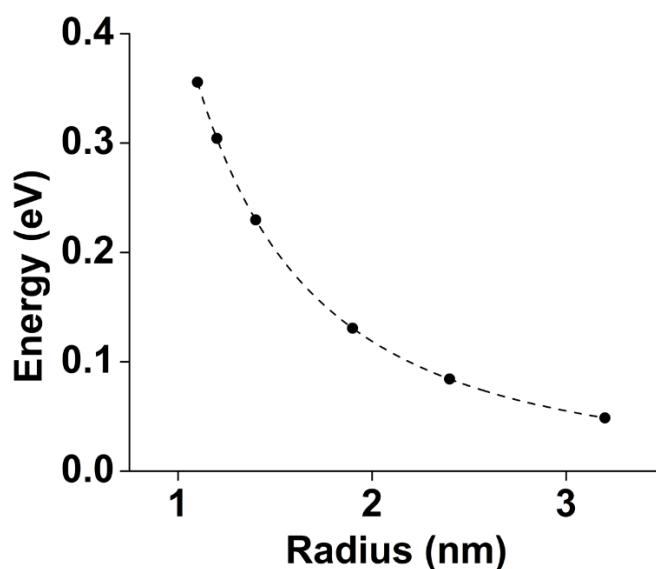


Figure 3.9. To calculate ΔR from the confinement energies from the spherical potential well model, we fit a calibration curve to calculated confinement energy for the non-delocalizing potential wells *vs.* radius. The resulting calibration curve is described by eq 3.7, which was used to calculate a radius for different surface coverages of delocalizing ligands. We subtracted the radius for a surface coverage of zero from this radius to obtain ΔR .

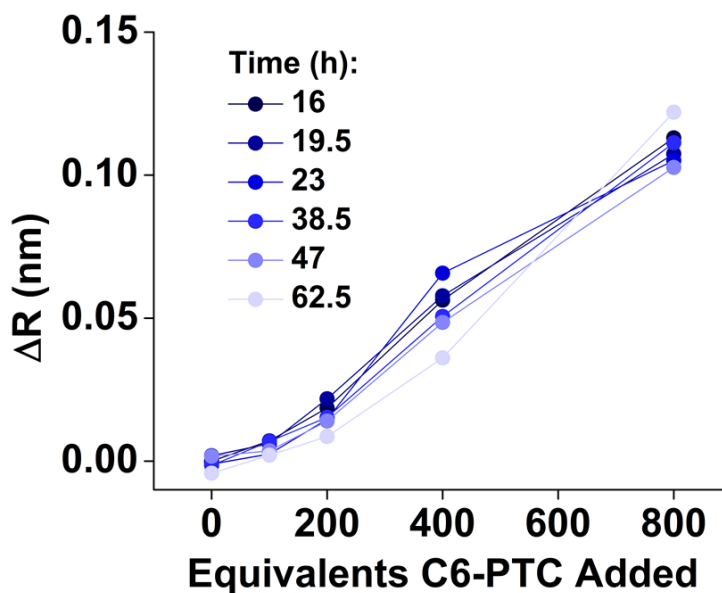


Figure 3.8. Plot of ΔR *vs.* equivalents of C6-PTC added to CdS QDs with $R = 2.5$, at a series of time points during the ligand exchange. We obtained these data from the same samples used to collect the NMR spectra shown in Figure 3.7. This plot shows that the bathochromic shift upon ligand exchange with C6-PTC stays fairly constant over time, which further implies that once bound, C6-PTC does not desorb from the QD surface.

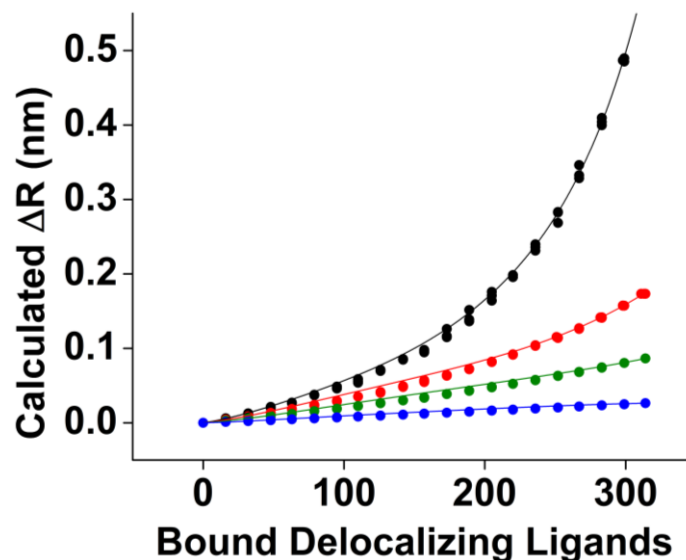


Figure 3.10. Plot of ΔR , calculated using a simple three-dimensional particle-in-a-spherical potential well model, vs. the number of bound delocalizing ligands for a 2.5-nm core radius. A similar plot for a core with a 1.9-nm radius is shown in the main text, Figure 3.3B.

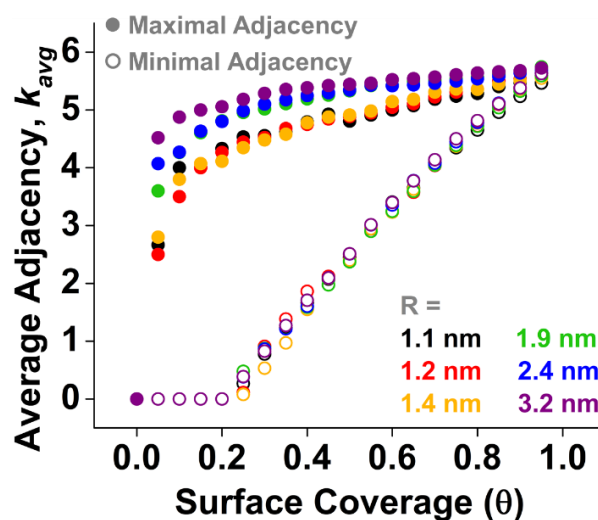


Figure 3.11. We calculated adjacency number, k , by tracking the number of neighboring delocalizing ligands for each bound delocalizing ligand in our 3D pseudopotential model. We plot the average adjacency, k_{avg} , of the bound delocalizing ligands as a function of surface coverage for several core sizes. Ligands placed as close together as possible are solid circles, and ligands placed maximally far apart are hollow circles. We see that, at surface coverages ≤ 0.2 , adjacency is zero for the minimally adjacent case; it then increases rapidly to reach an average adjacency of ~ 6 .

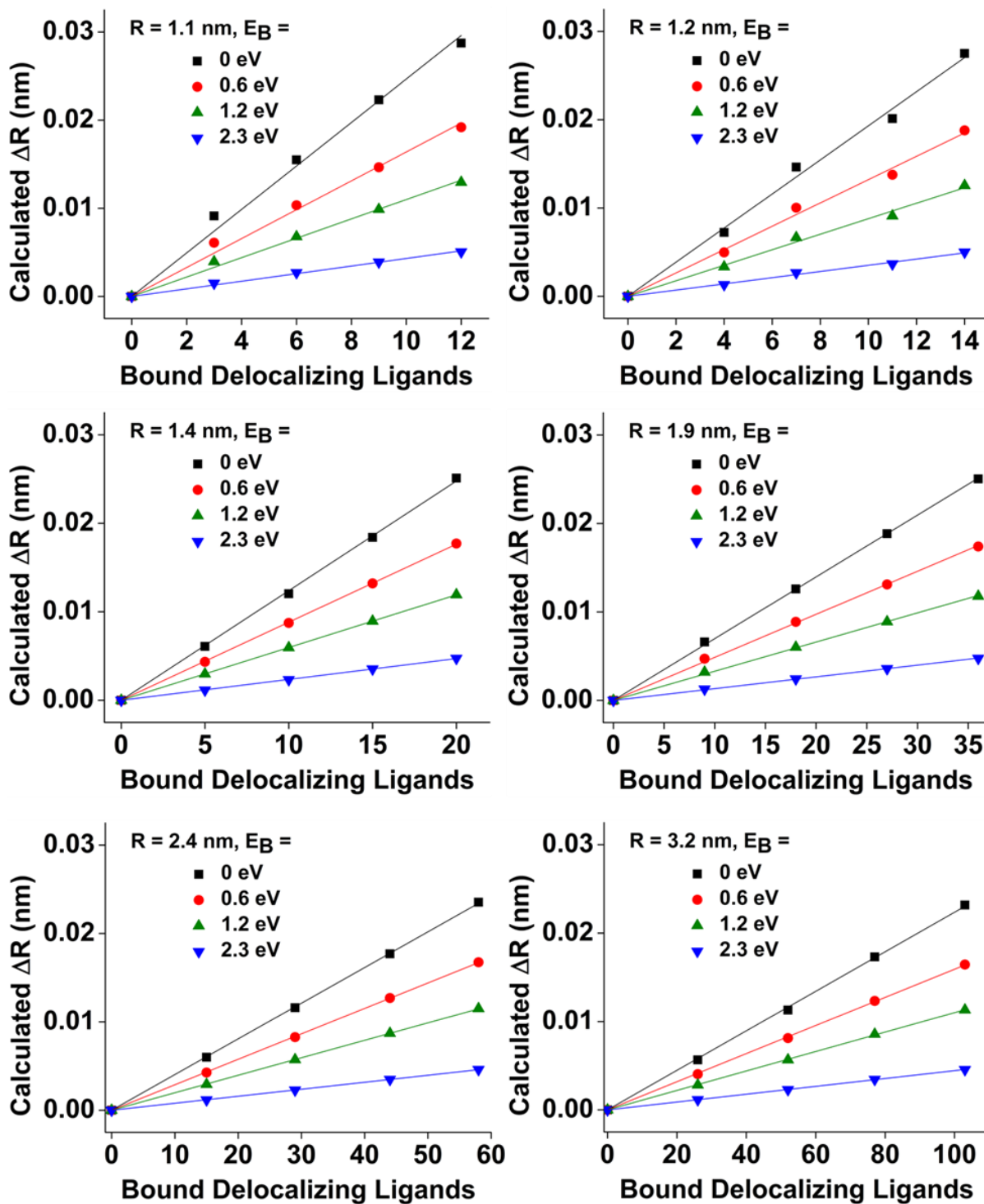


Figure 3.12. Linear fits of the calculated ΔR from the pseudopotential model *vs.* the number of bound delocalizing ligands for the zero adjacency case ($\theta \leq 0.2$, open circles, Figure 3.11), where ligands are placed maximally far apart on the surface. The slope of each line corresponds to Δr_0 . We report the slopes and fit errors in Table 3.1.

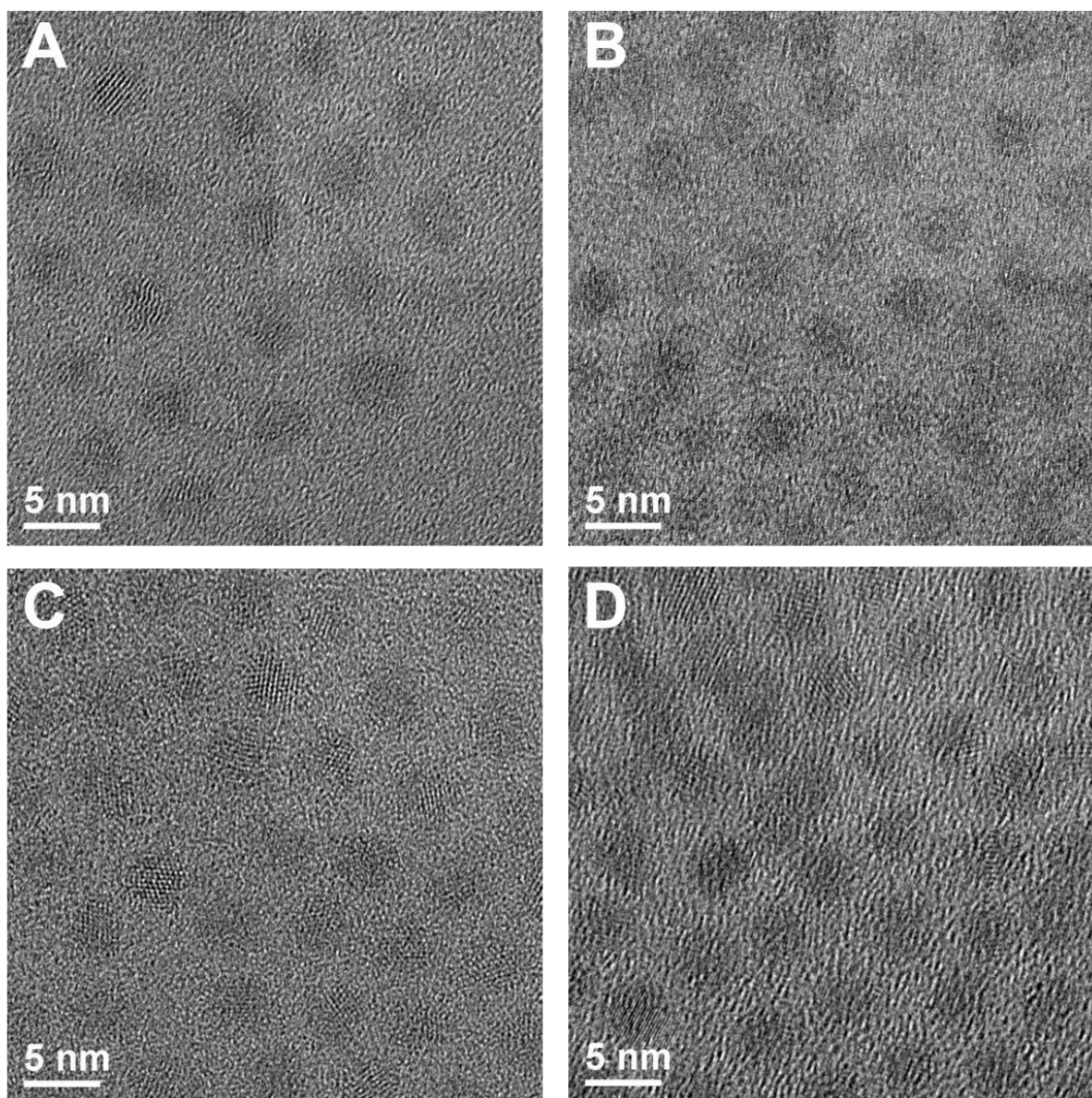


Figure 3.13. TEM images of oleate-capped (A, B) and C6-PTC-capped (C, D) CdS QDs. The oleate-capped CdS QDs (measured from 14 QDs) measure 3.7 ± 0.4 nm in diameter and the C6-PTC) capped CdS (measured from 12 QDs) measure 3.6 ± 0.3 nm in diameter from ImageJ analysis.

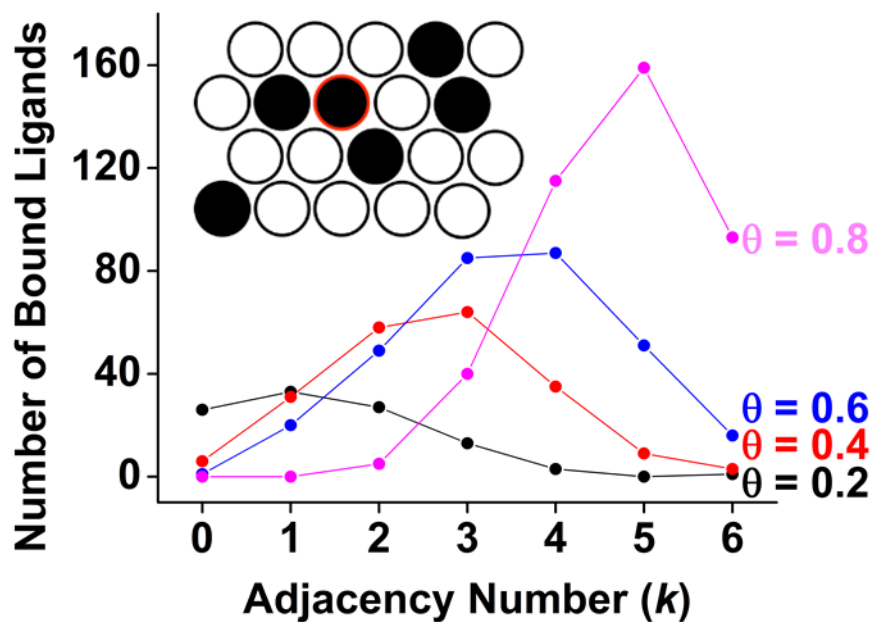


Figure 3.14. Adjacency distribution of ligands from simulation of $R = 3.2$ nm sphere with 515 surface sites for surface coverages ranging from 0.2 – 0.8. The solid lines are guides to the eye. Inset: Schematic representation of a section of the QD surface, showing the individual surface sites as circles. Open circles represent empty binding sites, and filled circles represent filled binding sites. Each site has 6 nearest-neighbor sites. The bound ligand outlined in red has two adjacent ligands ($k = 2$).

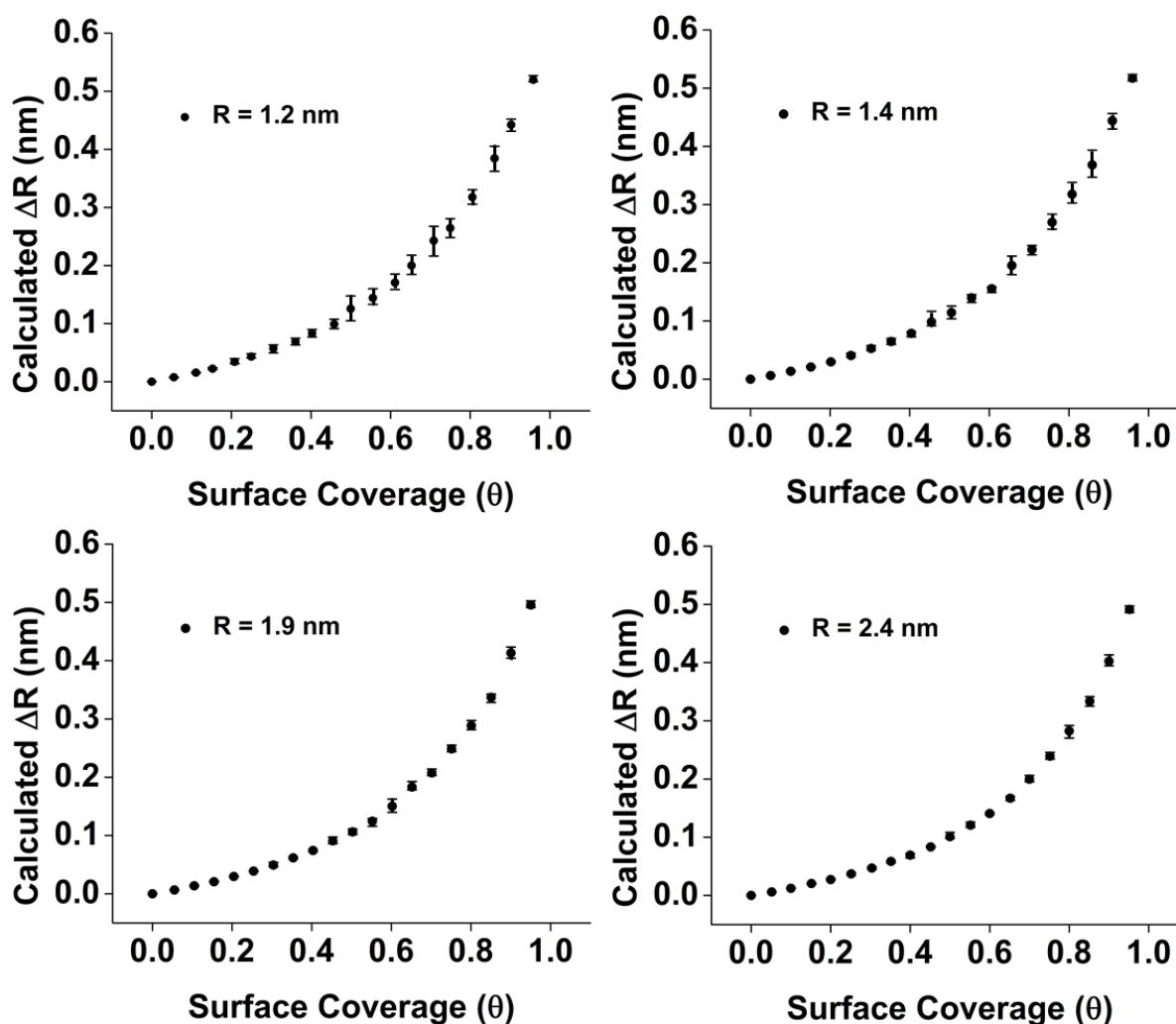


Figure 3.15. Plots of calculated ΔR (from our pseudopotential model) *vs.* delocalizing ligand surface coverage, showing five random trials of delocalizing ligand placement on the surface of a spherical potential well with four different radii. The points and error bars show the average and range, respectively, of the calculated ΔR values for a given arrangement of delocalizing ligands (that impose a barrier height of 0 eV) on the surface. It is evident that smaller sphere sizes show a much greater variation in ΔR at a given surface coverage. This phenomenon is due to different degrees of ligand adjacency, which has a greater impact on small spheres because each bound ligand takes up a greater fraction of the total surface area.

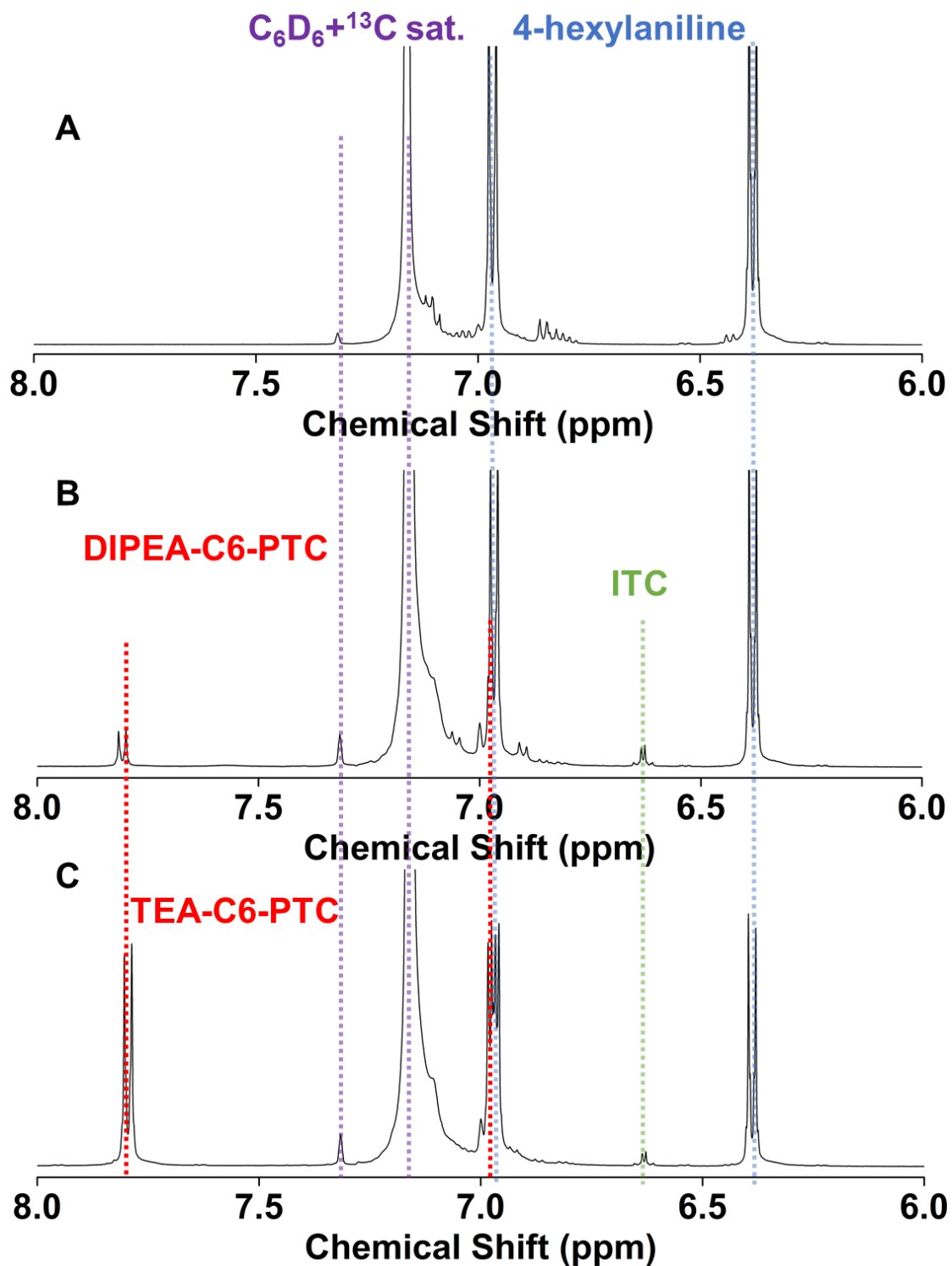


Figure 3.16. The aromatic region of ^1H NMR spectra of A) 4-hexylaniline, B) TEA-C6-PTC, and C) DIPEA-C6-PTC in d_6 -benzene. The vertical lines are guides to the eye, and highlight the peaks assigned to 4-hexylaniline (blue), 4-hexylphenylisothiocyanate (ITC, green), d_6 -benzene (purple), and C6-PTC (red).

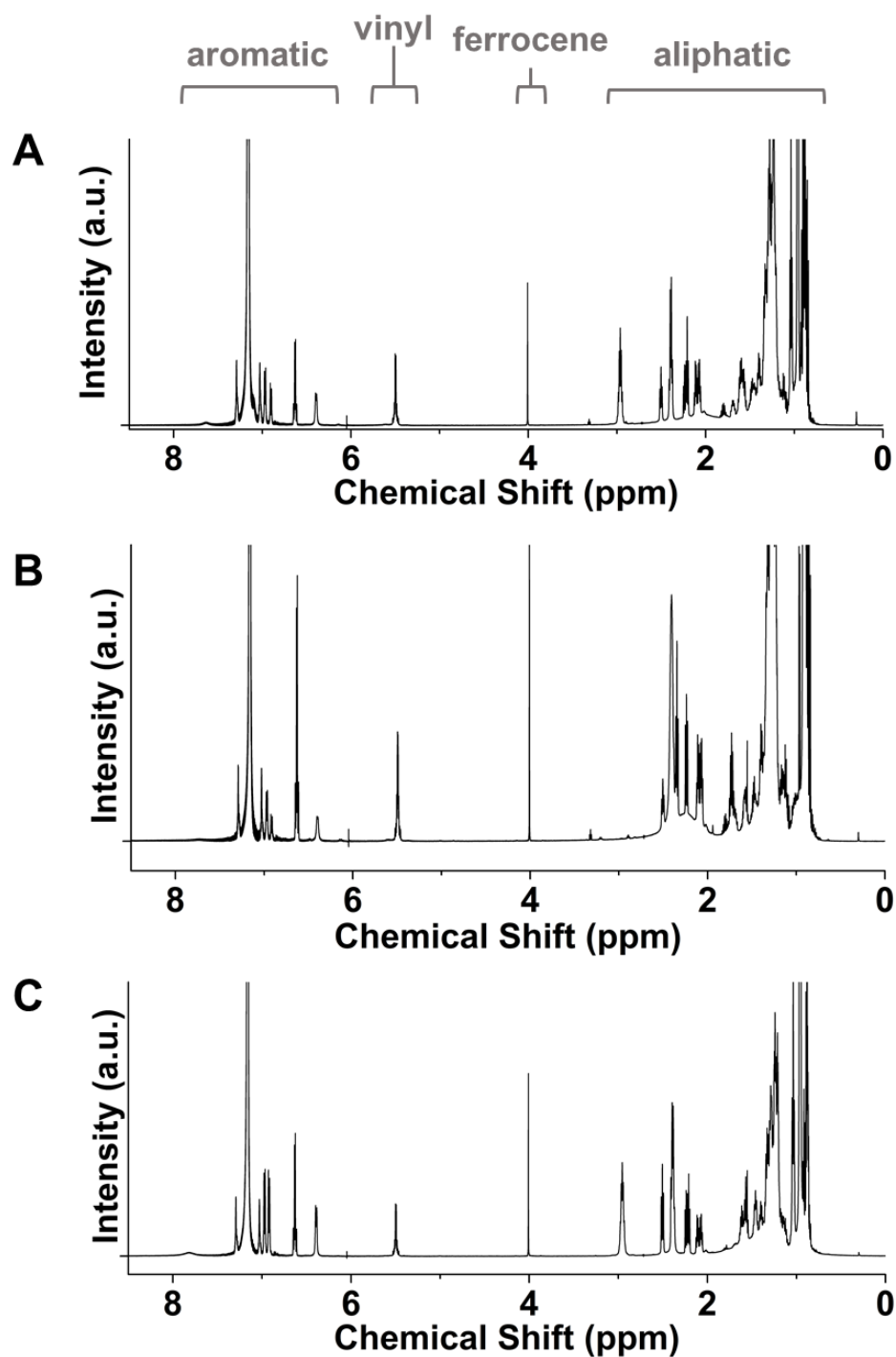


Figure 3.17. Full NMR spectra of ~717 molar equivalents of C6-PTC mixed with **A)** 2.5 nm CdS QDs with DIPEA as the counterion **B)** 2.5 nm CdS QDs with TEA as the counterion, and **C)** 1.9 nm CdS QDs with DIPEA as the counterion. These spectra possess a complex aliphatic region, easily interpretable vinyl region, and multiple aromatic peaks which we assign to the degradation products of C6-PTC. Further NMR details are discussed below, in Figures 3.18-3.21.

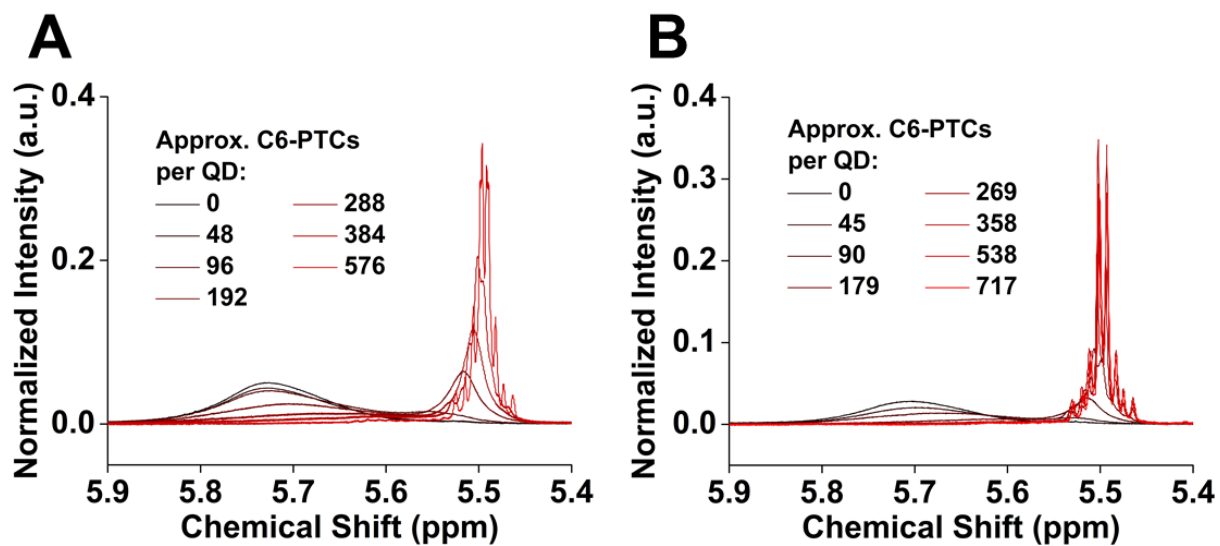


Figure 3.18. The vinyl region of the NMR spectra shown in Figure 3.17 (at all concentrations of C6-PTC), for **A)** 2.5 nm QDs with TEA as the counterion and **B)** 1.9 nm CdS with DIPEA as the counterion. The corresponding NMR spectra for 2.5 nm CdS QDs with DIPEA as the counterion are shown in the main text, Figure 2A.

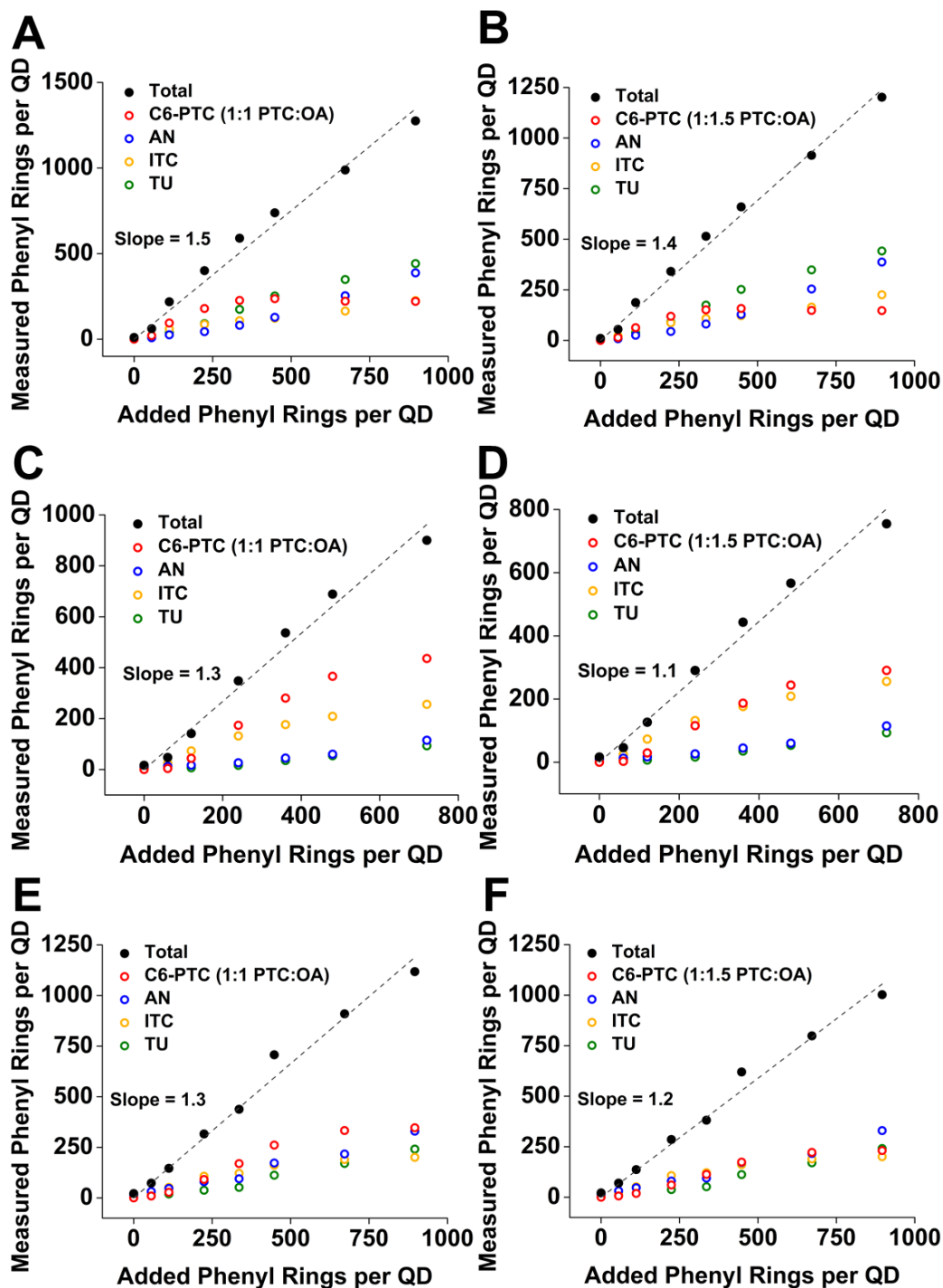


Figure 3.19. Plots showing the conservation of phenyl rings per QD (similar to **Figure 3.2B**) for alternate stoichiometries of the C6-PTC-for-oleate exchange. **A)** and **B)** show a one-to-one displacement of C6-PTC for oleic acid, and the case where one C6-PTC displaces an average of 1.5 oleates, respectively, for 1.9 nm CdS QDs with DIPEA counterion. **C)** and **D)** show the same for 2.5 nm CdS QDs with TEA counterion, and **E)** and **F)** show the corresponding plots for 2.5 nm CdS QDs with DIPEA counterion.

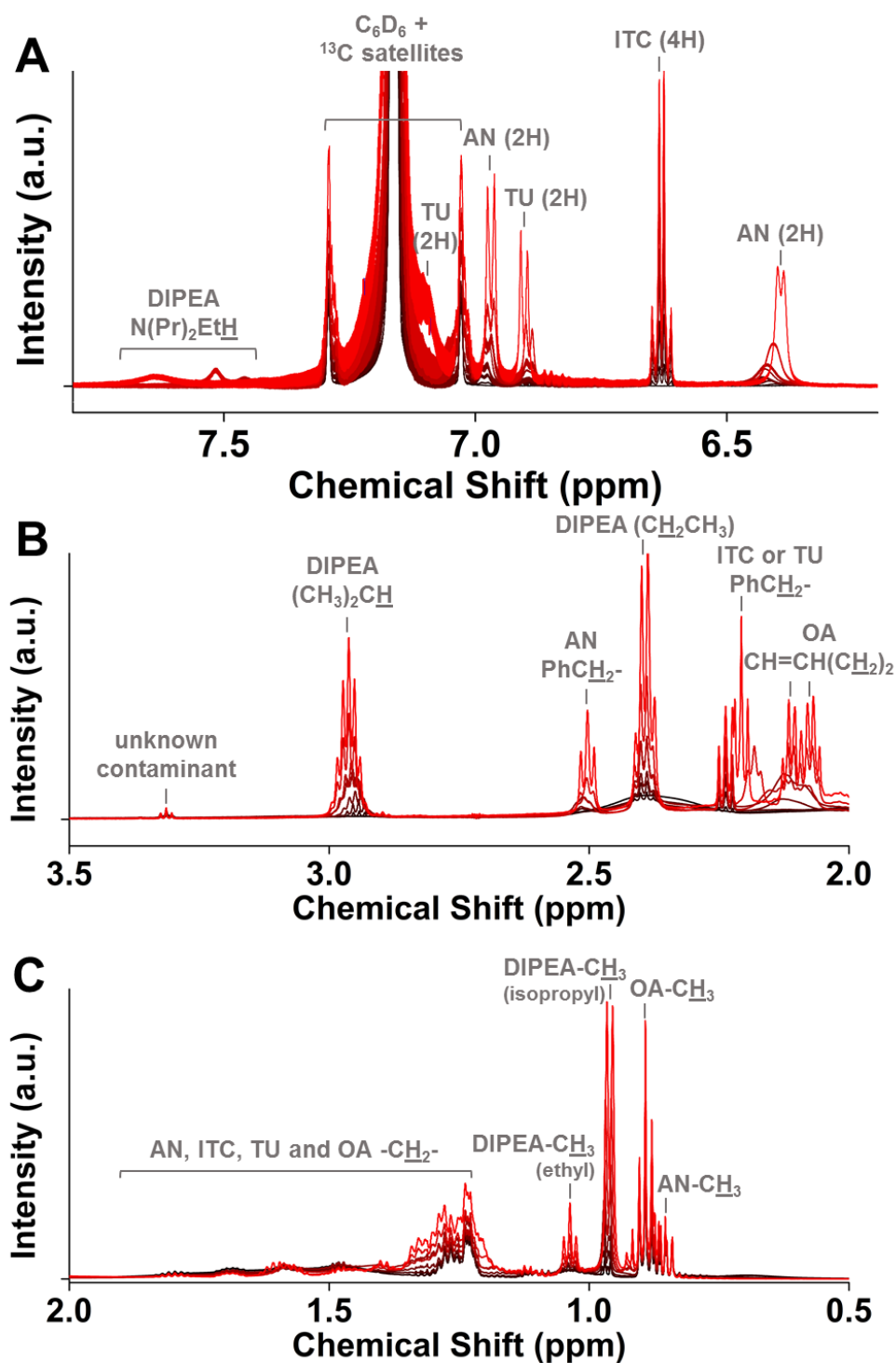


Figure 3.20. Peak assignments for the ${}^1\text{H}$ NMR spectra of samples of C6-PTC mixed with 2.5 nm CdS QDs with DIPEA as the counterion (the same samples depicted in **Figure 3.17A** and **Figure 2A** in the main text). Here, we show **A**) the aromatic region, **B**) the downfield aliphatic region from 2-3.5 ppm, and **C**) the upfield aliphatic region from 0.5-2 ppm.

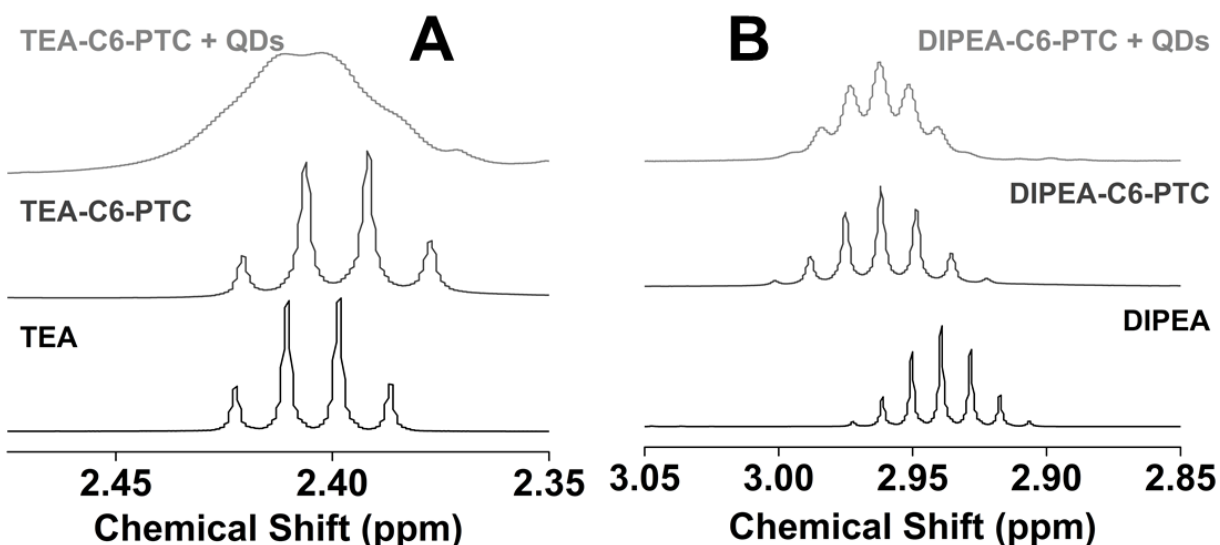


Figure 3.21. ^1H NMR signals of the **A)** TEA ethylene protons and **B)** DIPEA $(\text{CH}_3)_2\text{CH}$ - (isopropyl) proton for the free counterion, free C6-PTC, and C6-PTC + QDs showing the broadening of the counterion protons upon addition of QDs, which indicates adsorption of the counterion to the QD surface.

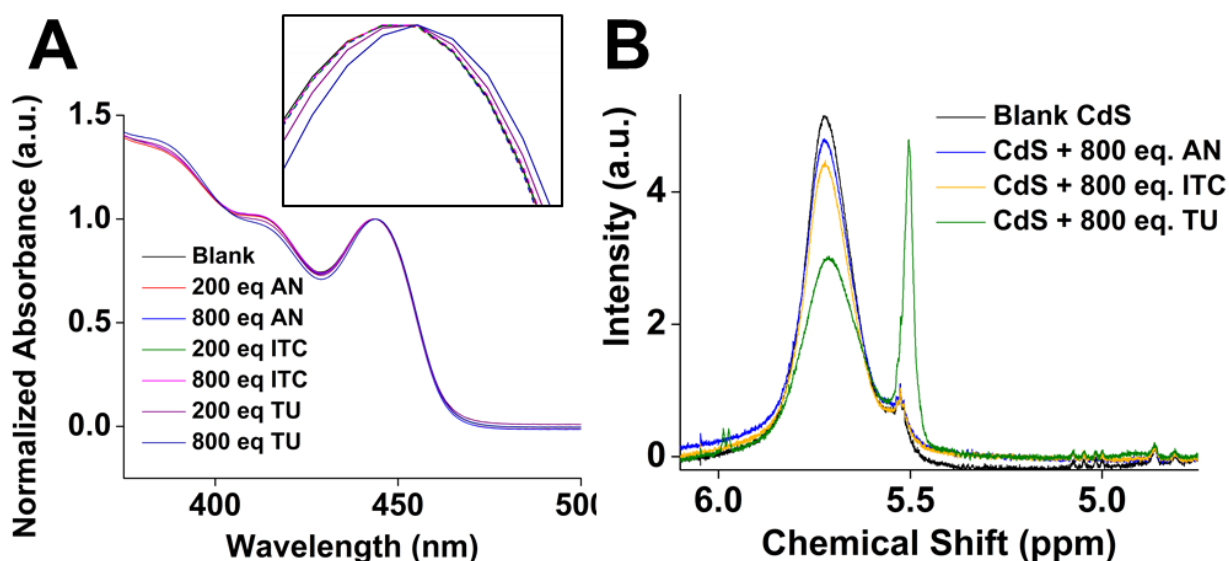


Figure 3.22. **A)** Absorption spectra of CdS QDs with 200 and 800 added equivalents of unsubstituted aniline (AN), phenylisothiocyanate (ITC), and N, N'-diphenylthiourea (TU). Only 800 equivalents of TU induces a detectable bathochromic shift of the spectrum. The inset shows a zoom-in of the excitonic peak; the spectra of the blank and TU samples are solid lines, whereas the other samples are dashed lines. **B)** The vinyl region of the spectra of CdS QDs (black), and mixtures of CdS QDs with 800 equivalents of aniline (AN, blue), phenylisothiocyanate (ITC, yellow), and N,N'-diphenylthiourea (TU, green). Only TU displaces oleate from the CdS QD surface when it is added.

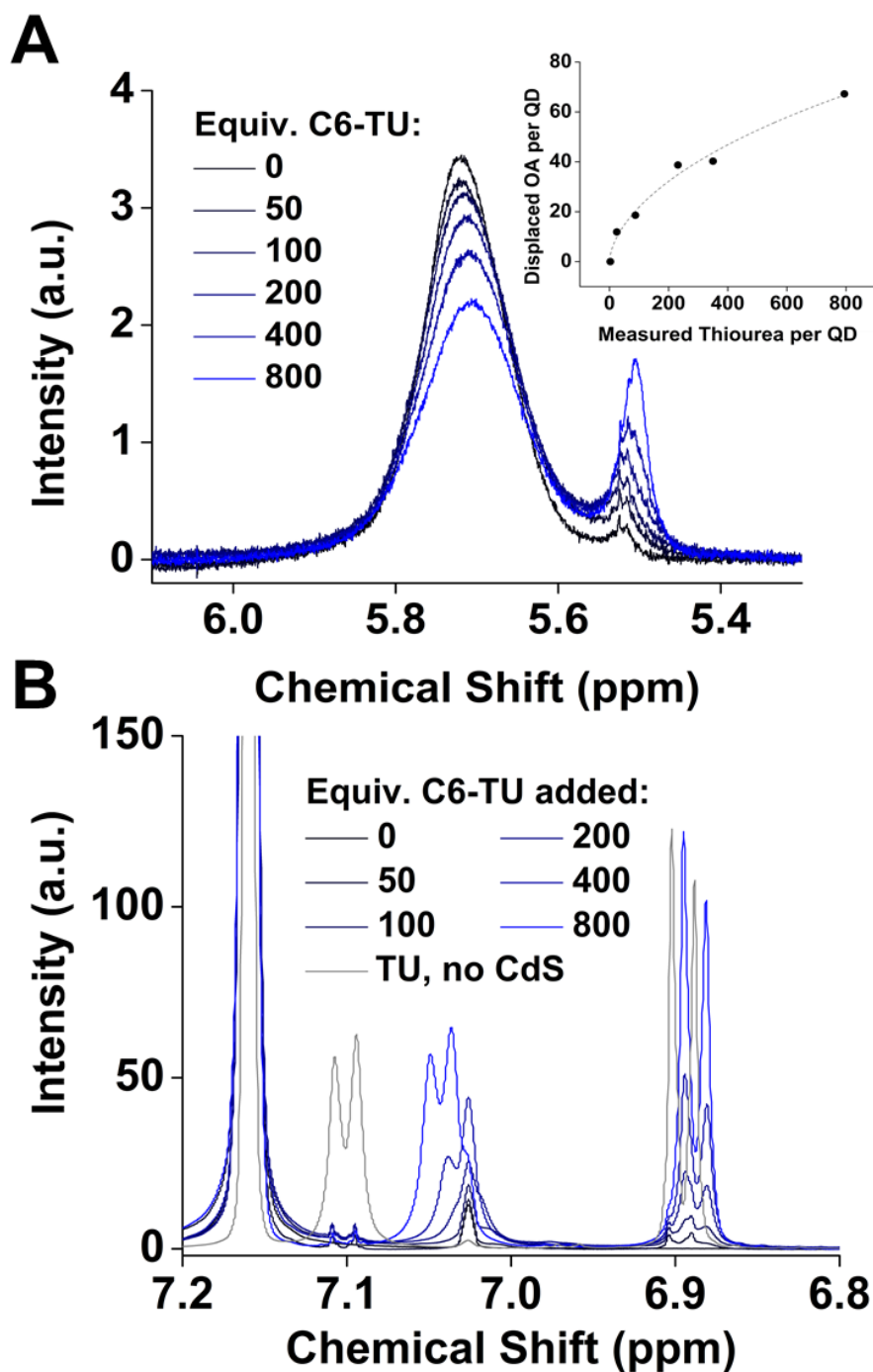


Figure 3.23. A) The vinyl region of ^1H NMR spectra of CdS QDs with 0-800 equivalents of N,N' -bis(4-hexylphenyl)thiourea (TU), showing partial oleate displacement. Inset: Plot of displaced oleate (OA) per QD *vs.* the measured TU per QD (as measured by direct integration of the TU NMR peaks), fit to a Langmuir-type function. **B)** Aromatic region of the NMR sequential NMR spectra of CdS QDs with 0-800 equivalents of N,N' -bis(4-hexylphenyl)thiourea (TU), showing moderate broadening and shifting of one of the aromatic peaks relative to free TU with no QDs (gray trace). There is some free TU present with QDs, but much of it is bound.

The Non-linearity of the Response of ΔR to N_{bound} . Our experimental plot of ΔR vs. N_{bound} , **Figure 3.3A**, for QDs with $R = 1.9$ nm shows a subtle curvature. We estimate – based on the estimated maximum number of bound C6-PTC ligands (calculated assuming the QD is a sphere and a C6-PTC footprint of ~ 0.23 nm²) – that we only reach a fractional surface coverage of 0.6-0.7 experimentally. The curvature we observe in the simulated data (**Figure 3.3B**) is most apparent when we plot ΔR up to high surface coverages (>0.7), so the non-linearity of our experimental data is less obvious than that of the simulated data. We also note that the experiments predict more non-linearity in the plot (over a given range of surface coverages) for smaller QDs than for larger QDs, which rationalizes the differences in the shapes of our experimental plots at different sizes.

We quantify the goodness of the linear vs. non-linear fits of the experimental data by comparing reduced R^2 value of a linear fit to that of a quadratic fit to that of our statistical model (described in the main text). **Figure 3.24** shows the plots of experimentally measured ΔR vs. the surface coverage of C6-PTC for the two sizes we studied. These plots are fit to three functions: (i) a line, with a fixed intercept of 0,0, for which $R^2 = 0.96$ for $R = 1.9$ nm and 0.97 for $R = 2.5$ nm; (ii) a generic quadratic function, for which $R^2 = 0.97$ for $R = 1.9$ nm and 0.97 for $R = 2.5$ nm; and (iii) our statistical model, as we describe in the main text, for which $R^2 = 0.98$ (shared between the two sizes to constrain the fit). For the larger size of QDs, all three functions fit similarly well, as judged by inspection and from the R^2 values. For the smaller size of QDs, however, the fit of the quadratic or statistical function is measurably better than that of the line. The quadratic function has no physical meaning, so we believe it is justifiable to rely on our statistical model to fit our data.

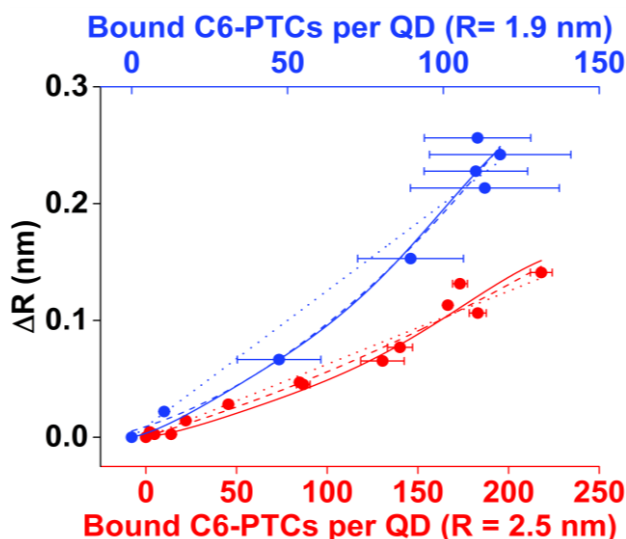


Figure 3.24. Plot of ΔR vs. C6-PTC surface coverage for CdS QDs with $R = 1.9$ nm (blue) and $R = 2.5$ nm (red). We show the fit to our model with a solid line, a quadratic function with a dashed line, and a linear function with a dotted line.

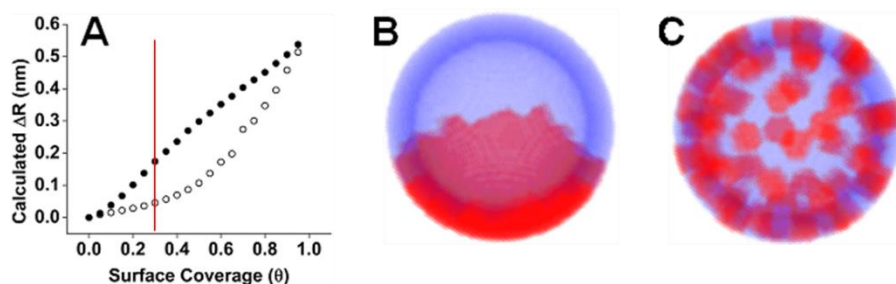


Figure 3.25. **A)** Calculated ΔR vs. fractional surface coverage of delocalizing ligand with a barrier height of 0 eV. The solid circles are data points where the delocalizing ligands have been placed in a Janus particle-like configuration with maximum adjacency, and the hollow circles are points where the delocalizing ligands are placed maximally far apart on the surface, with minimal adjacency. It is clear that, at a surface coverage, delocalizing ligands with more adjacency result in a greater ΔR , even though their distribution is less isotropic. **B),C)** are schematic images of what maximal (**B**) and minimal (**C**) adjacency looks like at a delocalizing ligand surface coverage of 30% (marked on **A** as a red line), where the native ligands are blue and the delocalizing ligands are red. Although the minimal adjacency case (**C**) is more isotropic, it has a smaller ΔR (hollow spheres) than the maximal adjacency case (**B**).

Table 3.1. Values of Δr_0 , Calculated from the Linear Fits of the Zero-Adjacency Case in the Minimal Adjacency Plots where $\theta \leq 0.2$ (Figure 3.12).

| <i>Barrier Height (Simulation Input)</i> | Δr_0 (nm) ^a | | | |
|--|--------------------------------|--------------------------------|---------------------------------|--------------------------------|
| | <i>0 eV</i> | <i>0.6 eV</i> | <i>1.2 eV</i> | <i>2.3 eV</i> |
| R = 1.1 nm | $(25 \pm 0.6) \times 10^{-4}$ | $(16 \pm 0.4) \times 10^{-4}$ | $(11 \pm 0.2) \times 10^{-4}$ | $(43 \pm 0.8) \times 10^{-5}$ |
| R = 1.2 nm | $(19 \pm 0.4) \times 10^{-4}$ | $(13 \pm 0.3) \times 10^{-4}$ | $(87 \pm 2) \times 10^{-5}$ | $(35 \pm 0.8) \times 10^{-5}$ |
| R = 1.4 nm | $(12 \pm 0.1) \times 10^{-4}$ | $(88 \pm 0.2) \times 10^{-5}$ | $(60 \pm 0.04) \times 10^{-5}$ | $(40 \pm 0.1) \times 10^{-5}$ |
| R = 1.9 nm | $(70 \pm 0.3) \times 10^{-5}$ | $(49 \pm 0.4) \times 10^{-5}$ | $(33 \pm 0.3) \times 10^{-5}$ | $(13 \pm 0.09) \times 10^{-5}$ |
| R = 2.4 nm | $(40 \pm 0.1) \times 10^{-5}$ | $(29 \pm 0.07) \times 10^{-5}$ | $(20 \pm 0.03) \times 10^{-5}$ | $(79 \pm 0.2) \times 10^{-6}$ |
| R = 3.2 nm | $(22 \pm 0.1) \times 10^{-5}$ | $(16 \pm 0.07) \times 10^{-5}$ | $(1.1 \pm 0.04) \times 10^{-6}$ | $(44 \pm 0.1) \times 10^{-6}$ |

^a The reported errors arise from the error of the slope from the linear fits in **Figure 3.12**.

Table 3.2. Experimental values of Δr_k from fits of Figure 3A to eq 5 and 6 in the main text.

| Radius (nm) | Δr_0 | C_1 | C_2 | C_3 | C_4 | C_5 | C_6 |
|-------------|----------------------|-------|-------|-------|-------|-------|-------|
| 1.9 | 5.8×10^{-4} | 1.87 | 1.00 | 1.00 | 4.37 | 2.37 | 1.00 |
| 2.5 | 2.0×10^{-4} | | | | | | |

Table 3.3. Values of ΔR for CdS QDs with R = 1.9 nm, Measured Before and After NMR Analysis.

| Equiv. C6-PTC Added | 0 | 45 | 90 | 179 | 269 | 358 | 538 | 717 |
|---------------------|---|-------|-------|------|------|------|------|------|
| Before NMR | 0 | 0.018 | 0.071 | 0.15 | 0.21 | 0.25 | 0.26 | 0.23 |
| After NMR | 0 | 0.026 | 0.062 | 0.15 | 0.22 | 0.24 | 0.26 | 0.23 |

3.7 Acknowledgements.

This material is based upon work supported by the National Science Foundation through Graduate Research Fellowships to R.D.H. and V.A.A. (Grant No. DGE-1324585). The portion of this research involving the pseudopotential calculations was also supported as part of the Center for Bio-Inspired Energy Science, an Energy Frontier Research Center funded by the U.S. Department of Energy (DOE), Office of Science, Basic Energy Sciences (BES), under Award # DE-SC0000989. Electron microscopy was performed in the *NUANCE* Center at Northwestern University. *NUANCE* is supported by the International Institute for Nanotechnology, MRSEC (NSF DMR-1121262), the Keck Foundation, the State of Illinois, and Northwestern University.

4 EFFECT OF AN EXCITON-DELOCALIZING LIGAND ON THE CONDUCTIVITY OF THIN PBS NANOCRYSTAL FILMS

Adapted from:

1. Harris, R.D.*; Bettis Homan, S.* *et al.* Electronic Processes within Quantum Dot-Molecule Complexes. *Chem. Rev.* **2016**, *116* (21), pp 12865–12919.
2. Harris, R.D.; Weiss, E.A. The Effect of an Exciton-Delocalizing Ligand on the Conductivity of Thin PbS Nanocrystal Films. Unpublished work.

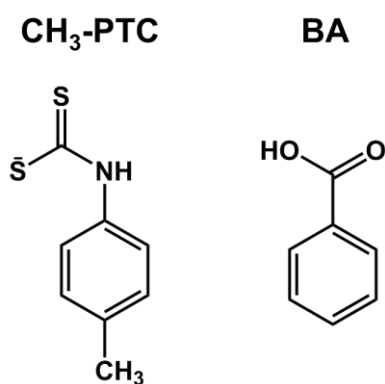
4.1 Chapter Summary

This chapter describes the increase in conductivity in lead sulfide quantum dot (PbS QD) films through treatment of the QDs with an exciton-delocalizing ligand, 4-methylphenyldithiocarbamate (CH₃-PTC). In this study, we demonstrate the potential of “so-called” strong coupling ligands(cite) to improve conductivity in QD thin films. We deposited between one and three monolayers of PbS QDs onto a glass substrate after treatment with either CH₃-PTC or benzoic acid (BA), which has a similar chemical structure and molecular length to CH₃-PTC but does not delocalize the QD exciton. We fabricated source and drain electrodes from a eutectic of gallium and indium (EGaIn) templated by polydimethylsiloxane (PDMS), and measured the current under bias, with 532-nm illumination or in the dark. Although the films were very fragile, which compromised their conductivity somewhat, we observed a greater film conductivity for films of CH₃-PTC-coated QDs than for films of BA-treated

QDs. When the QD films were treated with mixtures of CH₃-PTC and BA, we observe a conductive response only when the relative amount of CH₃-PTC is $\geq 75\%$. At concentrations of CH₃-PTC below this threshold, there is no detectable current through the film. Finally, we discuss some strategies to achieve substantial improvements to film durability and sample consistency.

4.2 Introduction

This chapter describes the effect of 4-methylphenyldithiocarbamate (CH₃-PTC), an exciton-



Scheme 4.1. The chemical structures of 4-methylphenyldithiocarbamate (CH₃-PTC) and benzoic acid (BA), the two QD ligands investigated in this study.

delocalizing ligand, on the conductivity of thin films of lead sulfide (PbS) nanocrystals (quantum dots, QDs). The goal of this project is to explore further avenues for increasing film conductivity beyond simple reduction of interparticle distance or the use of inorganic ligands to remove the interfacial energetic barrier imposed by the organic ligand shell. We prepared thin films of

PbS QDs with native oleic acid (OA) ligands and performed ligand exchanges with either CH₃-PTC or benzoic acid (BA) (**Scheme 4.1**). To ensure that the improved conductivity in PbS QD films is due to the unique coupling properties of CH₃-PTC and not the shortened interparticle distance alone, BA was chosen as the control ligand because it has a similar molecular length to CH₃-PTC, but does not delocalize the exciton. We then obtained ground state absorption measurements for each of the films and measured their conductivity.

We have shown previously that PTC decreases confinement of the excitonic hole for PbS, CdS, and CdSe QDs in solution and in films.^{26,52,55,128} Exciton-delocalizing ligands, while longer in length than thiocyanates and other commonly used ligands for film treatments, lower the energetic barrier to

charge transfer by coupling electronically to the inorganic QD core, and thereby improve charge transport through a film.

QDs are of interest for use in many different types of electronic devices, such as solar cells, LEDs, and transistors. The characteristics of QDs that make them appealing for such applications are their size-tunable optoelectronic properties,^{4,163} solution processability, and potential for multiple exciton generation from a single photon.¹⁶⁴ The current limitations of QD devices are toxicity (which is being addressed with the synthesis of heavy metal-free QDs)¹⁶⁵⁻¹⁶⁷ and the insulating organic ligand shell that arises from hot-injection synthesis procedures. The high-boiling point surfactants necessary to synthesize high-quality QDs (usually anionic carboxylic or phosphonic acids) typically contain long, aliphatic carbon chains that impose a high energetic barrier to charge transfer. Exchanging these insulating ligands for non-insulating ligands improves the likelihood of charge transfer.

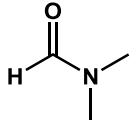
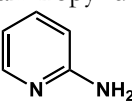
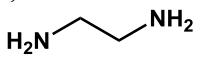
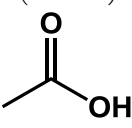
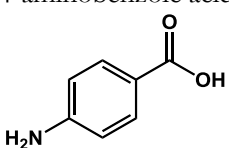
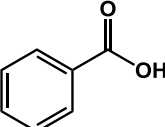
There are many examples in the literature of improved conductivity or overall efficiency in QD-based electronic devices achieved by increasing inter-QD coupling *via* ligand exchange with a shorter or more conjugated ligand.¹⁶⁸⁻¹⁸⁹ Thiols, for example, have been used in numerous studies to improve conductivity of QD films, due to their high binding affinity to the QD surface.^{143,169,172,176}

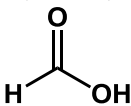
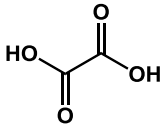
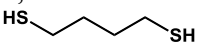
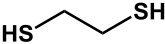
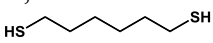
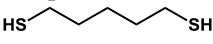
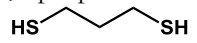
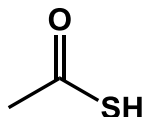
Treatment of QDs in films with short organic or inorganic ligands potentially induces exciton delocalization by facilitating inter-QD coupling.^{6,60,190-192} Zhang *et al.* showed that exchanging the native aliphatic ligands of CdSe QDs and CdSe/CdS/ZnS core/multishell QDs with inorganic metal chalcogenide ligands (SnS₄⁴⁻) resulted in delocalization of excitons in the solution phase and enhanced inter-QD coupling in the solid phase, as supported by a bathochromic shift in the optical spectra of solution-phase samples and enhanced conductivity of films. The Johnson group measured the apparent excitonic radius of inorganic-ligand-treated CdSe QD films (metal chalcogenides) *via* ultrafast cross-polarized transient grating spectroscopy and demonstrated that the exciton is more delocalized

in QDs with metal chalcogenide ligands and pyridine ligands (after thermally annealing) than with oleate ligands, and that the effective exciton size can expand to more than two QDs.⁶⁰ Wessels *et al.* demonstrated that films of gold nanoparticles cross-linked with difunctionalized *p*-phenylenebis(dithiocarbamate) show a 10^6 -fold improvement in conductivity over similar films treated with thiols.⁸⁷

Molecular length and conjugation may be combined with other properties of the ligand, such as the ability to shift the excitonic peak,^{143,193-194} as a means to improve device efficiency. **Table 4.1** and **Table 4.2** list the electrical properties of QD films (in the dark and under illumination, respectively), as a function of capping ligand. This study provides evidence that treatment of QD films with CH₃-PTC is a potentially advantageous processing step in the fabrication of QD-based devices. Increasing QD-QD coupling within films with the addition of CH₃-PTC has enormous potential to improve the efficacy of such devices.

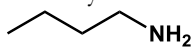
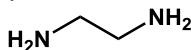
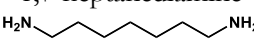
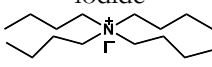
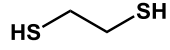
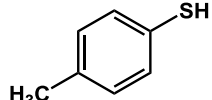
Table 4.1. Field-Effect Measurements of the Electrical Properties of Colloidal QD Films.

| Capping Ligand ^a | QD (diameter) | Conductivity (S cm ⁻¹) | Mobility (cm ² V ⁻¹ s ⁻¹) (h ⁺ or e ⁻) | Carrier Density (cm ⁻³) | Ref |
|--|--|--|--|---|------------|
| dimethylformamide (neat)  | PbSe (6.7 nm) | 2×10^{-4} | Not reported | Not reported | 168 |
| 2-aminopyridine  | In ₂ O ₃ (5.3 nm) | Not reported | 9.5 ± 0.2 (e ⁻) | Not reported | 179 |
| 1,2-ethanediamine  | PbS Cu ₂ S (4.4 nm) | 1.7×10^{-5} 3.2×10^{-1} | Not reported 5×10^{-3} (h ⁺) | Not reported 4×10^{20} | 174 172 |
| hydrazine (1 M) H₂N—NH₂ | PbSe (3.7 nm) | $(6 \pm 0.5) \times 10^{-3}$ | Not reported | Not reported | 171 |
| methylamine (1 M) H₃C—NH₂ | PbSe (3.7 nm) | $(1 \pm 0.95) \times 10^{-5}$ | Not reported | Not reported | 171 |
| acetic acid (10 mM)  | PbS (8.8 nm) PbSe (6.1 nm) | 1.1×10^{-4} 6.2×10^{-4} | $(3.8 \pm 0.5) \times 10^{-4}$ (h ⁺) $(6.9 \pm 1.6) \times 10^{-3}$ (h ⁺) | 2×10^{18} 6×10^{17} | 182 182 |
| 4-aminobenzoic acid  | PbSe (6.0 nm) In ₂ O ₃ (5.3 nm) | 2.3×10^{-3} Not reported | $(6.0 \pm 0.3) \times 10^{-3}$ (h ⁺) 2.6 ± 0.2 (e ⁻) | 2×10^{18} Not reported | 182 179 |
| methoxide CH₃O⁻ | PbSe (6.4 nm) | 5.0×10^{-2} | $(3.9 \pm 1.0) \times 10^{-1}$ (h ⁺) | $(8 \pm 2) \times 10^{17}$ | 194 |
| benzoic acid  | In ₂ O ₃ (5.3 nm) | Not reported | 3.07 ± 1.1 (e ⁻) | Not reported | 179 |

| | | | | | |
|---|-------------------------------|-------------------------------|--|-----------------------|-----|
| formic acid (10 mM) | PbS (8.8 nm) | 7.6×10^{-4} | $(2.4 \pm 0.7) \times 10^{-3}$ (h ⁺) | 2×10^{18} | 182 |
|  | PbSe (6.1 nm) | 1.0×10^{-2} | $(3.7 \pm 0.1) \times 10^{-2}$ (h ⁺) | 2×10^{18} | 182 |
| | PbSe (6.0 nm) | 4.3×10^{-2} | $(2.3 \pm 0.4) \times 10^{-2}$ (h ⁺) | 1×10^{19} | 182 |
| Oxalic acid (1 mM) | PbS (8.8 nm) | 3.2×10^{-5} | $(1.5 \pm 0.4) \times 10^{-4}$ (h ⁺) | 1×10^{18} | 182 |
|  | PbSe (6.1 nm) | 5.3×10^{-4} | $(2.3 \pm 1.5) \times 10^{-3}$ (h ⁺) | 2×10^{18} | 182 |
| | PbSe (6.0 nm) | 1.0×10^{-3} | $(2.5 \pm 0.2) \times 10^{-3}$ (h ⁺) | 3×10^{18} | 182 |
| (NH ₄) ₂ S | Cu _{2-x} S (5 nm) | 5.59 | 3.78 (h ⁺) | 9.42×10^{18} | 177 |
| 1,4-butanedithiol | PbSe (6.1 nm) | Not reported | 5×10^{-3} (e ⁻) | Not reported | 186 |
|  | | | | | |
| 1,2-ethanedithiol | Cu ₂ S (4.4 nm) | 6.4×10^{-5} | 2×10^{-5} (h ⁺) | 2×10^{19} | 172 |
|  | | | | | |
| | PbS (4.4 nm) | Not Reported | 8×10^{-3} (e ⁻) | Not reported | 176 |
| | PbS (5 nm) | 6×10^{-7} | 1×10^{-4} (h ⁺) | 2×10^{16} | 169 |
| | PbSe (3.7 nm) | $(1 \pm 0.55) \times 10^{-5}$ | Not reported | Not reported | 171 |
| | PbSe (5.8 nm) | 1×10^{-1} | Not reported | Not reported | 178 |
| | PbSe (6.1 nm) | Not reported | 7×10^{-2} (e ⁻) | Not reported | 186 |
| 1,6-hexanedithiol | PbSe (6.1 nm) | Not reported | 4×10^{-4} (e ⁻) | Not reported | 186 |
|  | | | | | |
| 1,5-pentanedithiol | PbSe (6.1 nm) | Not reported | 2×10^{-3} (e ⁻) | Not reported | 186 |
|  | | | | | |
| 1,3-propanedithiol | PbSe (6.1 nm) | Not reported | 4×10^{-2} (e ⁻) | Not reported | 186 |
|  | | | | | |
| thioacetic acid | PbS (~3 nm) | 4.4×10^{-7} | Not reported | Not reported | 189 |
|  | | | | | |

^aLigands listed in the protonation state reported in the cited reference.

Table 4.2. Measurements of Photo-electrical Properties of Colloidal QD Films.

| Capping Ligand ^a | QD (diameter) | Illumination Source or Technique | Conductivity (S cm ⁻¹) | Mobility (cm ² V ⁻¹ s ⁻¹) | Carrier Density (h ⁺ or e ⁻) (cm ⁻³) | Ref |
|---|------------------|---|---------------------------------------|--|--|-----|
| 1-butylamine  | CdSe (5.3 nm) | Incandescent light bulb (0.75 mW/cm ²) | 2×10^{-5} | 2×10^{-4} (e ⁻) | 6.2×10^{17} | 184 |
| 1,2-ethanediamine  | CdSe (2.8 nm) | TMRC | Not reported | 4×10^{-3} (e ⁻ /h ⁺) ^b | Not reported | 181 |
| | PbSe (5.5 nm) | TRTS | 1.5 | 6.3 (e ⁻ /h ⁺) ^b | 1.5×10^{18} | 185 |
| 1,7-heptanediamine  | CdSe (5.3 nm) | Incandescent light bulb (0.75 mW/cm ²) | 2×10^{-8} | 6×10^{-6} (e ⁻) | 2.1×10^{16} | 184 |
| NaOH | CdSe (5.3 nm) | Incandescent light bulb (0.75 mW/cm ²) | 5×10^{-4} | 1×10^{-2} (e ⁻) | 3.1×10^{17} | 184 |
| tetrabutylammonium iodide  | PbSe (5.5 nm) | TRTS | 9×10^{-1} | 4.2 (e ⁻ /h ⁺) ^b | 1.3×10^{18} | 185 |
| NH ₄ SCN | PbSe (5.5 nm) | TRTS | 20 | 31 (e ⁻ /h ⁺) ^b | 4.0×10^{18} | 185 |
| Na ₂ S | PbSe (5.5 nm) | TRTS | 10 | 25 (e ⁻ /h ⁺) ^b | 2.5×10^{18} | 185 |
| SnS ₄ | CdSe (3.2 nm) | 150 W Xenon lamp | 5.2×10^{-1} | Not reported | Not reported | 183 |
| 1,2-ethanedithiol  | PbSe (5.5 nm) | TRTS | 1.5 | 5.8 (e ⁻ /h ⁺) ^b | 1.6×10^{18} | 185 |
| 4-methylthiophenol  | PbS (2.8 nm) | Solar-simulated illumination | 5×10^{-6} | 1×10^{-6} (h ⁺) | 5×10^{17} | 143 |

^aLigands listed in the protonation state reported in the cited reference.^bThe total mobility for both electron and hole.

4.3 Results and Discussion

4.3.1. The Effect of Film Thickness on the Optical and Electronic Properties of Ligand-

Exchanged QD Films. We fabricated a series of PbS QD films with one, two, and three monolayers (MLs), and characterized them by ground state absorption spectroscopy and potentiometry measurements using a procedure adapted from McPhail *et al.*⁶ Briefly, we submerged a float glass slide in 2-3 mL of acetonitrile (ACN), then pipetted 50 μ L of PbS QDs in hexanes on one side of the container, a polytetrafluoroethylene (PTFE) crucible (**Figure 4.1**). Due to the immiscibility of hexanes

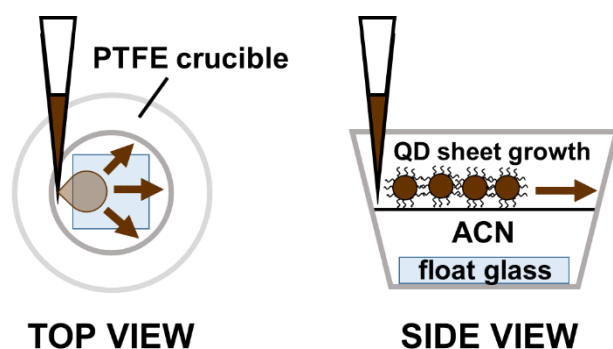


Figure 4.1. Schematic showing the film deposition technique used in this study. QDs in hexanes were pipetted over a float glass slide submerged in acetonitrile (ACN). Due to the immiscibility of hexanes and ACN, the QDs self-assemble into a single monolayer at the air-solvent interface.

and ACN, the QDs self-assemble into a single ML sheet across the surface of the ACN. We exchanged the native oleate ligands present on the QDs with either 4-methylphenyldithiocarbamate ($\text{CH}_3\text{-PTC}$) or benzoic acid (BA) by injecting a solution of one of these ligands dissolved in ACN below the surface of the QD film, and allowing the QDs to equilibrate for 30 minutes. To deposit the QD film on the glass, the ACN subphase was removed with a pipette. To create thicker films, this deposition process was repeated up to two more times on the same glass slide. We used an integrating sphere to characterize the overall optical properties of the film in the ground state. Upon exchange with $\text{CH}_3\text{-PTC}$, we observed a substantial bathochromic shift in the first excitonic peak of the 1-ML PbS QD film (**Figure 4.2A**). We quantify this bathochromic shift using the parameter ΔR , which is defined as the apparent increase in excitonic radius of the QD that would result in a similar bathochromic shift of the absorbance spectrum. PbS QDs have a maximum ΔR of ~ 0.15 nm at all sizes.⁵⁵ In our 1-ML films, we observed a 51-nm shift in

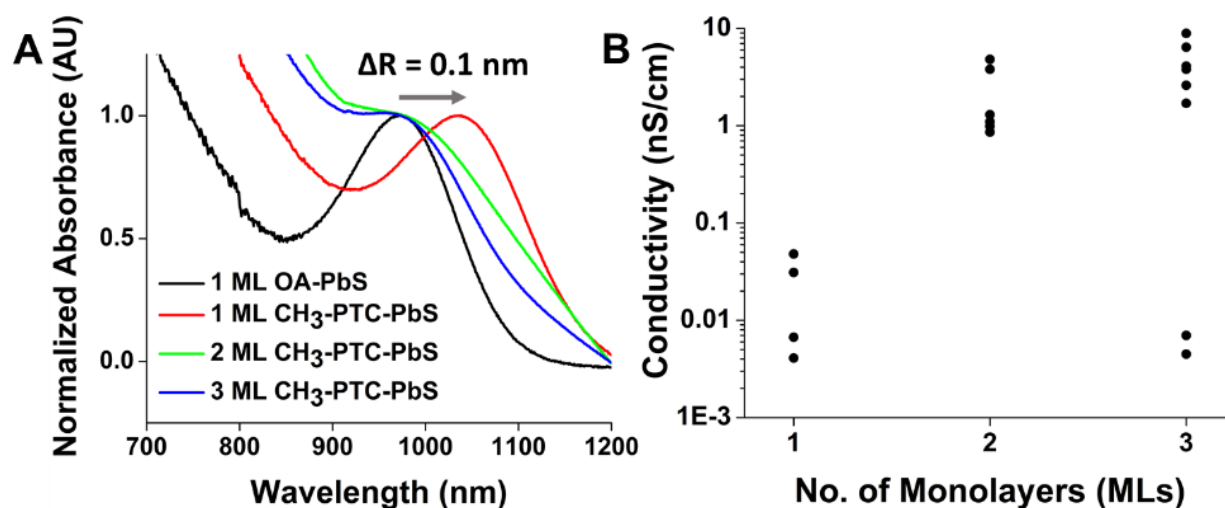


Figure 4.2. **A)** The bathochromic shift of the first excitonic peak of PbS QDs upon exchange with CH₃-PTC, in a QD film composed of one to three QD monolayers. We quantify the bathochromic shift using the parameter ΔR , the apparent increase in excitonic radius of the QDs, which we obtain from empirically derived sizing curves.⁴ **B)** A plot of the measured conductivity (in the dark) of CH₃-PTC-treated PbS QD films as a function of the film thickness in monolayers. Each data point corresponds to a single measurement on a section of QD film (some films had multiple measurements taken from different areas).

the position of the first excitonic peak, which corresponds to a ΔR of 0.1 nm. When we increased the thickness of the film to two and three monolayers, however, the observable bathochromic shift became negligible (**Figure 4.2A**). We believe that the increased film thickness caused some QDs to exchange with CH₃-PTC to a greater extent than others, leading to a distribution of bathochromic shifts that, in aggregate, show a broadened absorption spectrum rather than a clearly defined bathochromic shift.

In terms of measurable conductivity, for films treated with CH₃-PTC, 1-ML PbS QD films had a conductivity of less than 0.1 nanosiemens/cm (nS/cm), whereas the overall conductivity generally increased with increasing film thickness (despite a great degree of variability). For films exchanged with CH₃-PTC, the relationship between film thickness and measured conductivity (in the dark) is shown in **Figure 4.2B**. We hypothesize that thicker CH₃-PTC-exchanged films have higher

conductivity because the deposition of each successive ML fills in cracks or vacancies left behind by the previous ML.

4.3.2. CH₃-PTC-exchanged PbS Films are More Conductive than BA-exchanged Films. We

treated PbS QD films with mixtures of CH₃-PTC and BA. We used BA, a non-delocalizing ligand of

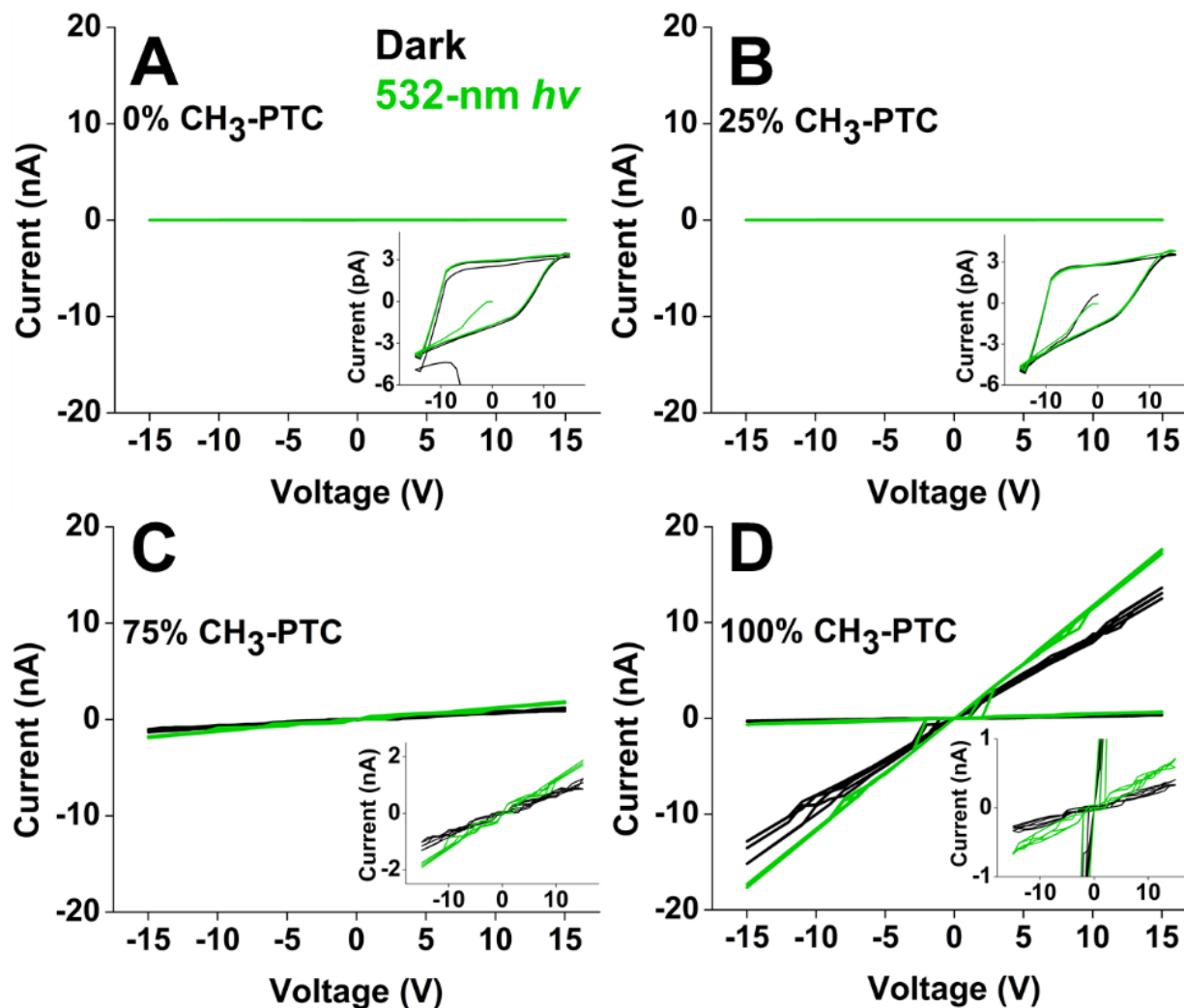


Figure 4.3. Current vs. voltage curves for PbS QD films treated with mixtures of benzoic acid (BA) and CH₃-PTC. Where there is less than 100% CH₃-PTC, the remainder of the ligand mixture is composed of BA (for example, 25% CH₃-PTC films were exchanged with a 1:3 mixture of CH₃-PTC:BA). We treated each QD film with approximately 1000 molar equivalents of ligand per QD. The black traces correspond to measurements taken in the dark, and the green traces correspond to measurements taken under 532-nm illumination. The insets show the same data zoomed in to show the y-axis range. From these figures, we observe hysteresis at low CH₃-PTC concentration, with a “turn-on” of conductivity that occurs between 25% and 75% CH₃-PTC. From 75% to 100% CH₃-PTC, we observe an order of magnitude increase in conductivity.

similar length and chemical structure to CH₃-PTC, as a control (refer to **Scheme 4.1**). The use of a ligand with similar (and even slightly shorter) length to CH₃-PTC allows us to attribute the difference in film conductivity to electronic effects at the QD-ligand interface, rather than differences in inter-QD spacing. We applied a varying bias from -15 V to +15 V for three cycles, and measured the resulting current.

The results of these experiments are plotted in **Figure 4.3**. For four identical PbS QD films, we exchanged the native oleate surface ligands with **A**) 100% BA, **B**) a 1:3 ratio of CH₃-PTC to BA, **C**) a 3:1 ratio of CH₃-PTC to BA, and **D**) 100% CH₃-PTC. We prepared these samples in duplicate; only one sample is shown in **A-C** for clarity because the samples measured within a small error of one another. We show results from both duplicate films in **D** because they differ from one another. For **A-D**, we also show the inset to zoom in on the full range of measured current. From the plots in **Figure 4.3**, we observe that the strongest conductive response occurs for one of the samples in **D**, the 100% CH₃-PTC sample, which has a conductivity of 8.8 nS/cm in the dark and 12 nS/cm under 532-nm illumination. The other, less conductive sample has a conductivity of 0.2 nS/cm in the dark and 0.4 nS/cm under

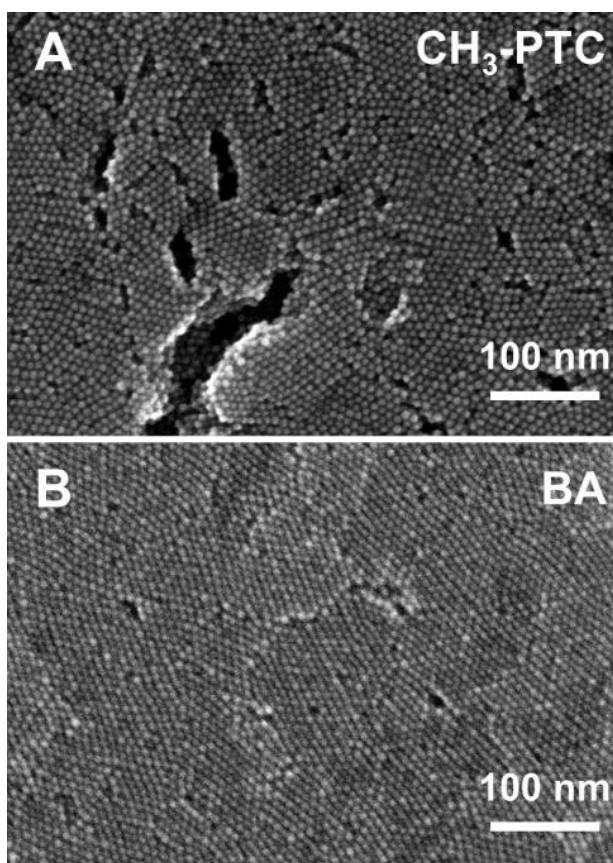


Figure 4.4. SEM images of PbS QD films exchanged with **A**) 4-methylphenyldithiocarbamate (CH₃-PTC) or **B**) benzoic acid (BA). We observe no major structural or packing differences between these two films; both have approximately hexagonally close-packed QDs with many cracks and defects present.

532-nm illumination. On average, however, the PbS QD films treated with 100% CH₃-PTC are the most conductive.

We observe no conductive response at all for samples treated with 0% and 25% CH₃-PTC. We measure a conductivity of 0.7 nS/cm in the dark and 1.2 nS/cm under 532-nm illumination for PbS QD films treated with a mixture of CH₃-PTC and BA containing 75% CH₃-PTC. From 25% to 75% CH₃-PTC, there is an activation of the conductivity, which indicates that a minimum threshold of CH₃-PTC is required to observe any conductive response of a PbS QD film. In comparing the measurements taken in the dark to those obtained under 532-nm illumination, we observe a slight increase in the measured conductivity under light, which is expected for visible excitation of PbS.

We believe that the discrepancy between the two samples treated with 100% CH₃-PTC is due to variability in film morphology on the microscale. **Figure 4.4** shows Scanning Electron Microscopy (SEM) images of our PbS QD films treated with either **A)** CH₃-PTC or **B)** BA. From these images, we observe ordered domains of ~ 10-100 nm, with defects and occasionally larger cracks. These larger cracks are qualitatively more prevalent in the CH₃-PTC-treated film, which is possibly due to the methyl group disrupting the packing order of the QDs. Both films approximate a hexagonal-close-packed structure.

4.4 Conclusions and Outlook

As discussed above, preparation and characterization of BA- and CH₃-PTC-treated films in duplicate gave inconsistent results for films exchanged with CH₃-PTC alone, to the tune of nearly one order of magnitude in conductivity. We attribute the inconsistency between films to the heterogeneity of the films as a result of the ligand exchange process and subsequent deposition. **Figure 4.5** depicts the same PbS QD film as **Figure 4.4A**, but at a weaker magnification, which further highlights the presence of microscale cracks.

We propose three strategies for continuing this work in order to solve the problems outlined above. Future work should focus on (i) optimizing the deposition of QD films to promote durability and homogeneity, (ii) utilizing cross-linking ligands to further stabilize the films and increase conductivity upon ligand exchange, and iii) improving the fabrication of electrodes used in the conductivity measurements to shorten the distance between the source and drain electrodes, which should also increase the overall measured conductivity.

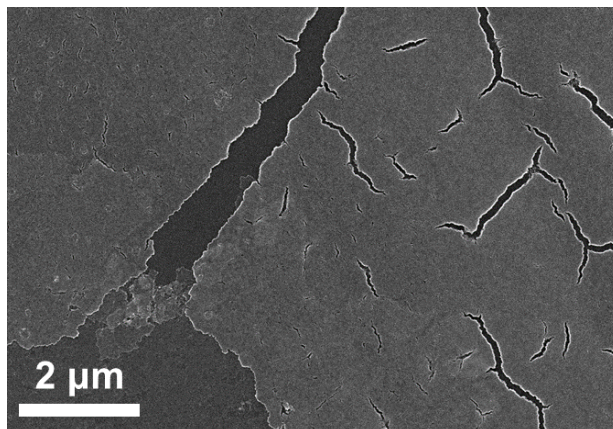


Figure 4.5. SEM image of a 2-ML PbS QD film treated with PTC. This image reveals large cracks and heterogeneities present in the film, which is the likely culprit of our reproducibility problems and lower than expected conductivity of PTC-treated PbS QD films.

The layer-by-layer (LbL) deposition of the QD films utilized in this study is likely the largest contributor to the film inhomogeneity described above. More contiguous films can be fabricated using spin-coating from a nonpolar solvent and subsequently performing the ligand exchange after deposition¹⁹⁵, or LbL dip-coating in alternating solutions of QDs and ligand.¹⁹⁶ In **Figure 4.6**, we treated two spin-coated PbS QD films with either **A)** BA or **B)** CH₃-PTC. Whereas our BA-treated LbL films displayed hysteresis, our BA-treated spin-coated films show a small conductive response. The maximum measured current, at an applied potential of +15 V, for CH₃-PTC-treated spin-coated PbS films is ~2 nA, whereas the maximum current for similarly prepared BA-treated films is ~20 pA (this corresponds to an illuminated conductivity of 0.83 and 8.2×10^{-3} nS/cm, respectively). The 100-fold improvement in conductivity going from BA to CH₃-PTC is a promising positive result, and the appearance of a conductive response for BA-treated films indicates that spin-coating produces films with fewer defects than our LbL deposition technique.

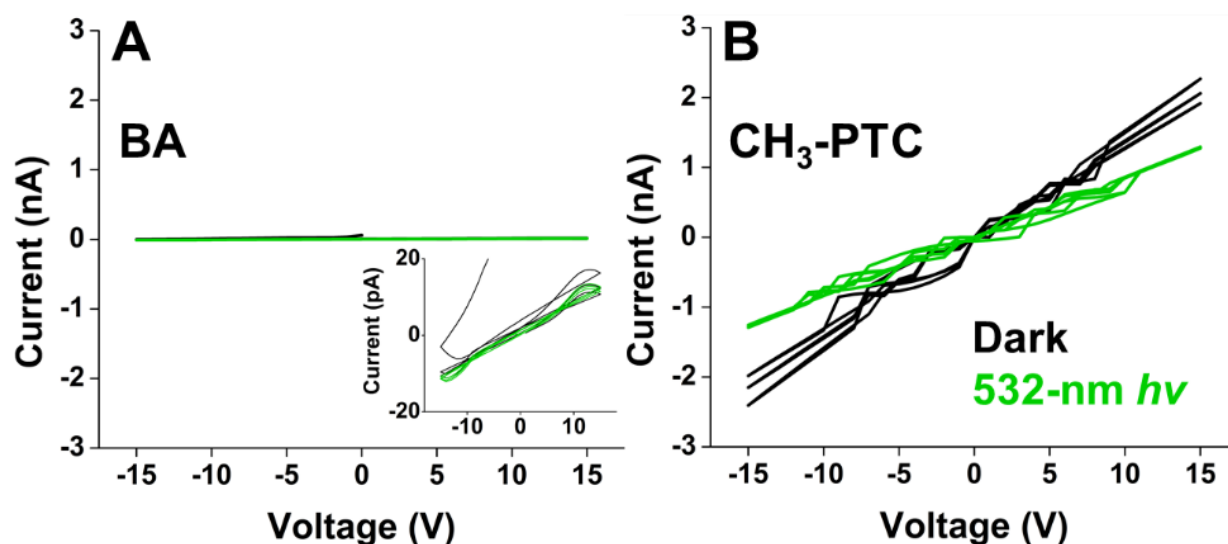


Figure 4.6. Current vs. voltage curves for spin-coated PbS QD films treated with **A)** BA and **B)** CH₃-PTC. The black traces correspond to measurements taken in the dark, and the green traces correspond to measurements taken under 532-nm illumination. The maximum current for CH₃-PTC-treated films is ~ 2 nA, and the corresponding maximum current for BA-treated PbS QD films is ~ 20 pA.

The use of cross-linking ligands may also improve the robustness of the QD films. Future experiments could involve the use of phenylene *bis*(dithiocarbamate) (PBTC) and terephthalic acid, the crosslinking analogues of CH₃-PTC and BA, as post-deposition treatments.

In addition to optimization of the film deposition and ligand exchange strategies, we also propose to increase the reproducibility of our conductivity measurements by using elastomeric stamps to fabricate source-drain electrodes with a smaller interelectrode spacing. This method would utilize a modified polydimethylsiloxane (PDMS) polymer as a soft stamp to transfer thermally evaporated gold electrodes to the QD film surface. **Figure 4.7** shows a proposed schematic of the electrode fabrication and transfer process, adapted from previous work.¹⁹⁷ In this proposed method, a slightly

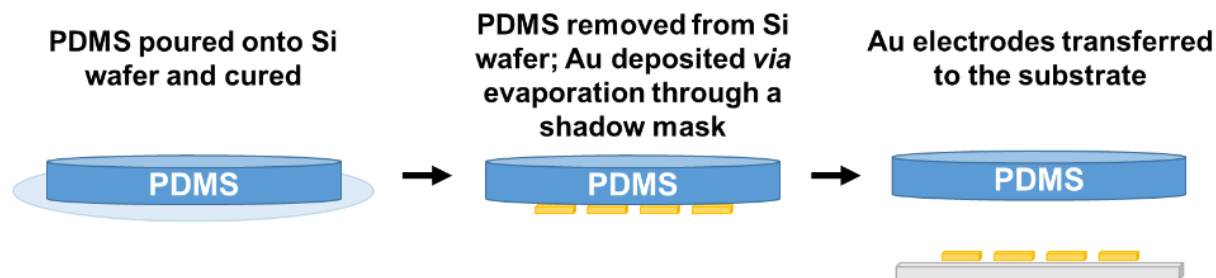


Figure 4.7. Schematic of the proposed future electrode fabrication and deposition process. First, a PDMS stamp is poured onto a smooth silicon wafer and cured using half of the typical amount of crosslinking agent. Once cured, the PDMS stamp is removed from the silicon wafer, and gold electrodes are deposited by thermal evaporation through a prefabricated shadow mask. Finally, the stamp is pressed onto the substrate to transfer the electrodes onto the surface of the QD film.

“undercooked” PDMS stamp is prepared on a silicon wafer by using about half the amount of crosslinking agent recommended by the manufacturer. Once cured, this soft stamp becomes a substrate for thermal evaporation of gold through a shadow mask, which would allow us a high degree of control over patterning, as well as precise formation of electrodes at smaller (0.1-100 μm) scales. We hypothesize that a more standardized electrode fabrication with a smaller path length for the charges to travel will decrease the likelihood of measuring conductivity across large film defects, and allow for a greater number of measurements on a single film.

Although our results are preliminary, this work has demonstrated a clear trend towards improving the conductivity of thin PbS QD films with an exciton-delocalizing ligand, $\text{CH}_3\text{-PTC}$, relative to a non-delocalizing ligand of similar molecular length and structure (BA). With the suggested improvements outlined above, a future graduate student could make great strides towards a robust publication-quality dataset.

4.5 Experimental Methods

PbS QD Synthesis and Purification. We synthesized PbS QDs ($R = 1.8 \text{ nm}$) using a procedure adapted from that reported by Hines and Scholes.⁴⁴ We added 2 mL of oleic acid (OA), 18 mL of 1-octadecene (ODE), and 0.36 g of PbO in a three-neck 50-mL round-bottom flask, and heated the mixture to

150 °C with stirring under nitrogen flow for 30 min until the solution became clear and colorless. After cooling the solution to 110 °C, we injected 8 mL of a hexamethyldisilathiane (TMS)₂S solution, initially prepared by adding 0.17 mL of (TMS)₂S in 8 mL of ODE, into the round-bottom flask. The PbO reaction mixture went from colorless to dark brown ~3 s after injection of (TMS)₂S. We allowed the QDs to grow for 10 min, and then submerged the flask in an ice bath until the reaction mixture reached room temperature.

We purified the QDs by equally dividing the room-temperature PbS QDs dispersions into two falcon tubes to which we added acetone in a 1:1 ratio by volume. The tubes were centrifuged at 3500 rpm for 5 min, which produced a brown pellet and a supernatant containing excess ODE. After removing the acetone, we redispersed the pellets in a minimal amount of hexanes, added methanol in 2:1 excess (by volume), and centrifuged the tubes at 3500 rpm for 5 min. The methanol wash also resulted in a brown pellet and a supernatant containing excess ligands and small nanocrystalline clusters. We repeated the methanol wash a second time, centrifuged the mixture, dried the resulting pellets over nitrogen, and redispersed them in chloroform to make stock solutions of PbS QDs.

Synthesis of Ammonium CH₃-PTC. We synthesized the ammonium salt of CH₃-PTC by adding two equivalents of carbon-disulfide drop-wise to one equivalent of 4-methylaniline in a rapidly stirring suspension of five equivalents of aqueous ammonium hydroxide (28-30%) at 0 °C, and stirring overnight. We washed the resulting white powder with chloroform and hexanes and dried under N₂ flow for several minutes.

Film Preparation and Ligand Exchange. We deposited monolayers of PbS QDs onto float glass slides *via* self-assembly at the liquid-air interface. First, we sonicated the glass slides for five minutes in methanol, followed by five minutes in acetone, to clean the surface. We gently dried the slides with a stream of nitrogen and placed them inside 25-mL Teflon crucibles. We added 2-3 mL acetonitrile to

each crucible, and gently trickled 50 μL of 15 μM PbS QDs in hexanes down the wall of the crucible and allowed the QDs to spread across the surface of the acetonitrile subphase. We allowed the layer of QDs to equilibrate for 30-60 s before injecting 1000 equivalents of PTC, dissolved in 50 μL acetonitrile, below the surface of the film. We covered the crucible with a watch glass and allowed the ligand exchange to proceed for 30 minutes.

To create a film with several monolayers, we added additional 50 μL aliquots of PbS QDs and PTC/acetonitrile solution as described above until we reached the desired film thickness.

Ground State Absorption Measurements. We acquired ground state absorption spectra on a Varian Cary 5000 spectrometer. The spectrometer was fitted with an integrating sphere so that we could measure the films directly. We corrected the baselines of all spectra with a virgin glass slide prior to measurement.

Electrode Fabrication. We prepared 2 mm diameter, circular eutectic gallium-indium (EGaIn) source and drain contacts with a 1 mm intercontact separation set in 6 mm diameter polydimethylsiloxane (PDMS) disks. These PDMS disks provided a template to hold the conformal EGaIn contacts within a well-defined contact area and separation distance; the electrometer's source and drain leads contacted the QD film directly through this EGaIn (**Figure 4.8**).⁶

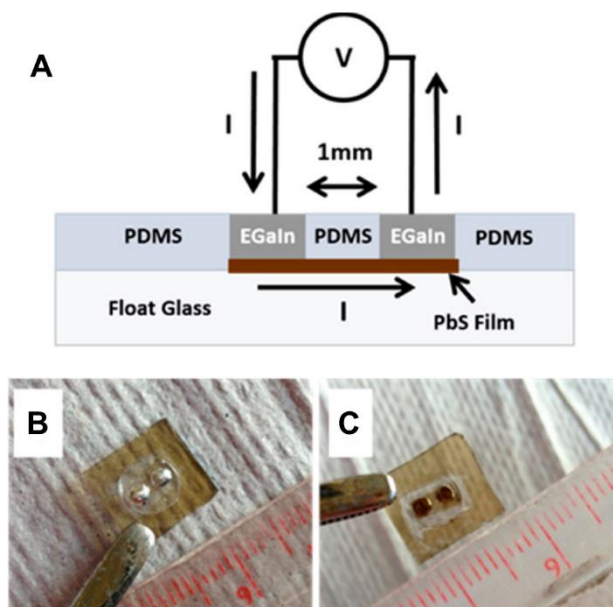


Figure 4.8. Our electrochemical measurement setup. **A)** Schematic of the PbS QD film on top of a float glass substrate. We used conformal electrodes fabricated from a eutectic of gallium and indium (EGaIn) templated by PDMS. We applied a potential across these electrodes and measured the resulting current across the film, for PbS QD films treated with different ligands. **B)** Top and **C)** bottom views of the EGaIn electrodes on top of a QD film. Adapted from McPhail *et al.*⁶

Conductivity Measurements. We performed all electrical measurements using a Keithley 6430 Sub-Femtoamp Remote SourceMeter controlled by a custom LabView 8.0 Virtual Instrument console. For photoresponse studies, we globally illuminated the film at 532 nm with a Thorlabs CPS 532 laser diode passed through a 20° square beam diffuser to produce 1 mW/cm² power density. All sample preparation and measurements were carried out under dry nitrogen atmosphere to prevent photooxidation of the film.⁶

Scanning Electron Microscopy. We performed field-emission scanning electron microscopy (FE-SEM) using a Hitachi SU8030 microscope with a 20 keV accelerating voltage and a 10 μA emission current. We prepared QD films as described above, except that p-type Si < 100>/SiO₂ wafers were used instead of glass slides.

5 INCREASED YIELD OF HOLE TRANSFER FROM CDS QDS TO A TETHERED ZINC PHTHALOCYANINE WITH AN EXCITON-DELOCALIZING LINKER

Adapted From: Harris, R.D.; Lian, S.; Weiss, E.A. Increased Yield and Rate of Hole Transfer from CdS QDs to a Tethered Zinc Phthalocyanine with an Exciton-Delocalizing Linker. Unpublished work.

5.1 Chapter Summary

This chapter describes the use of a strongly exciton-delocalizing linker, N-4-pyridinylcarbamodithioate, to improve the hole extraction efficiency from a photoexcited cadmium sulfide quantum dot (CdS QD) to a tethered zinc phthalocyanine acceptor relative to a moderately delocalizing linker, 4-mercaptopyridine. We selectively photoexcite the CdS QDs, and subsequently observe the appearance of a positive peak at 500 nm, which corresponds to the radical cation of zinc phthalocyanine. Although these results are promising, they are not yet definitive since we have yet to obtain transient absorption data from QD-linker and zinc phthalocyanine control samples. Future work on this project will involve optimizing the solvent or hole acceptor to achieve consistent solubility over time for all of our samples, in order to obtain these control spectra.

5.2 Introduction

This chapter describes the potential improvement in hole transfer (hT) yield and rate from a photoexcited cadmium sulfide quantum dot (CdS QD) to a zinc phthalocyanine (ZnPc) using an exciton-delocalizing molecular linker, N-4-pyridinylcarbamdithioate (pyr-NCS₂). The strongly delocalizing dithiocarbamate functionality should allow us to achieve a greater yield and rate of hole transfer relative to a moderately delocalizing linker, 4-mercaptopyridine (pyr-SH).

The use of QDs for applications such as photocatalysis or solar electricity generation requires the efficient separation of the exciton into an electron and hole. To reduce the probability of charge carrier recombination, these two charge carriers must be extracted on similar timescales. Due to the larger effective mass of the photoexcited hole, it tends to be the rate-limiting step (occurring at 10s of nanoseconds to 100s of picoseconds)¹⁹⁸⁻¹⁹⁹ in charge transfer processes as opposed to electron transfer (which occurs at 10s of picoseconds to 10s of femtoseconds).²⁰⁰⁻²⁰⁴ Increasing the rate of hole transfer, therefore, is more likely to reduce the incidence of charge carrier recombination.

In a previous paper, we demonstrated that phenylene bis(dithiocarbamate) (PBDT) linkers can be used to improve the yield of electron transfer from a photoexcited zinc porphyrin to a CdSe QD by increasing the number and proximity of porphyrin molecules bound to the QD surface.¹³³ Since PBDTs and their derivatives, such as phenyldithiocarbamate (PTC), are known to delocalize the excitonic hole, however, their use in improving electron transfer did not capitalize on their exciton-delocalizing properties to improve charge transfer. Our group's previous work on PTC-capped QDs established that PTC predominantly affects confinement of the hole, and should thereby improve hT via a delocalization mechanism.^{52,55,128}

In another previous study, we used a covalently bound linker-hole acceptor system to show that a dithiocarbamate delocalizing linker will increase the rate of charge transfer to a phenothiazine hole

acceptor by a factor of 20 relative to a carboxylate non-delocalizing linker.¹²⁹ In our system, we increase the yield and rate of hT using a dative linkage, which allows for increased flexibility and adaptability in the design and fabrication of QD-based devices where alternative or multiple molecular redox partners are desired.

In this work, we chose ZnPc as the hole acceptor because (i) it has the appropriate HOMO and LUMO energies for favorable hole transfer from a QD donor, and (ii) ZnPc and its radical cation possess optical features that do not interfere with absorption of CdS QDs. A number of studies have utilized phthalocyanines as photosensitizers for charge or energy transfer processes.²⁰⁵⁻²¹¹ Arvani *et al.* studied hT between QDs and zinc phthalocyanines, but this study did not examine the effect of surface chemistry on the yield and rate of hT within QD-molecule complexes.²⁰⁷ We will use surface chemistry to our advantage to optimize the hT process, and facilitate hT from the QD to the phthalocyanine acceptor.

We exchanged oleate-capped CdS QDs with increasing amounts (up to 100 added molar equivalents) of either pyr-NCS₂ or pyr-SH, and quantified the decrease in quantum confinement of the QDs using ground state absorption spectroscopy. We use the quantity “ ΔR ,” the apparent increase in QD excitonic radius, to describe the reduction in quantum confinement.

After treatment with either pyr-NCS₂ or pyr-SH, we added 100 equivalents of ZnPc to form donor-linker-acceptor complexes, CdS-NCS₂-ZnPc and CdS-SH-ZnPc, respectively. For the CdS-NHCS₂-ZnPc complex, we used transient absorption (TA) spectroscopy to photoexcite the CdS QDs at 420 nm, slightly red of their band edge absorption. We subsequently observed a signal at 500 nm, which we believe indicates hole transfer (hT) via the formation of the ZnPc radical cation (ZnPc⁺), the oxidized form of ZnPc. Due to issues maintaining solubility of the ZnPc in our solvent, DCM, we

were unable to obtain the corresponding spectra for CdS-SH-ZnPc or ZnPc alone. We address these challenges in the future work section below.

This work is the first to demonstrate the use of a non-covalent, hole-delocalizing linker ligand to improve the rate and yield of hole extraction from a photoexcited QD. The use of QD linker ligands, as opposed to covalently linking the ligand to the QD's molecular redox partner, allows ligand-treated QDs to be used as photosensitizers for a wide array of charge transfer partners for photovoltaic or photocatalytic applications.

5.3 Experimental

Synthesis and Purification of CdS Quantum Dots. We synthesized oleate-coated CdS QDs with $R = 1.9$ nm by adding 90% technical grade oleic acid (2.2 mL, 6.95 mmol), 90% technical grade octadecene (7.0 mL, 21.9 mmol), and cadmium oxide (0.180 g, 1.40 mmol) to a dry, three-neck round bottom flask, and heating the reaction mixture to 260 °C under an N₂ atmosphere with vigorous stirring. Once the solution became clear, we injected elemental sulfur (0.032 g, 1 mmol) dissolved in 2 mL of octadecene and allowed the QDs to grow for three minutes at 250 °C.

In order to extract the unused cadmium precursor, we added an equal volume of a 1:1 (v:v) mixture of CH₃OH and CHCl₃ to the QD colloidal dispersion and centrifuged the mixture at 3500 RPM for five minutes. The cadmium precursor separated into the bottom CH₃OH:CHCl₃ layer, while the QDs remained in the top layer of octadecene. We decanted this top layer, precipitated the QDs by the addition of ~8 mL acetone and centrifugation, discarded the supernatant, and redispersed the QDs in hexanes. We filtered the final redispersed solution using 0.45- μ m syringe filters to remove any remaining aggregated QDs.

Synthesis of the Triethylammonium Salt of N-4-pyridinylcarbamidithioate (pyr-NCS₂). We synthesized pyr-NCS₂ using a procedure adapted from Knott.²¹² We dissolved 4-aminopyridine (1.2 g, 12 mmol) in

7.5 mL hot pyridine (~ 80 °C) in a 50-mL 3-neck flask. The solution was cooled to ~ 35 °C, and carbon disulfide (0.83 mL, 14 mmol) and triethylamine (2.0 mL, 14 mmol) were added. After ~ 16 h of gentle stirring, a pale orange solid formed in the flask. We then added 25 mL diethyl ether and gravity filtered the solid. We washed the solid with cold ethanol and dried it under nitrogen to obtain a light orange powder, which we stored in the freezer until use. ^1H NMR (500 MHz, Methanol- d_4) δ 8.30 (d, 2H), 8.10 (d, 2H), 3.62 (q, 2H), 1.18 (t, 3H); ^{13}C NMR (126 MHz, Methanol- d_4) δ 219.38, 160.15, 144.03, 116.33.

Ligand Exchange Procedure for the Formation of QD-ZnP Complexes. We performed ligand exchanges in dichloromethane (DCM) using methanol (MeOH) as a co-solvent for the ligand. We prepared 1- μM solutions of oleate-capped CdS QDs in DCM by diluting the appropriate amount of our stock solution. Then, we prepared 0.01-M solutions of our ligands in MeOH and added the desired volume of ligand to each sample. We also added the appropriate quantities of neat MeOH to each sample, such that each sample had the same amount of DCM and MeOH with varying amounts of ligand. We stirred the samples for 20 minutes to allow the system to come to equilibrium.

Steady State Absorption and Photoluminescence Spectroscopy. We acquired ground state absorption spectra of all samples on a Varian Cary 5000 spectrometer. We recorded the emission spectra of the samples with a Fluorolog-3 spectrofluorometer (Horiba Jobin Yvon). All spectra were recorded in a quartz cuvette with a 2-mm path length. We corrected the baselines of all spectra with neat solvent prior to measurement.

Transient Absorption Spectroscopy. All TA spectra were obtained on samples dispersed in degassed DCM in 2-mm quartz cuvettes with stirring. Our TA setup is described elsewhere.

Spectroelectrochemical Measurements. We performed spectroelectrochemistry on ZnPc in a 0.1M solution of tetrabutylammonium hexafluorophosphate as the supporting electrolyte in

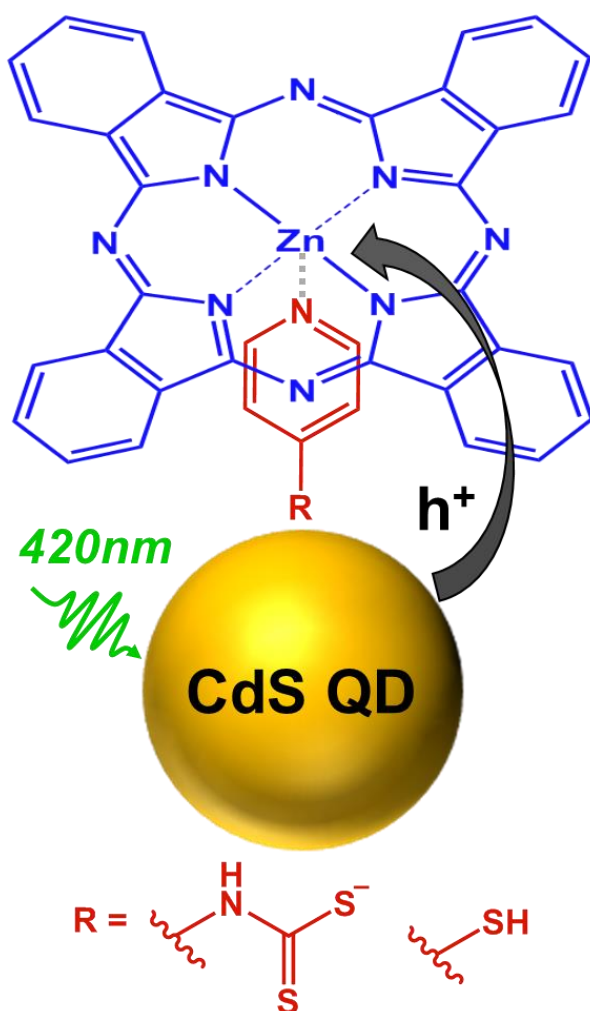


Figure 5.1. Schematic of the QD-linker-ZnPc conjugates employed in this study and photoinduced h^+ scheme. The QD is selectively excited at 430 nm, and subsequently transfers a hole to the ZnPc. We refer to these complexes as “CdS-NCS₂-ZnPc” and “CdS-SH-ZnPc” in the text.

complexes, so the overall coordination number of the Zn is five.²¹³

Figure 5.2 shows the ground state absorption spectra of CdS QDs, ZnPc, and a mixture of the two species in dichloromethane (DCM), as well as ZnPc with 50-150 molar equivalents of either the pyr-SH or pyr-NHCS₂ linkers and the QD-linker-ZnPc complexes. The spectrum of the CdS QDs is shown in black, and has a first excitonic absorption peak at 414 nm ($R = 1.9$ nm). The absorption

dichloromethane (DCM) to observe the electrochemical formation of ZnPc⁺. We used an indium tin oxide working electrode, platinum wire counterelectrode, and silver wire pseudoreference. We applied a positive 0.8 V potential and obtained ground state absorption spectra of the solution over time, from 0-75 minutes.

5.4 Preliminary Results and Discussion

Figure 5.1 shows a schematic of the donor-linker-acceptor system used in this study. The donor is CdS QDs with a radius of 1.9 nm, the acceptor is ZnPc, and they are linked together by a pyridine derivative with a head group that is either (i) strongly delocalizing, in the case of pyr-NCS₂, or (ii) moderately delocalizing, in the case of pyr-SH. ZnPc is known to coordinate to only a single pyridine ligand in these types of

spectrum of ZnPc only is shown in blue, and a mixture of CdS QDs with ZnPc is shown in navy. The band edge of these QDs has minimal overlap with the absorption of the ZnPc Soret band, so we are able to photoexcite our QDs selectively.

We also show the ground state absorption spectra for ZnPc mixed with both of our ligands, pyr-SH (teal-light green) and pyr-NHCS₂ (violet-maroon), as well as the fully linked CdS-linker-ZnPc complexes (lime and red for pyr-SH and pyr-NHCS₂, respectively). When exchanged with these ligands, the band edge of the QDs undergoes a bathochromic shift to ~420 nm. We observe a decrease in extinction coefficient of the ZnPc upon complexation with both pyr-NHCS₂ and pyr-SH, but no other optoelectronic effects.

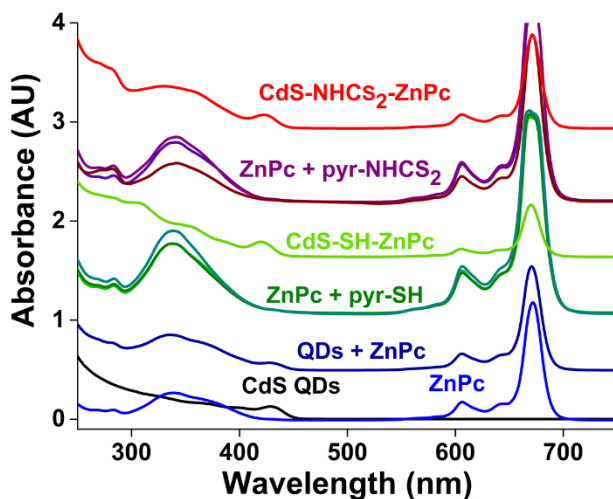


Figure 5.2. Ground state absorption spectra of the CdS QDs (black), ZnPc (blue), a mixture of CdS QDs with 250 molar equivalents of ZnPc (navy), ZnPc with 50-150 molar equivalents of pyr-SH (teal-light green), CdS-SH-ZnPc (lime green), ZnPc with 50-150 molar equivalents of pyr-NHCS₂ (violet-maroon), and CdS-NHCS₂-ZnPc (red). Spectra have been vertically offset for clarity.

In order to link the ZnPc hole acceptor to the QDs, we first performed ligand exchanges with either (i) pyr-NCS₂ or (ii) pyr-SH to replace some of the native oleate ligands on the QD surface. Both of these ligands induce a bathochromic shift in the first excitonic absorption peak of the QDs, **Figure 5.3A**. When we added more than 100 equivalents of our ligands, we observed aggregation of the QDs. To obtain a reliable ΔR for these samples, we collected an absorbance spectrum before and after filtering the QD-ligand mixtures through a 0.2 μm PTFE membrane, and rely on the peak position of the post-filtration spectrum to calculate ΔR . We show only the normalized spectra of filtered samples in **Figure 5.3A**. The increase in excitonic radius, in this case, should be due only to QD-ligand

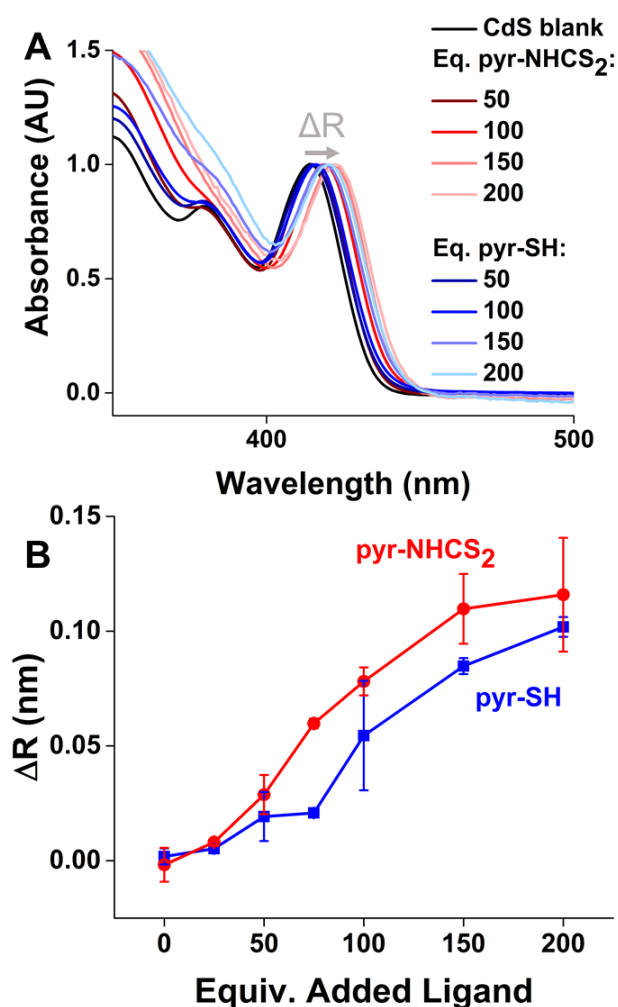


Figure 5.3. A) Normalized ground state absorption spectra for CdS QDs exchanged with 50–200 equivalents of pyr-NCS₂ (shades of red) and pyr-SH (shades of blue). B) Plot of ΔR , the apparent increase in excitonic radius, as a function of added ligand (pyr-NCS₂ or pyr-SH). The points and error bars correspond to the average and standard deviation, respectively, of three identically prepared samples of oleate-capped CdS QDs exchanged with one of these ligands. For the same quantity of ligand added to the CdS QDs, the pyr-NCS₂ delocalizes the QD exciton to a greater degree than pyr-SH. To obtain these ΔR values, we took the average first excitonic peak of six blank CdS QD samples, and used this peak position as R_{init} . The value of ΔR is equal to $R - R_{\text{init}}$, where R is calculated from λ_{abs} using the calibration curves from Yu *et al.*⁴

coupling and not aggregation of the QDs. In order to successfully synthesize the full CdS-linker-ZnPc complexes, we add no more than 100 molar equivalents of each linker ligand.

We quantify the extent of this bathochromic shift using the parameter ΔR ($R - R_{\text{init}}$), the apparent increase in excitonic radius, which we determine by converting the position of the first excitonic peak of the QDs from λ_{abs} to excitonic radius R using experimentally derived calibration curves from Yu *et al.*⁴ Figure 5.3B shows a plot of ΔR vs. the number of added molar equivalents of pyr-NCS₂ (red) or pyr-SH (blue). The R_{init} value used for 50, 100, 150, and 200 molar equivalents of added ligand in this plot is the average of six blank CdS QD samples. The points at zero added equivalents of ligand on this plot arise from performing the $R - R_{\text{init}}$ calculation for each individual sample relative to this average. The points and error bars correspond to the average and standard deviation, respectively, of the ΔR of three identically prepared mixtures of CdS QDs and added ligand.

The points at 25 and 75 added equivalents were obtained on a different day, so for these points, the R_{init} value used is the average of three blank CdS QD samples prepared at the same time. The ΔR points and error bars are calculated as described above.

From this plot, we see that, while both pyr-NCS₂ and pyr-SH cause a bathochromic shift in the first excitonic absorption peak of CdS QDs, pyr-NCS₂ delocalizes the exciton to a greater extent. We therefore expect more efficient hole transfer from the QD to the ZnPc using the pyr-NHCS₂ linker.

We attempted TA experiments to show the formation of the oxidized form of ZnPc, ZnPc⁺, upon selective excitation of the CdS QD. The full TA spectra from 1-2000 ps are shown in **Figure 5.4A**. The bleach at 606 nm corresponds to direct absorption by the Q-band of ZnPc. The large absorption feature at 450 nm and below is due to the excitation wavelength at 420 nm.

Upon direct excitation of the QD, we observe

a positive peak at 500 nm that decays over time. We compare this signal to our spectroelectrochemical

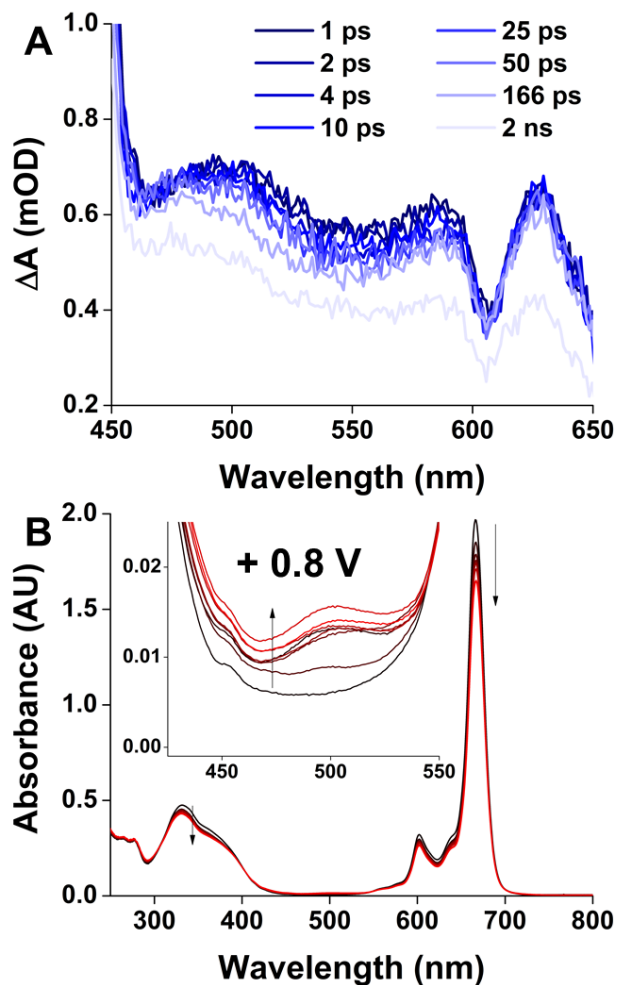


Figure 5.4. **A)** Full TA spectra of the CdS-NHCS₂-ZnPc complex from 1-2000 ps after excitation at 420 nm. The bleach at 606 nm corresponds to direct absorption of the ZnPc Q-band. The peak at 500 nm appears to correspond to the oxidized form of ZnPc, ZnPc⁺. The large absorption below 450 nm is from the excitation at 420 nm. **B)** Spectroelectrochemistry of ZnPc in DCM, with an applied potential of +0.8 V vs. Ag (pseudoreference). The gradient from black to red shows an increase in time (0-75 minutes). Over time, the Soret and Q-band of neutral ZnPc (325 and 680 nm, respectively) decrease, and we observe the appearance of a peak at 500 nm, which corresponds to the radical cation of ZnPc.³

data, **Figure 5.4B**. We applied a +0.8 V potential relative to a silver wire pseudoreference, and observed the evolution of a peak at 500 nm. This evidence, as well as evidence from the literature,³ indicate possible rapid hole transfer from the photoexcited QD to the ZnPc using a pyr-NHCS₂ linker.

5.5 Conclusions and Future Work

Thus far, we have established that the oxidized form of ZnPc, ZnPc⁺, has an optical signal at 500 nm. Direct excitation of CdS QDs in our CdS-NHCS₂-ZnPc complex shows a positive signal at this wavelength, but more control experiments are necessary to verify the formation of this species, as well as to determine the relative efficiencies of photoinduced hole transfer for both pyr-SH and pyr-NHCS₂ linkers. For these experiments to be successful, we must first address the issue of solubility of the ZnPc and its complexes with QDs.

5.5.1. Alternatives to DCM. ZnPc is only marginally soluble in our chosen solvent, DCM. While the achievable concentration of ZnPc is sufficient for electrochemical and spectroelectrochemical analysis, its instability at the concentrations necessary for transient absorption spectroscopy poses a problem. Solubility studies conducted on ZnPc indicate that more polar solvents, such as DMSO, might solubilize the ZnPc more effectively.²¹⁴ Unfortunately, our attempts at electrochemical oxidation of the ZnPc in DMSO were unsuccessful, likely because the DMSO donates an electron as soon as the ZnPc⁺ is formed.²¹⁵

Additionally, we must also consider the solubility of the CdS QDs, which are primarily capped with nonpolar oleate. Ligand exchanges are possible to bring the QDs into a more polar solvent, but as we observed with DMSO, polar solvents with basic character do not allow for cation formation. Of the solvents studied by Ghani *et al.*, the only nonpolar, nonbasic solvent in which ZnPc is measurably soluble is anisole.²¹⁴ Immediate next steps would include electrochemical oxidation of ZnPc in anisole to observe formation of the radical cation species, as well as exchanges of the CdS

QDs with both of our linker ligands in this solvent. If the solubility of our CdS-linker-ZnPc complex can be maintained in anisole, we hope to perform transient absorption studies on both complexes, as well as QD-linker and ZnPc by themselves as controls.

5.5.2. Chemical Functionalization of ZnPc. If the unsubstituted ZnPc still cannot be solubilized using anisole, we propose to modify it chemically to increase the solubility in nonpolar solvents such as DCM. This would be accomplished by either addition of thiobutyl or butoxy functional groups to the outer rings of the ZnPc, according to procedures detailed by Kobayashi *et al.*²¹⁶

6 CONCLUSIONS AND OUTLOOK

6.1 Dissertation Summary

This dissertation describes the exchange of native, electronically insulating ligands on QD surfaces for ligands that decrease the energetic barrier to quantum confinement. In Chapter 2, we introduced the characterization of the QD ligand shell using NMR. We discussed two instances of correlating QD photoluminescence with surface chemistry: i) the increase in PLQY of CdSe QDs with added PTC, and ii) the relatively constant PLQY of CdS QDs upon desorption of cadmium oleate from the surface.

In Chapter 3, we described the quantification of 4-hexylphenyldithiocarbamate (C6-PTC) on the surface of CdS QDs by ^1H NMR. In this study, we determined the relationship between the number of delocalizing ligands bound to the QD surface, and the degree of delocalization experienced by the exciton. This relationship, in which an increasing amount of delocalization occurs per bound (C6-PTC) as surface coverage increases, is heavily influenced by the packing geometry of the delocalizing ligands on the surface. Simulations of tightly packed and spread-out delocalizing ligands on a QD surface showed that, for the same percent surface coverage, the tightly packed ligands induce a greater degree of exciton delocalization than spread-out ligands.

The focus of this dissertation shifted in Chapter 4 to the fabrication of thin films of PbS QDs treated with either a delocalizing ligand, 4-methylphenyldithiocarbamate (CH_3 -PTC), or a non-delocalizing ligand of similar length, benzoic acid (BA). We found that CH_3 -PTC does improve the conductivity of films relative to BA, but our analysis was hampered by the mechanical fragility of the films. Improvements to film deposition and electrode fabrication have the potential to make the difference in film performance with different ligand treatments even more apparent.

Chapter 5 discussed the potential improvement in hole transfer efficiency from a photoexcited CdS QD to a zinc phthalocyanine molecule using a strongly exciton-delocalizing linker molecule. We are currently limited by solubility of the phthalocyanine, but expect to achieve stronger evidence for hole transfer improvement upon optimization of the solvent system.

Overall, this thesis combines quantitative NMR surface characterization and the use of exciton-delocalizing ligands to improve the optoelectronic properties of QDs by decreasing the energetic barrier to charge transfer. Both of these themes share the central idea of decreasing quantum confinement of QDs by manipulating the surface chemistry, which has the potential to lead to interesting ideas for rational design of functional nanomaterials based on strongly coupled quantum dot-ligand complexes.

6.2 Future Directions and Outlook

The effects of ligand adjacency on their ability to delocalize a QD exciton could be investigated further by attempting to create different spatial arrangements of ligands experimentally on the QD surface. Experimental verification of the greater delocalizing ability of tightly packed patches of delocalizing ligands relative to evenly distributed ligands, and even tuning the degree of phase segregation on the QD surface, would provide additional confirmation of ligand adjacency effects. The degree of phase segregation on the QD surface could be driven by the chemical functionalization of the PTC ligand with different substituent lengths, degrees of fluorination, branching, or phenyl functionalization,²¹⁷ and could be characterized by 1D and 2D NMR.²¹⁸

The ability to direct the degree of ligand adjacency in order to control the amount of delocalization would be a unique new capability to expand the “toolbox” of rational design of hierarchical materials. The work performed in this dissertation provides the foundation for further development of this capability.

In Chapter 4, where we utilized an exciton-delocalizing ligand to improve the conductivity of thin films of PbS QDs, we can improve the mechanical properties of the films using spin-coating rather than layer-by-layer deposition. We also propose the use of crosslinking analogues for CH₃-PTC and BA for additional durability.

In addition, we put forth a different procedure for electrode fabrication involving templated Au stamps, which will decrease the distance between source and drain electrodes and minimize the chances of measuring conductivity across a crack in the film.

Finally, we aim to improve the yield and/or rate of hole transfer from a photoexcited CdS QD to a tethered zinc phthalocyanine hole acceptor. Improvements in solubility of the zinc phthalocyanine will be made by changing the solvent system from dichloromethane to anisole, or *via* chemical functionalization of the outer rings of the phthalocyanine. Improving hole transfer to a redox partner through exciton delocalization is one of the major pathways towards eliminating charge recombination.

REFERENCES

- (1) Owen, J. The Coordination Chemistry of Nanocrystal Surfaces *Science* **2015**, *347*, 615-616.
- (2) Fritzing, B.; Capek, R. K.; Lambert, K.; Martins, J. C.; Hens, Z. Utilizing Self-Exchange to Address the Binding of Carboxylic Acid Ligands to CdSe Quantum Dots *J. Am. Chem. Soc.* **2010**, *132*, 10195-10201.
- (3) Nyokong, T.; Gasyna, Z.; Stillman, M. J. Phthalocyanine Pi-Cation-Radical Species - Photochemical and Electrochemical Preparation of [Znpc(-1)].+ in Solution *Inorg Chem* **1987**, *26*, 548-553.
- (4) Yu, W. W.; Qu, L. H.; Guo, W. Z.; Peng, X. G. Experimental Determination of the Extinction Coefficient of CdTe, CdSe, and CdS Nanocrystals *Chemistry of Materials* **2003**, *15*, 2854-2860.
- (5) Sonstrom, P.; Baumer, M. Supported Colloidal Nanoparticles in Heterogeneous Gas Phase Catalysis: On the Way to Tailored Catalysts *Phys Chem Chem Phys* **2011**, *13*, 19270-19284.
- (6) McPhail, M. R.; Weiss, E. A. Influence of Interparticle Structure on the Steady-State and Transient Current within Arrays of Thiocyanate-Treated PbS Nanocubes *Chem Mater* **2015**, *27*, 5605-5613.
- (7) de Mello Donegá, C.; SpringerLink (Online service) *Nanoparticles : Workhorses of Nanoscience*.
- (8) Rossetti, R.; Brus, L. Electron-Hole Recombination Emission as a Probe of Surface-Chemistry in Aqueous Cds Colloids *J Phys Chem-Us* **1982**, *86*, 4470-4472.
- (9) Efros, A. L.; Rosen, M. The Electronic Structure of Semiconductor Nanocrystals *Annu Rev Mater Sci* **2000**, *30*, 475-521.
- (10) Anderson, N. C.; Hendricks, M. P.; Choi, J. J.; Owen, J. S. Ligand Exchange and the Stoichiometry of Metal Chalcogenide Nanocrystals: Spectroscopic Observation of Facile Metal-Carboxylate Displacement and Binding *J. Am. Chem. Soc.* **2013**, *135*, 18536-18548.
- (11) Wei, H. H.-Y.; Evans, C. M.; Swartz, B. D.; Neukirch, A. J.; Young, J.; Prezhd, O. V.; Krauss, T. D. Colloidal Semiconductor Quantum Dots with Tunable Surface Composition *Nano Lett.* **2012**, *12*, 4465-4471.
- (12) Peterson, M. D.; Jensen, S. C.; Weinberg, D. J.; Weiss, E. A. Mechanisms for Adsorption of Methyl Viologen on CdS Quantum Dots *ACS Nano* **2014**, *8*, 2826-2837.
- (13) Morris-Cohen, A. J.; Donakowski, M. D.; Knowles, K. E.; Weiss, E. A. The Effect of a Common Purification Procedure on the Chemical Composition of the Surfaces of CdSe Quantum Dots Synthesized with Trioctylphosphine Oxide *J. Phys. Chem. C* **2010**, *114*, 897-906.
- (14) Jasieniak, J.; Mulvaney, P. From Cd-Rich to Se-Rich – the Manipulation of CdSe Nanocrystal Surface Stoichiometry *J. Am. Chem. Soc.* **2007**, *129*, 2841-2848.
- (15) Krause, M. M.; Kambhampati, P. Linking Surface Chemistry to Optical Properties of Semiconductor Nanocrystals *Phys. Chem. Chem. Phys.* **2015**, *17*, 18882-18894.
- (16) Moreels, I.; Lambert, K.; De Muynck, D.; Vanhaecke, F.; Poelman, D.; Martins, J. C.; Allan, G.; Hens, Z. Composition and Size-Dependent Extinction Coefficient of Colloidal PbSe Quantum Dots *Chemistry of Materials* **2007**, *19*, 6101-6106.
- (17) Omogo, B.; Aldana, J. F.; Heyes, C. D. Radiative and Nonradiative Lifetime Engineering of Quantum Dots in Multiple Solvents by Surface Atom Stoichiometry and Ligands *The Journal of Physical Chemistry C* **2013**, *117*, 2317-2327.

- (18) Sluydts, M.; De Nolf, K.; Van Speybroeck, V.; Cottenier, S.; Hens, Z. Ligand Addition Energies and the Stoichiometry of Colloidal Nanocrystals *ACS Nano* **2016**, *10*, 1462-1474.
- (19) Walsh, B. R.; Saari, J. I.; Krause, M. M.; Nick, R.; Coe-Sullivan, S.; Kambhampati, P. Controlling the Surface of Semiconductor Nanocrystals for Efficient Light Emission from Single Excitons to Multiexcitons *The Journal of Physical Chemistry C* **2015**, *119*, 16383-16389.
- (20) Cirillo, M.; Strubbe, F.; Neyts, K.; Hens, Z. Thermal Charging of Colloidal Quantum Dots in Apolar Solvents: A Current Transient Analysis *ACS Nano* **2011**, *5*, 1345-1352.
- (21) Liu, W.; Howarth, M.; Greytak, A. B.; Zheng, Y.; Nocera, D. G.; Ting, A. Y.; Bawendi, M. G. Compact Biocompatible Quantum Dots Functionalized for Cellular Imaging *Journal of the American Chemical Society* **2008**, *130*, 1274-1284.
- (22) Liu, J.; Kilina, S. V.; Tretiak, S.; Prezhdo, O. V. Ligands Slow Down Pure-Dephasing in Semiconductor Quantum Dots *ACS Nano* **2015**, *9*, 9106-9116.
- (23) Ulusoy, M.; Jonczyk, R.; Walter, J.-G.; Springer, S.; Lavrentieva, A.; Stahl, F.; Green, M.; Scheper, T. Aqueous Synthesis of Pegylated Quantum Dots with Increased Colloidal Stability and Reduced Cytotoxicity *Bioconjugate Chemistry* **2015**.
- (24) Kim, W. D.; Kim, J.-H.; Lee, S.; Lee, S.; Woo, J. Y.; Lee, K.; Chae, W.-S.; Jeong, S.; Bae, W. K.; McGuire, J. A. *et al.* Role of Surface States in Photocatalysis: Study of Chlorine-Passivated CdSe Nanocrystals for Photocatalytic Hydrogen Generation *Chemistry of Materials* **2016**.
- (25) Pan, Y.; Li, Y. R.; Zhao, Y.; Akins, D. L. Synthesis and Characterization of Quantum Dots: A Case Study Using PbS *Journal of Chemical Education* **2015**, *92*, 1860-1865.
- (26) Frederick, M. T.; Weiss, E. A. Relaxation of Exciton Confinement in CdSe Quantum Dots by Modification with a Conjugated Dithiocarbamate Ligand *ACS Nano* **2010**, *4*, 3195-3200.
- (27) Frederick, M. T.; Amin, V. A.; Weiss, E. A. Optical Properties of Strongly Coupled Quantum Dot-Ligand Systems *J. Phys. Chem. Lett.* **2013**, *4*, 634-640.
- (28) Amin, V. A.; Aruda, K. O.; Lau, B.; Rasmussen, A. M.; Edme, K.; Weiss, E. A. Dependence of the Band Gap of CdSe Quantum Dots on the Surface Coverage and Binding Mode of an Exciton-Delocalizing Ligand, Methylthiophenolate *The Journal of Physical Chemistry C* **2015**, *119*, 19423-19429.
- (29) Koole, R.; Luigjes, B.; Tachiya, M.; Pool, R.; Vlugt, T. J. H.; de Mello Donegá, C.; Meijerink, A.; Vanmaekelbergh, D. Differences in Cross-Link Chemistry between Rigid and Flexible Dithiol Molecules Revealed by Optical Studies of CdTe Quantum Dots *The Journal of Physical Chemistry C* **2007**, *111*, 11208-11215.
- (30) Liang, Y.; Thorne, J. E.; Parkinson, B. A. Controlling the Electronic Coupling between CdSe Quantum Dots and Thiol Capping Ligands Via Ph and Ligand Selection *Langmuir* **2012**, *28*, 11072-11077.
- (31) Giansante, C.; Infante, I.; Fabiano, E.; Grisorio, R.; Suranna, G. P.; Gigli, G. "Darker-Than-Black" PbS Quantum Dots: Enhancing Optical Absorption of Colloidal Semiconductor Nanocrystals Via Short Conjugated Ligands *Journal of the American Chemical Society* **2015**, *137*, 1875-1886.
- (32) Giansante, C.; Carbone, L.; Giannini, C.; Altamura, D.; Ameer, Z.; Maruccio, G.; Loiudice, A.; Belviso, M. R.; Cozzoli, P. D.; Rizzo, A. *et al.* Colloidal Arenethiolate-Capped PbS Quantum Dots: Optoelectronic Properties, Self-Assembly, and Application in Solution-Cast Photovoltaics *The Journal of Physical Chemistry C* **2013**, *117*, 13305-13317.
- (33) Azpiroz, J. M.; De Angelis, F. Ligand Induced Spectral Changes in CdSe Quantum Dots *ACS Applied Materials & Interfaces* **2015**, *7*, 19736-19745.

- (34) Gao, Y.; Peng, X. Crystal Structure Control of CdSe Nanocrystals in Growth and Nucleation: Dominating Effects of Surface Versus Interior Structure *Journal of the American Chemical Society* **2014**, *136*, 6724-6732.
- (35) Subila, K. B.; Kishore Kumar, G.; Shivaprasad, S. M.; George Thomas, K. Luminescence Properties of CdSe Quantum Dots: Role of Crystal Structure and Surface Composition *The Journal of Physical Chemistry Letters* **2013**, *4*, 2774-2779.
- (36) Mangel, S.; Aronovitch, E.; Enyashin, A. N.; Houben, L.; Bar-Sadan, M. Atomic-Scale Evolution of a Growing Core–Shell Nanoparticle *Journal of the American Chemical Society* **2014**, *136*, 12564-12567.
- (37) Orfield, N. J.; McBride, J. R.; Wang, F.; Buck, M. R.; Keene, J. D.; Reid, K. R.; Htoon, H.; Hollingsworth, J. A.; Rosenthal, S. J. Quantum Yield Heterogeneity among Single Nonblinking Quantum Dots Revealed by Atomic Structure–Quantum Optics Correlation *ACS Nano* **2016**.
- (38) Murray, C. B.; Norris, D. J.; Bawendi, M. G. Synthesis and Characterization of Nearly Monodisperse Cde (E = Sulfur, Selenium, Tellurium) Semiconductor Nanocrystallites *Journal of the American Chemical Society* **1993**, *115*, 8706-8715.
- (39) Aldana, J.; Wang, Y. A.; Peng, X. Photochemical Instability of CdSe Nanocrystals Coated by Hydrophilic Thiols *Journal of the American Chemical Society* **2001**, *123*, 8844-8850.
- (40) Young, A. G.; Al-Salim, N.; Green, D. P.; McQuillan, A. J. Attenuated Total Reflection Infrared Studies of Oleate and Trioctylphosphine Oxide Ligand Adsorption and Exchange Reactions on CdS Quantum Dot Films *Langmuir* **2008**, *24*, 3841-3849.
- (41) Tan, R.; Blom, D. A.; Ma, S.; Greytak, A. B. Probing Surface Saturation Conditions in Alternating Layer Growth of CdSe/CdS Core/Shell Quantum Dots *Chem. Mater.* **2013**, *25*, 3724-3736.
- (42) Qu, L.; Peng, X. Control of Photoluminescence Properties of CdSe Nanocrystals in Growth *Journal of the American Chemical Society* **2002**, *124*, 2049-2055.
- (43) García-Rodríguez, R.; Liu, H. Mechanistic Insights into the Role of Alkylamine in the Synthesis of CdSe Nanocrystals *Journal of the American Chemical Society* **2014**, *136*, 1968-1975.
- (44) Hines, M. A.; Scholes, G. D. Colloidal PbS Nanocrystals with Size-Tunable near-Infrared Emission: Observation of Post-Synthesis Self-Narrowing of the Particle Size Distribution *Advanced Materials* **2003**, *15*, 1844-1849.
- (45) Carbone, L.; Nobile, C.; De Giorgi, M.; Sala, F. D.; Morello, G.; Pompa, P.; Hytch, M.; Snoeck, E.; Fiore, A.; Franchini, I. R. *et al.* Synthesis and Micrometer-Scale Assembly of Colloidal CdSe/CdS Nanorods Prepared by a Seeded Growth Approach *Nano Letters* **2007**, *7*, 2942-2950.
- (46) Wheeler, L. M.; Nichols, A. W.; Chernomordik, B. D.; Anderson, N. C.; Beard, M. C.; Neale, N. R. All-Inorganic Germanium Nanocrystal Films by Cationic Ligand Exchange *Nano Letters* **2016**.
- (47) Hendricks, M. P.; Campos, M. P.; Cleveland, G. T.; Jen-La Plante, I.; Owen, J. S. A Tunable Library of Substituted Thiourea Precursors to Metal Sulfide Nanocrystals *Science* **2015**, *348*, 1226-1230.
- (48) Aldeek, F.; Hawkins, D.; Palomo, V.; Safi, M.; Palui, G.; Dawson, P. E.; Alabugin, I.; Mattoussi, H. Uv and Sunlight Driven Photoligation of Quantum Dots: Understanding the Photochemical Transformation of the Ligands *Journal of the American Chemical Society* **2015**, *137*, 2704-2714.

- (49) Peterson, M. D.; Cass, L. C.; Harris, R. D.; Edme, K.; Sung, K.; Weiss, E. A. The Role of Ligands in Determining the Exciton Relaxation Dynamics in Semiconductor Quantum Dots *Annual Review of Physical Chemistry, Vol 65* **2014**, *65*, 317-339.
- (50) Kilina, S.; Velizhanin, K. A.; Ivanov, S.; Prezhdo, O. V.; Tretiak, S. Surface Ligands Increase Photoexcitation Relaxation Rates in CdSe Quantum Dots *ACS Nano* **2012**, *6*, 6515-6524.
- (51) Guyot-Sionnest, P.; Wehrenberg, B.; Yu, D. Intraband Relaxation in CdSe Nanocrystals and the Strong Influence of the Surface Ligands *The Journal of Chemical Physics* **2005**, *123*, 074709.
- (52) Frederick, M. T.; Amin, V. A.; Swenson, N. K.; Ho, A. Y.; Weiss, E. A. Control of Exciton Confinement in Quantum Dot–Organic Complexes through Energetic Alignment of Interfacial Orbitals *Nano Letters* **2013**, *13*, 287-292.
- (53) Frederick, M. T.; Amin, V. A.; Weiss, E. A. Optical Properties of Strongly Coupled Quantum Dot–Ligand Systems *The Journal of Physical Chemistry Letters* **2013**, *4*, 634-640.
- (54) Hines, D. A.; Kamat, P. V. Recent Advances in Quantum Dot Surface Chemistry *Acs Applied Materials & Interfaces* **2014**, *6*, 3041-3057.
- (55) Frederick, M. T.; Amin, V. A.; Cass, L. C.; Weiss, E. A. A Molecule to Detect and Perturb the Confinement of Charge Carriers in Quantum Dots *Nano Lett* **2011**, *11*, 5455-5460.
- (56) Teunis, M. B.; Dolai, S.; Sardar, R. Effects of Surface-Passivating Ligands and Ultrasmall CdSe Nanocrystal Size on the Delocalization of Exciton Confinement *Langmuir* **2014**, *30*, 7851-7858.
- (57) Zhang, H.; Hu, B.; Sun, L.; Hovden, R.; Wise, F. W.; Muller, D. A.; Robinson, R. D. Surfactant Ligand Removal and Rational Fabrication of Inorganically Connected Quantum Dots *Nano Letters* **2011**, *11*, 5356-5361.
- (58) Turk, M. E.; Vora, P. M.; Fafarman, A. T.; Diroll, B. T.; Murray, C. B.; Kagan, C. R.; Kikkawa, J. M. Ultrafast Electron Trapping in Ligand-Exchanged Quantum Dot Assemblies *Acs Nano* **2015**, *9*, 1440-1447.
- (59) Liu, L.; Zhang, X.; Ji, L.; Li, H.; Yu, H.; Xu, F.; Hu, J.; Yang, D.; Dong, A. Size-Dependent Ligand Exchange of Colloidal CdSe Nanocrystals with S²⁻ Ions *RSC Advances* **2015**, *5*, 90570-90577.
- (60) Crisp, R. W.; Schrauben, J. N.; Beard, M. C.; Luther, J. M.; Johnson, J. C. Coherent Exciton Delocalization in Strongly Coupled Quantum Dot Arrays *Nano Letters* **2013**, *13*, 4862-4869.
- (61) Kovalenko, M. V.; Scheele, M.; Talapin, D. V. Colloidal Nanocrystals with Molecular Metal Chalcogenide Surface Ligands *Science* **2009**, *324*, 1417-1420.
- (62) Nag, A.; Kovalenko, M. V.; Lee, J.-S.; Liu, W.; Spokoyny, B.; Talapin, D. V. Metal-Free Inorganic Ligands for Colloidal Nanocrystals: S²⁻, Hs⁻, Se²⁻, Hse⁻, Te²⁻, Hte⁻, Tes³²⁻, Oh⁻, and Nh₂⁻ as Surface Ligands *Journal of the American Chemical Society* **2011**, *133*, 10612-10620.
- (63) Fafarman, A. T.; Koh, W.-k.; Diroll, B. T.; Kim, D. K.; Ko, D.-K.; Oh, S. J.; Ye, X.; Doan-Nguyen, V.; Crump, M. R.; Reifsnnyder, D. C. *et al.* Thiocyanate-Capped Nanocrystal Colloids: Vibrational Reporter of Surface Chemistry and Solution-Based Route to Enhanced Coupling in Nanocrystal Solids *Journal of the American Chemical Society* **2011**, *133*, 15753-15761.
- (64) Sarkar, S. K.; Chandrasekharan, N.; Gorer, S.; Hodes, G. Reversible Adsorption-Enhanced Quantum Confinement in Semiconductor Quantum Dots *Applied physics letters* **2002**, *81*, 5045-5047.
- (65) Hughes, B. K.; Ruddy, D. A.; Blackburn, J. L.; Smith, D. K.; Bergren, M. R.; Nozik, A. J.; Johnson, J. C.; Beard, M. C. Control of PbSe Quantum Dot Surface Chemistry and Photophysics Using an Alkylselenide Ligand *ACS Nano* **2012**, *6*, 5498-5506.

- (66) Baker, D. R.; Kamat, P. V. Tuning the Emission of CdSe Quantum Dots by Controlled Trap Enhancement *Langmuir* **2010**, *26*, 11272-11276.
- (67) Pan, Z.; Zhang, H.; Cheng, K.; Hou, Y.; Hua, J.; Zhong, X. Highly Efficient Inverted Type-I CdS/CdSe Core/Shell Structure QD-Sensitized Solar Cells *ACS Nano* **2012**, *6*, 3982-3991.
- (68) Buckley, J. J.; Couderc, E.; Greaney, M. J.; Munteanu, J.; Riche, C. T.; Bradforth, S. E.; Brutchey, R. L. Chalcogenol Ligand Toolbox for CdSe Nanocrystals and Their Influence on Exciton Relaxation Pathways *ACS Nano* **2014**, *8*, 2512-2521.
- (69) Majetich, S. A.; Carter, A. C.; Belot, J.; Mccullough, R. D. H-1-Nmr Characterization of the Cdse Nanocrystallite Surface *J Phys Chem-Us* **1994**, *98*, 13705-13710.
- (70) Zaera, F. Probing Liquid/Solid Interfaces at the Molecular Level *Chem Rev* **2012**, *112*, 2920-2986.
- (71) Hens, Z.; Martins, J. C. A Solution Nmr Toolbox for Characterizing the Surface Chemistry of Colloidal Nanocrystals *Chemistry of Materials* **2013**, *25*, 1211-1221.
- (72) Moreels, I.; Justo, Y.; De Geyter, B.; Haustraete, K.; Martins, J. C.; Hens, Z. Size-Tunable, Bright, and Stable PbS Quantum Dots: A Surface Chemistry Study *Acs Nano* **2011**, *5*, 2004-2012.
- (73) Sachleben, J. R.; Colvin, V.; Emsley, L.; Wooten, E. W.; Alivisatos, A. P. Solution-State Nmr Studies of the Surface Structure and Dynamics of Semiconductor Nanocrystals *J Phys Chem B* **1998**, *102*, 10117-10128.
- (74) Badia, A.; Gao, W.; Singh, S.; Demers, L.; Cuccia, L.; Reven, L. Structure and Chain Dynamics of Alkanethiol-Capped Gold Colloids *Langmuir* **1996**, *12*, 1262-1269.
- (75) Schmitt, H.; Badia, A.; Dickinson, L.; Reven, L.; Lennox, R. B. The Effect of Terminal Hydrogen Bonding on the Structure and Dynamics of Nanoparticle Self-Assembled Monolayers (Sams): An Nmr Dynamics Study *Advanced Materials* **1998**, *10*, 475-+.
- (76) Berrettini, M. G.; Braun, G.; Hu, J. G.; Strouse, G. F. Nmr Analysis of Surfaces and Interfaces in 2-Nm CdSe *Journal of the American Chemical Society* **2004**, *126*, 7063-7070.
- (77) Matylitsky, V. V.; Dworak, L.; Breus, V. V.; Basche, T.; Wachtveitl, J. Ultrafast Charge Separation in Multiexcited CdSe Quantum Dots Mediated by Adsorbed Electron Acceptors *Journal of the American Chemical Society* **2009**, *131*, 2424-2425.
- (78) Tyagi, P. Multilayer Edge Molecular Electronics Devices: A Review *J Mater Chem* **2011**, *21*, 4733-4742.
- (79) Ji, M. B.; Park, S.; Connor, S. T.; Mokari, T.; Cui, Y.; Gaffney, K. J. Efficient Multiple Exciton Generation Observed in Colloidal PbSe Quantum Dots with Temporally and Spectrally Resolved Intraband Excitation *Nano Letters* **2009**, *9*, 1217-1222.
- (80) Huang, J.; Huang, Z. Q.; Yang, Y.; Zhu, H. M.; Lian, T. Q. Multiple Exciton Dissociation in CdSe Quantum Dots by Ultrafast Electron Transfer to Adsorbed Methylene Blue *Journal of the American Chemical Society* **2010**, *132*, 4858-4864.
- (81) Konstantatos, G.; Howard, I.; Fischer, A.; Hoogland, S.; Clifford, J.; Klem, E.; Levina, L.; Sargent, E. H. Ultrasensitive Solution-Cast Quantum Dot Photodetectors *Nature* **2006**, *442*, 180-183.
- (82) Talapin, D. V.; Shevchenko, E. V.; Kornowski, A.; Gaponik, N.; Haase, M.; Rogach, A. L.; Weller, H. A New Approach to Crystallization of CdSe Nanoparticles into Ordered Three-Dimensional Superlattices *Advanced Materials* **2001**, *13*, 1868-1871.
- (83) Weiss, E. A.; Chiechi, R. C.; Kaufman, G. K.; Kriebel, J. K.; Li, Z. F.; Duati, M.; Rampi, M. A.; Whitesides, G. M. Influence of Defects on the Electrical Characteristics of Mercury-

- Drop Junctions: Self-Assembled Monolayers of N-Alkanethiolates on Rough and Smooth Silver *Journal of the American Chemical Society* **2007**, *129*, 4336-4349.
- (84) Jarosz, M. V.; Porter, V. J.; Fisher, B. R.; Kastner, M. A.; Bawendi, M. G. Photoconductivity Studies of Treated CdSe Quantum Dot Films Exhibiting Increased Exciton Ionization Efficiency *Phys Rev B* **2004**, *70*, 195327.
- (85) Lilly, G. D.; Whalley, A. C.; Grunder, S.; Valente, C.; Frederick, M. T.; Stoddart, J. F.; Weiss, E. A. Switchable Photoconductivity of Quantum Dot Films Using Cross-Linking Ligands with Light-Sensitive Structures *J Mater Chem* **2011**, *21*, 11492-11497.
- (86) Yu, W. W.; Peng, X. Formation of High-Quality CdS and Other II-VI Semiconductor Nanocrystals in Noncoordinating Solvents: Tunable Reactivity of Monomers *Angewandte Chemie, International Edition* **2002**, *41*, 2368-2371.
- (87) Wessels, J. M.; Nothofer, H. G.; Ford, W. E.; von Wrochem, F.; Scholz, F.; Vossmeier, T.; Schroedter, A.; Weller, H.; Yasuda, A. Optical and Electrical Properties of Three-Dimensional Interlinked Gold Nanoparticle Assemblies *Journal of the American Chemical Society* **2004**, *126*, 3349-3356.
- (88) Karlin, K. Progress in Inorganic Chemistry *Progress in Inorganic Chemistry; John Wiley & Sons, Inc* **2005**, *53*, 429-463.
- (89) Zotti, G.; Vercelli, B.; Berlin, A.; Virgili, T. Multi Layers of CdSe Nanocrystals and Bis(Dithiocarbamate) Linkers Displaying Record Photoconduction *J Phys Chem C* **2012**, *116*, 25689-25693.
- (90) Querner, C.; Reiss, P.; Bleuse, J.; Pron, A. Chelating Ligands for Nanocrystals' Surface Functionalization *Journal of the American Chemical Society* **2004**, *126*, 11574-11582.
- (91) Malicki, M.; Knowles, K. E.; Weiss, E. A. Gating of Hole Transfer from Photoexcited PbS Quantum Dots to Aminoferrocene by the Ligand Shell of the Dots *Chem Commun* **2013**, *49*, 4400-4402.
- (92) Wuister, S. F.; Donega, C. D.; Meijerink, A. Influence of Thiol Capping on the Exciton Luminescence and Decay Kinetics of CdTe and CdSe Quantum *J Phys Chem B* **2004**, *108*, 17393-17397.
- (93) Wang, C. W.; Moffitt, M. G. Surface-Tunable Photoluminescence from Block Copolymer-Stabilized Cadmium Sulfide Quantum Dots *Langmuir* **2004**, *20*, 11784-11796.
- (94) Hens, Z.; Martins, J. C. A Solution Nmr Toolbox for Characterizing the Surface Chemistry of Colloidal Nanocrystals *Chem. Mater.* **2013**, *25*, 1211-1221.
- (95) Fritzinger, B.; Moreels, I.; Lommens, P.; Koole, R.; Hens, Z.; Martins, J. C. In Situ Observation of Rapid Ligand Exchange in Colloidal Nanocrystal Suspensions Using Transfer Noe Nuclear Magnetic Resonance Spectroscopy *J. Am. Chem. Soc.* **2009**, *131*, 3024-3032.
- (96) Morris-Cohen, A. J.; Vasilenko, V.; Amin, V. A.; Reuter, M. G.; Weiss, E. A. Model for Adsorption of Ligands to Colloidal Quantum Dots with Concentration-Dependent Surface Structure *ACS Nano* **2012**, *6*, 557-565.
- (97) Krause, M. M.; Jethi, L.; Mack, T. G.; Kambhampati, P. Ligand Surface Chemistry Dictates Light Emission from Nanocrystals *J. Phys. Chem. Lett.* **2015**, *6*, 4292-4296.
- (98) Boulesbaa, A.; Issac, A.; Stockwell, D.; Huang, Z.; Huang, J.; Guo, J.; Lian, T. Ultrafast Charge Separation at CdS Quantum Dot/Rhodamine B Molecule Interface *J. Am. Chem. Soc.* **2007**, *129*, 15132-15133.

- (99) Kishimoto, F.; Imai, T.; Fujii, S.; Mochizuki, D.; Maitani, M. M.; Suzuki, E.; Wada, Y. Microwave-Enhanced Photocatalysis on CdS Quantum Dots - Evidence of Acceleration of Photoinduced Electron Transfer *Sci. Rep.* **2015**, *5*, 11308, 1-9.
- (100) Ge, L.; Zuo, F.; Liu, J.; Ma, Q.; Wang, C.; Sun, D.; Bartels, L.; Feng, P. Synthesis and Efficient Visible Light Photocatalytic Hydrogen Evolution of Polymeric G-C₃N₄ Coupled with CdS Quantum Dots *J. Phys. Chem. C* **2012**, *116*, 13708-13714.
- (101) Strandwitz, N. C.; Khan, A.; Boettcher, S. W.; Mikhailovsky, A. A.; Hawker, C. J.; Nguyen, T.-Q.; Stucky, G. D. One- and Two-Photon Induced Polymerization of Methylmethacrylate Using Colloidal CdS Semiconductor Quantum Dots *J. Am. Chem. Soc.* **2008**, *130*, 8280-8288.
- (102) Bradshaw, L. R.; Hauser, A.; McLaurin, E. J.; Gamelin, D. R. Luminescence Saturation Via Mn²⁺-Exciton Cross Relaxation in Colloidal Doped Semiconductor Nanocrystals *J. Phys. Chem. C* **2012**, *116*, 9300-9310.
- (103) Weinberg, D. J.; Dyar, S. M.; Khademi, Z.; Malicki, M.; Marder, S. R.; Wasielewski, M. R.; Weiss, E. A. Spin-Selective Charge Recombination in Complexes of CdS Quantum Dots and Organic Hole Acceptors *J. Am. Chem. Soc.* **2014**, *136*, 14513-14518.
- (104) Filella, M.; Town, R. M.; Bugarín, M. G. Cadmium Succinate and Cadmium Malate Stability Constants Revisited *J. Chem. Eng. Data* **1999**, *44*, 1009-1019.
- (105) McPhail, M. R.; Weiss, E. A. Role of Organosulfur Compounds in the Growth and Final Surface Chemistry of PbS Quantum Dots *Chem. Mater.* **2014**, *26*, 3377-3384.
- (106) Resch, U.; Eychmueller, A.; Haase, M.; Weller, H. Absorption and Fluorescence Behavior of Redispersible Cadmium Sulfide Colloids in Various Organic Solvents *Langmuir* **1992**, *8*, 2215-2218.
- (107) Kalyuzhny, G.; Murray, R. W. Ligand Effects on Optical Properties of CdSe Nanocrystals *J. Phys. Chem. B* **2005**, *109*, 7012-7021.
- (108) Munro, A. M.; Jen-La Plante, I.; Ng, M. S.; Ginger, D. S. Quantitative Study of the Effects of Surface Ligand Concentration on CdSe Nanocrystal Photoluminescence *J. Phys. Chem. C* **2007**, *111*, 6220-6227.
- (109) Munro, A. M.; Ginger, D. S. Photoluminescence Quenching of Single CdSe Nanocrystals by Ligand Adsorption *Nano Lett.* **2008**, *8*, 2585-2590.
- (110) Williams, E. S.; Major, K. J.; Tobias, A.; Woodall, D.; Morales, V.; Lippincott, C.; Moyer, P. J.; Jones, M. Characterizing the Influence of Topo on Exciton Recombination Dynamics in Colloidal CdSe Quantum Dots *J. Phys. Chem. C* **2013**, *117*, 4227-4237.
- (111) Morris-Cohen, A. J.; Malicki, M.; Peterson, M. D.; Slavin, J. W. J.; Weiss, E. A. Chemical, Structural, and Quantitative Analysis of the Ligand Shells of Colloidal Quantum Dots *Chemistry of Materials* **2013**, *25*, 1155-1165.
- (112) Garcia-Rodriguez, R.; Liu, H. Solution Structure of Cadmium Carboxylate and Its Implications for the Synthesis of Cadmium Chalcogenide Nanocrystals *Chem. Commun.* **2013**, *49*, 7857-7859.
- (113) García-Rodríguez, R.; Liu, H. A Nuclear Magnetic Resonance Study of the Binding of Trimethylphosphine Selenide to Cadmium Oleate *J. Phys. Chem. A* **2014**, *118*, 7314-7319.
- (114) Liu, H.; Owen, J. S.; Alivisatos, A. P. Mechanistic Study of Precursor Evolution in Colloidal Group II-VI Semiconductor Nanocrystal Synthesis *J. Am. Chem. Soc.* **2007**, *129*, 305-312.
- (115) Grabolle, M.; Spieles, M.; Lesnyak, V.; Gaponik, N.; Eychmüller, A.; Resch-Genger, U. Determination of the Fluorescence Quantum Yield of Quantum Dots: Suitable Procedures and Achievable Uncertainties *Anal. Chem.* **2009**, *81*, 6285-6294.

- (116) Malicki, M.; Knowles, K. E.; Weiss, E. A. Gating of Hole Transfer from Photoexcited PbS Quantum Dots to Aminoferrocene by the Ligand Shell of the Dots *Chem. Commun.* **2013**, *49*, 4400-4402.
- (117) Greaney, M. J.; Couderc, E.; Zhao, J.; Nail, B. A.; Mecklenburg, M.; Thornbury, W.; Osterloh, F. E.; Bradforth, S. E.; Brutchey, R. L. Controlling the Trap State Landscape of Colloidal CdSe Nanocrystals with Cadmium Halide Ligands *Chem. Mater.* **2015**, *27*, 744-756.
- (118) De Roo, J.; Justo, Y.; De Keukeleere, K.; Van den Broeck, F.; Martins, J. C.; Van Driessche, I.; Hens, Z. Carboxylic-Acid-Passivated Metal Oxide Nanocrystals: Ligand Exchange Characteristics of a New Binding Motif *Angew Chem Int Edit* **2015**, *54*, 6488-6491.
- (119) Sachleben, J. R.; Colvin, V.; Emsley, L.; Wooten, E. W.; Alivisatos, A. P. Solution-State Nmr Studies of the Surface Structure and Dynamics of Semiconductor Nanocrystals *J. Phys. Chem. B* **1998**, *102*, 10117-10128.
- (120) Cass, L. C.; Malicki, M.; Weiss, E. A. The Chemical Environments of Oleate Species within Samples of Oleate-Coated PbS Quantum Dots *Anal. Chem.* **2013**, *85*, 6974-6979.
- (121) Aruda, K. O.; Bohlmann Kunz, M.; Tagliazucchi, M.; Weiss, E. A. Temperature-Dependent Permeability of the Ligand Shell of PbS Quantum Dots Probed by Electron Transfer to Benzoquinone *J. Phys. Chem. Lett.* **2015**, *6*, 2841-2846.
- (122) Myung, N.; Bae, Y.; Bard, A. J. Enhancement of the Photoluminescence of CdSe Nanocrystals Dispersed in CHCl_3 by Oxygen Passivation of Surface States *Nano Lett.* **2003**, *3*, 747-749.
- (123) Knowles, K. E.; Tagliazucchi, M.; Malicki, M.; Swenson, N. K.; Weiss, E. A. Electron Transfer as a Probe of the Permeability of Organic Monolayers on the Surfaces of Colloidal PbS Quantum Dots *J. Phys. Chem. C* **2013**, *117*, 15849-15857.
- (124) Morris-Cohen, A. J.; Frederick, M. T.; Lilly, G. D.; McArthur, E. A.; Weiss, E. A. Organic Surfactant-Controlled Composition of the Surfaces of CdSe Quantum Dots *J. Phys. Chem. Lett.* **2010**, *1*, 1078-1081.
- (125) Weinberg, D. J.; He, C.; Weiss, E. A. Control of the Redox Activity of Quantum Dots through Introduction of Fluoroalkanethiolates into Their Ligand Shells *Journal of the American Chemical Society* **2016**, *138*, 2319-2326.
- (126) Amin, V. A.; Aruda, K. O.; Lau, B.; Rasmussen, A. M.; Edme, K.; Weiss, E. A. Dependence of the Band Gap of CdSe Quantum Dots on the Surface Coverage and Binding Mode of an Exciton-Delocalizing Ligand, Methylthiophenolate *J Phys Chem C* **2015**, *119*, 19423-19429.
- (127) Aruda, K. O.; Amin, V. A.; Thompson, C. M.; Lau, B.; Nepomnyashchii, A. B.; Weiss, E. A. Description of the Adsorption and Exciton Delocalizing Properties of P-Substituted Thiophenols on CdSe Quantum Dots *Langmuir* **2016**, *32*, 3354-3364.
- (128) Harris, R. D.; Amin, V. A.; Lau, B.; Weiss, E. A. Role of Interligand Coupling in Determining the Interfacial Electronic Structure of Colloidal CdS Quantum Dots *Acc Nano* **2016**, *10*, 1395-1403.
- (129) Lian, S. C.; Weinberg, D. J.; Harris, R. D.; Kodaimati, M. S.; Weiss, E. A. Subpicosecond Photoinduced Hole Transfer from a CdS Quantum Dot to a Molecular Acceptor Bound through an Exciton-Delocalizing Ligand *Acc Nano* **2016**, *10*, 6372-6382.
- (130) Boulesbaa, A.; Issac, A.; Stockwell, D.; Huang, Z.; Huang, J.; Guo, J.; Lian, T. Ultrafast Charge Separation at CdS Quantum Dot/Rhodamine B Molecule Interface *J Am Chem Soc* **2007**, *129*, 15132-+.
- (131) Song, N. H.; Zhu, H. M.; Jin, S. Y.; Zhan, W.; Lian, T. Q. Poisson-Distributed Electron-Transfer Dynamics from Single Quantum Dots to C60 Molecules *Acc Nano* **2011**, *5*, 613-621.

- (132) Knowles, K. E.; Tagliacruzchi, M.; Malicki, M.; Swenson, N. K.; Weiss, E. A. Electron Transfer as a Probe of the Permeability of Organic Monolayers on the Surfaces of Colloidal PbS Quantum Dots *J Phys Chem C* **2013**, *117*, 15849-15857.
- (133) Jin, S. Y.; Tagliacruzchi, M.; Son, H. J.; Harris, R. D.; Aruda, K. O.; Weinberg, D. J.; Nepomnyashchii, A. B.; Farha, O. K.; Hupp, J. T.; Weiss, E. A. Enhancement of the Yield of Photoinduced Charge Separation in Zinc Porphyrin-Quantum Dot Complexes by a Bis(Dithiocarbamate) Linkage *J Phys Chem C* **2015**, *119*, 5195-5202.
- (134) Song, Y.; Chen, S. W. Janus Nanoparticles: Preparation, Characterization, and Applications *Chem-Asian J* **2014**, *9*, 418-430.
- (135) Chen, O.; Yang, Y. A.; Wang, T.; Wu, H. M.; Niu, C. G.; Yang, J. H.; Cao, Y. C. Surface-Functionalization-Dependent Optical Properties of II-VI Semiconductor Nanocrystals *Journal of the American Chemical Society* **2011**, *133*, 17504-17512.
- (136) Boles, M. A.; Talapin, D. V. Self-Assembly of Tetrahedral CdSe Nanocrystals: Effective "Patchiness" Via Anisotropic Steric Interaction *Journal of the American Chemical Society* **2014**, *136*, 5868-5871.
- (137) Santos, A.; Millan, J. A.; Glotzer, S. C. Faceted Patchy Particles through Entropy-Driven Patterning of Mixed Ligand Sams *Nanoscale* **2012**, *4*, 2640-2650.
- (138) Poon, Z.; Lee, J. A.; Huang, S. W.; Prevost, R. J.; Hammond, P. T. Highly Stable, Ligand-Clustered "Patchy" Micelle Nanocarriers for Systemic Tumor Targeting *Nanomed-Nanotechnol* **2011**, *7*, 201-209.
- (139) Jin, S. Y.; Harris, R. D.; Lau, B.; Aruda, K. O.; Amin, V. A.; Weiss, E. A. Enhanced Rate of Radiative Decay in CdSe Quantum Dots Upon Adsorption of an Exciton-Delocalizing Ligand *Nano Letters* **2014**, *14*, 5323-5328.
- (140) Azpiroz, J. M.; De Angelis, F. Ligand Induced Spectral Changes in CdSe Quantum Dots *ACS applied materials & interfaces* **2015**, *7*, 19736-19745.
- (141) Wu, K. F.; Chen, Z. Y.; Lv, H. J.; Zhu, H. M.; Hill, C. L.; Lian, T. Q. Hole Removal Rate Limits Photodriven H₂ Generation Efficiency in CdS-Pt and CdSe/CdS-Pt Semiconductor Nanorod-Metal Tip Heterostructures *Journal of the American Chemical Society* **2014**, *136*, 7708-7716.
- (142) Olshansky, J. H.; Ding, T. X.; Lee, Y. V.; Leone, S. R.; Alivisatos, A. P. Hole Transfer from Photoexcited Quantum Dots: The Relationship between Driving Force and Rate *Journal of the American Chemical Society* **2015**, *137*, 15567-15575.
- (143) Giansante, C.; Carbone, L.; Giannini, C.; Altamura, D.; Ameer, Z.; Maruccio, G.; Loiudice, A.; Belviso, M. R.; Cozzoli, P. D.; Rizzo, A. *et al.* Colloidal Arenethiolate-Capped PbS Quantum Dots: Optoelectronic Properties, Self-Assembly, and Application in Solution-Cast Photovoltaics *J Phys Chem C* **2013**, *117*, 13305-13317.
- (144) Xie, Y. Z.; Teunis, M. B.; Pandit, B.; Sardar, R.; Liu, J. J. Molecule-Like CdSe Nanoclusters Passivated with Strongly Interacting Ligands: Energy Level Alignment and Photoinduced Ultrafast Charge Transfer Processes *J Phys Chem C* **2015**, *119*, 2813-2821.
- (145) Teunis, M. B.; Dolai, S.; Sardar, R. Effects of Surface-Passivating Ligands and Ultrasmall CdSe Nanocrystal Size on the De Localization of Exciton Confinement *Langmuir* **2014**, *30*, 7851-7858.
- (146) Lawrence, K. N.; Johnson, M. A.; Dolai, S.; Kumbhar, A.; Sardar, R. Solvent-Like Ligand-Coated Ultrasmall Cadmium Selenide Nanocrystals: Strong Electronic Coupling in a Self-Organized Assembly *Nanoscale* **2015**, *7*, 11667-11677.

- (147) Tan, Y. Z.; Jin, S.; Hamers, R. J. Photostability of CdSe Quantum Dots Functionalized with Aromatic Dithiocarbamate Ligands *ACS Applied Materials & Interfaces* **2013**, *5*, 12975-12983.
- (148) Marbella, L. E.; Millstone, J. E. Nmr Techniques for Noble Metal Nanoparticles *Chemistry of Materials* **2015**, *27*, 2721-2739.
- (149) Donakowski, M. D.; Godbe, J. M.; Sknepnek, R.; Knowles, K. E.; de la Cruz, M. O.; Weiss, E. A. A Quantitative Description of the Binding Equilibria of Para-Substituted Aniline Ligands and CdSe Quantum Dots *J Phys Chem C* **2010**, *114*, 22526-22534.
- (150) Gomes, R.; Hassinen, A.; Szczygiel, A.; Zhao, Q. A.; Vantomme, A.; Martins, J. C.; Hens, Z. Binding of Phosphonic Acids to CdSe Quantum Dots: A Solution Nmr Study *J Phys Chem Lett* **2011**, *2*, 145-152.
- (151) Sachleben, J. R.; Wooten, E. W.; Emsley, L.; Pines, A.; Colvin, V. L.; Alivisatos, A. P. Nmr-Studies of the Surface-Structure and Dynamics of Semiconductor Nanocrystals *Chem Phys Lett* **1992**, *198*, 431-436.
- (152) Cros-Gagneux, A.; Delpech, F.; Nayral, C.; Cornejo, A.; Coppel, Y.; Chaudret, B. Surface Chemistry of Inp Quantum Dots: A Comprehensive Study *Journal of the American Chemical Society* **2010**, *132*, 18147-18157.
- (153) Morris-Cohen, A. J.; Frederick, M. T.; Lilly, G. D.; McArthur, E. A.; Weiss, E. A. Organic Surfactant-Controlled Composition of the Surfaces of CdSe Quantum Dots *J Phys Chem Lett* **2010**, *1*, 1078-1081.
- (154) Fritzing, B.; Capek, R. K.; Lambert, K.; Martins, J. C.; Hens, Z. Utilizing Self-Exchange to Address the Binding of Carboxylic Acid Ligands to CdSe Quantum Dots *J Am Chem Soc* **2010**, *132*, 10195-10201.
- (155) Hassinen, A.; Gomes, R.; De Nolf, K.; Zhao, Q.; Vantomme, A.; Martins, J. C.; Hens, Z. Surface Chemistry of CdTe Quantum Dots Synthesized in Mixtures of Phosphonic Acids and Amines: Formation of a Mixed Ligand Shell *J Phys Chem C* **2013**, *117*, 13936-13943.
- (156) Moreels, I.; Fritzing, B.; Martins, J. C.; Hens, Z. Surface Chemistry of Colloidal PbSe Nanocrystals *Journal of the American Chemical Society* **2008**, *130*, 15081-15086.
- (157) Terrill, R. H.; Postlethwaite, T. A.; Chen, C. H.; Poon, C. D.; Terzis, A.; Chen, A. D.; Hutchison, J. E.; Clark, M. R.; Wignall, G.; Londono, J. D. *et al.* Monolayers in Three Dimensions: Nmr, Sxrs, Thermal, and Electron Hopping Studies of Alkanethiol Stabilized Gold Clusters *Journal of the American Chemical Society* **1995**, *117*, 12537-12548.
- (158) Anderson, N. C.; Hendricks, M. P.; Choi, J. J.; Owen, J. S. Ligand Exchange and the Stoichiometry of Metal Chalcogenide Nanocrystals: Spectroscopic Observation of Facile Metal-Carboxylate Displacement and Binding *J Am Chem Soc* **2013**, *135*, 18536-18548.
- (159) Greaney, M. J.; Couderc, E.; Zhao, J.; Nail, B. A.; Mecklenburg, M.; Thornbury, W.; Osterloh, F. E.; Bradforth, S. E.; Brutchey, R. L. Controlling the Trap State Landscape of Colloidal CdSe Nanocrystals with Cadmium Halide Ligands *Chem Mater* **2015**, *27*, 744-756.
- (160) Lias, S. G.; National Institute of Science and Technology: Gaithersburg MD, 20899, 2011.
- (161) Duchesne, L.; Wells, G.; Fernig, D. G.; Harris, S. A.; Levy, R. Supramolecular Domains in Mixed Peptide Self-Assembled Monolayers on Gold Nanoparticles *ChemBiochem* **2008**, *9*, 2127-2134.
- (162) Ramadas, K.; Janarthanan, N.; Velmathi, S. Lac Sulfur Assisted Synthesis of Symmetrical Thioureas *Synthetic Commun* **1997**, *27*, 2255-2260.
- (163) Cademartiri, L.; Montanari, E.; Calestani, G.; Migliori, A.; Guagliardi, A.; Ozin, G. A. Size-Dependent Extinction Coefficients of PbS Quantum Dots *Journal of the American Chemical Society* **2006**, *128*, 10337-10346.

- (164) Luther, J. M.; Beard, M. C.; Song, Q.; Law, M.; Ellingson, R. J.; Nozik, A. J. Multiple Exciton Generation in Films of Electronically Coupled PbSe Quantum Dots *Nano Letters* **2007**, *7*, 1779-1784.
- (165) Knowles, K. E.; Hartstein, K. H.; Kilburn, T. B.; Marchioro, A.; Nelson, H. D.; Whitham, P. J.; Gamelin, D. R. Luminescent Colloidal Semiconductor Nanocrystals Containing Copper: Synthesis, Photophysics, and Applications *Chem Rev* **2016**, *116*, 10820-10851.
- (166) Reiss, P.; Carriere, M.; Lincheneau, C.; Vaure, L.; Tamang, S. Synthesis of Semiconductor Nanocrystals, Focusing on Nontoxic and Earth-Abundant Materials *Chem Rev* **2016**, *116*, 10731-10819.
- (167) Grim, J. Q.; Manna, L.; Moreels, I. A Sustainable Future for Photonic Colloidal Nanocrystals *Chem Soc Rev* **2015**, *44*, 5897-5914.
- (168) Baumgardner, W. J.; Whitham, K.; Hanrath, T. Confined-but-Connected Quantum Solids Via Controlled Ligand Displacement *Nano Letters* **2013**, *13*, 3225-3231.
- (169) Klem, E. J. D.; Shukla, H.; Hinds, S.; MacNeil, D. D.; Levina, L.; Sargent, E. H. Impact of Dithiol Treatment and Air Annealing on the Conductivity, Mobility, and Hole Density in PbS Colloidal Quantum Dot Solids *Applied Physics Letters* **2008**, *92*.
- (170) Lee, J. S.; Kovalenko, M. V.; Huang, J.; Chung, D. S.; Talapin, D. V. Band-Like Transport, High Electron Mobility and High Photoconductivity in All-Inorganic Nanocrystal Arrays *Nat Nanotechnol* **2011**, *6*, 348-352.
- (171) Beard, M. C.; Midgett, A. G.; Law, M.; Semonin, O. E.; Ellingson, R. J.; Nozik, A. J. Variations in the Quantum Efficiency of Multiple Exciton Generation for a Series of Chemically Treated PbSe Nanocrystal Films *Nano Letters* **2009**, *9*, 836-845.
- (172) Brewer, A. S.; Arnold, M. S. Field-Effect Measurements of Mobility and Carrier Concentration of Cu₂s Colloidal Quantum Dot Thin Films after Ligand Exchange *Thin Solid Films* **2014**, *567*, 91-95.
- (173) Gao, Y. N.; Aerts, M.; Sandeep, C. S. S.; Talgorn, E.; Savenije, T. J.; Kinge, S.; Siebbeles, L. D. A.; Houtepen, A. J. Photoconductivity of PbSe Quantum-Dot Solids: Dependence on Ligand Anchor Group and Length *Acc Nano* **2012**, *6*, 9606-9614.
- (174) Mentzel, T. S.; Wanger, D. D.; Ray, N.; Walker, B. J.; Strasfeld, D.; Bawendi, M. G.; Kastner, M. A. Nanopatterned Electrically Conductive Films of Semiconductor Nanocrystals *Nano Letters* **2012**, *12*, 4404-4408.
- (175) Oh, S. J.; Wang, Z. Q.; Berry, N. E.; Choi, J. H.; Zhao, T. S.; Gauding, E. A.; Paik, T.; Lai, Y. M.; Murray, C. B.; Kagan, C. R. Engineering Charge Injection and Charge Transport for High Performance PbSe Nanocrystal Thin Film Devices and Circuits *Nano Letters* **2014**, *14*, 6210-6216.
- (176) Osedach, T. P.; Zhao, N.; Andrew, T. L.; Brown, P. R.; Wanger, D. D.; Strasfeld, D. B.; Chang, L. Y.; Bawendi, M. G.; Bulovic, V. Bias-Stress Effect in 1,2-Ethanedithiol-Treated PbS Quantum Dot Field-Effect Transistors *Acc Nano* **2012**, *6*, 3121-3127.
- (177) Otelaja, O. O.; Ha, D. H.; Ly, T.; Zhang, H. T.; Robinson, R. D. Highly Conductive Cu₂-Xs Nanoparticle Films through Room-Temperature Processing and an Order of Magnitude Enhancement of Conductivity Via Electrophoretic Deposition *Acc Applied Materials & Interfaces* **2014**, *6*, 18911-18920.
- (178) Otto, T. N.; Yu, D. Positive Temperature Coefficient of Resistance and Bistable Conduction in Lead Selenide Quantum Dot Thin Films *J Phys Chem C* **2013**, *117*, 3713-3717.

- (179) Pham, H. T.; Jeong, H.-D. Newly Observed Temperature and Surface Ligand Dependence of Electron Mobility in Indium Oxide Nanocrystal Solids *Acs Applied Materials & Interfaces* **2015**, *7*, 11660-11667.
- (180) Talapin, D. V.; Murray, C. B. PbSe Nanocrystal Solids for N- and P-Channel Thin Film Field-Effect Transistors *Science* **2005**, *310*, 86-89.
- (181) Talgorn, E.; Moysidou, E.; Abellon, R. D.; Savenije, T. J.; Goossens, A.; Houtepen, A. J.; Siebbeles, L. D. A. Highly Photoconductive CdSe Quantum-Dot Films: Influence of Capping Molecules and Film Preparation Procedure *J Phys Chem C* **2010**, *114*, 3441-3447.
- (182) Zarghami, M. H.; Liu, Y.; Gibbs, M.; Gebremichael, E.; Webster, C.; Law, M. P-Type PbSe and PbS Quantum Dot Solids Prepared with Short-Chain Acids and Diacids *Acs Nano* **2010**, *4*, 2475-2485.
- (183) Zhang, Y. Q.; Cao, X. A. Evaluation of All-Inorganic CdSe Quantum Dot Thin Films for Optoelectronic Applications *Nanotechnology* **2012**, *23*.
- (184) Yu, D.; Wehrenberg, B. L.; Jha, P.; Ma, J.; Guyot-Sionnest, P. Electronic Transport of N-Type CdSe Quantum Dot Films: Effect of Film Treatment *J Appl Phys* **2006**, *99*.
- (185) Guglietta, G. W.; Diroll, B. T.; Gaulding, E. A.; Fordham, J. L.; Li, S. M.; Murray, C. B.; Baxter, J. B. Lifetime, Mobility, and Diffusion of Photoexcited Carriers in Ligand-Exchanged Lead Selenide Nanocrystal Films Measured by Time-Resolved Terahertz Spectroscopy *Acs Nano* **2015**, *9*, 1820-1828.
- (186) Liu, Y.; Gibbs, M.; Puthussery, J.; Gaik, S.; Ihly, R.; Hillhouse, H. W.; Law, M. Dependence of Carrier Mobility on Nanocrystal Size and Ligand Length in PbSe Nanocrystal Solids *Nano Letters* **2010**, *10*, 1960-1969.
- (187) Li, W.; Dittrich, T.; Jackel, F.; Feldmann, J. Optical and Electronic Properties of Pyrite Nanocrystal Thin Films: The Role of Ligands *Small* **2014**, *10*, 1194-1201.
- (188) Korala, L.; Wang, Z. J.; Liu, Y.; Maldonado, S.; Brock, S. L. Uniform Thin Films of CdSe and CdSe(ZnS) Core(Shell) Quantum Dots by Sol-Gel Assembly: Enabling Photoelectrochemical Characterization and Electronic Applications *Acs Nano* **2013**, *7*, 1215-1223.
- (189) Dao, T. D.; Hafez, M. E.; Beloborodov, I. S.; Jeong, H. D. Thioacetic-Acid Capped PbS Quantum Dot Solids Exhibiting Thermally Activated Charge Hopping Transport *B Korean Chem Soc* **2014**, *35*, 457-465.
- (190) Kagan, C. R.; Murray, C. B. Charge Transport in Strongly Coupled Quantum Dot Solids *Nat Nano* **2015**, *10*, 1013-1026.
- (191) Weidman, M. C.; Yager, K. G.; Tisdale, W. A. Interparticle Spacing and Structural Ordering in Superlattice PbS Nanocrystal Solids Undergoing Ligand Exchange *Chemistry of Materials* **2015**, *27*, 474-482.
- (192) Zhang, Y. Q.; Cao, X. A. Optical Characterization of CdSe Quantum Dots with Metal Chalcogenide Ligands in Solutions and Solids *Applied Physics Letters* **2011**, *99*, 023106.
- (193) Yaacobi-Gross, N.; Soreni-Harari, M.; Zimin, M.; Kababya, S.; Schmidt, A.; Tessler, N. Molecular Control of Quantum-Dot Internal Electric Field and Its Application to CdSe-Based Solar Cells *Nat Mater* **2011**, *10*, 974-979.
- (194) Scheele, M.; Engel, J. H.; Ferry, V. E.; Hanifi, D.; Liu, Y.; Alivisatos, A. P. Nonmonotonic Size Dependence in the Hole Mobility of Methoxide-Stabilized PbSe Quantum Dot Solids *Acs Nano* **2013**, *7*, 6774-6781.

- (195) Law, M.; Luther, J. M.; Song, O.; Hughes, B. K.; Perkins, C. L.; Nozik, A. J. Structural, Optical, and Electrical Properties of PbSe Nanocrystal Solids Treated Thermally or with Simple Amines *Journal of the American Chemical Society* **2008**, *130*, 5974-5985.
- (196) Luther, J. M.; Law, M.; Song, Q.; Perkins, C. L.; Beard, M. C.; Nozik, A. J. Structural, Optical and Electrical Properties of Self-Assembled Films of PbSe Nanocrystals Treated with 1,2-Ethanedithiol *Acs Nano* **2008**, *2*, 271-280.
- (197) Swisher, S. L. Master's Thesis, University of California at Berkeley, 2012.
- (198) Huang, J.; Huang, Z.; Jin, S.; Lian, T. Exciton Dissociation in CdSe Quantum Dots by Hole Transfer to Phenothiazine *The Journal of Physical Chemistry C* **2008**, *112*, 19734-19738.
- (199) Singhal, P.; Ghosh, H. N. Ultrafast Hole/Electron Transfer Dynamics in a CdSe Quantum Dot Sensitized by Pyrogallol Red: A Super-Sensitization System *The Journal of Physical Chemistry C* **2014**, *118*, 16358-16365.
- (200) Morris-Cohen, A. J.; Frederick, M. T.; Cass, L. C.; Weiss, E. A. Simultaneous Determination of the Adsorption Constant and the Photoinduced Electron Transfer Rate for a Cds Quantum Dot-Viologen Complex *Journal of the American Chemical Society* **2011**, *133*, 10146-10154.
- (201) Huang, J.; Stockwell, D.; Huang, Z.; Mohler, D. L.; Lian, T. Photoinduced Ultrafast Electron Transfer from CdSe Quantum Dots to Re-Bipyridyl Complexes *Journal of the American Chemical Society* **2008**, *130*, 5632-5633.
- (202) Robel, I.; Kuno, M.; Kamat, P. V. Size-Dependent Electron Injection from Excited CdSe Quantum Dots into TiO₂ Nanoparticles *Journal of the American Chemical Society* **2007**, *129*, 4136-4137.
- (203) Kamat, P. V. Boosting the Efficiency of Quantum Dot Sensitized Solar Cells through Modulation of Interfacial Charge Transfer *Accounts of Chemical Research* **2012**, *45*, 1906-1915.
- (204) Christians, J. A.; Kamat, P. V. Trap and Transfer. Two-Step Hole Injection across the Sb₂S₃/Cusc Interface in Solid-State Solar Cells *ACS Nano* **2013**, *7*, 7967-7974.
- (205) Bankole, O. M.; Achadu, O. J.; Nyokong, T. Nonlinear Interactions of Zinc Phthalocyanine-Graphene Quantum Dots Nanocomposites: Investigation of Effects of Surface Functionalization with Heteroatoms *J Fluoresc* **2017**, *27*, 755-766.
- (206) Osifeko, O.; Nyokong, T. Synthesis and Physicochemical Properties of Zinc and Indium Phthalocyanines Conjugated to Quantum Dots, Gold and Magnetic Nanoparticles *Dyes Pigments* **2016**, *131*, 186-200.
- (207) Arvani, M.; Virkki, K.; Abou-Chahine, F.; Efimov, A.; Schramm, A.; Tkachenko, N. V.; Lupo, D. Photoinduced Hole Transfer in QD-Phthalocyanine Hybrids *Phys Chem Chem Phys* **2016**, *18*, 27414-27421.
- (208) Iagatti, A.; Doria, S.; Marcelli, A.; Angelini, N.; Notarantonio, S.; Paoletti, A. M.; Pennesi, G.; Rossi, G.; Zanotti, G.; Calogero, G. *et al.* Photophysical Processes Occurring in a Zn-Phthalocyanine in Ethanol Solution and on TiO₂ Nanostructures *J Phys Chem C* **2015**, *119*, 20256-20264.
- (209) Sharma, D.; Steen, G.; Kortnerik, J. P.; Garcia-Iglesias, M.; Vazquez, P.; Torres, T.; Herek, J. L.; Huijser, A. Impact of the Anchoring Ligand on Electron Injection and Recombination Dynamics at the Interface of Novel Asymmetric Push-Pull Zinc Phthalocyanines and TiO₂ *J Phys Chem C* **2013**, *117*, 25397-25404.
- (210) D'Souza, S.; Antunes, E.; Litwinski, C.; Nyokong, T. Photophysical Behavior of Zinc Monoaminophthalocyanines Linked to Mercaptopropionic Acid-Capped CdTe Quantum Dots *J Photoch Photobio A* **2011**, *220*, 11-19.

- (211) Souza, S. D.; Antunes, E.; Nyokong, T. Synthesis and Photophysical Studies of CdTe Quantum Dot-Monosubstituted Zinc Phthalocyanine Conjugates *Inorg Chim Acta* **2011**, *367*, 173-181.
- (212) Knott, E. B. Heterocyclyl-Rhodanines and Heterocyclyl-2-Thiohydantoins *J Chem Soc* **1956**, 1644-1649.
- (213) Taube, R. New Aspects of Chemistry of Transition-Metal Phthalocyanines *Pure Appl Chem* **1974**, *38*, 427-438.
- (214) Ghani, F.; Kristen, J.; Riegler, H. Solubility Properties of Unsubstituted Metal Phthalocyanines in Different Types of Solvents *J Chem Eng Data* **2012**, *57*, 439-449.
- (215) Tran, N. L.; Bohrer, F. I.; Trogler, W. C.; Kummel, A. C. A Density Functional Theory Study of the Correlation between Analyte Basicity, Znpc Adsorption Strength, and Sensor Response *J Chem Phys* **2009**, *130*.
- (216) Kobayashi, N.; Ogata, H.; Nonaka, N.; Luk'yanets, E. A. Effect of Peripheral Substitution on the Electronic Absorption and Fluorescence Spectra of Metal-Free and Zinc Phthalocyanines *Chem-Eur J* **2003**, *9*, 5123-5134.
- (217) Ologan, M.; Marson, D.; Polizzi, S.; Pengo, P.; Boccardo, S.; Pricl, S.; Posocco, P.; Pasquato, L. Patchy and Janus Nanoparticles by Self-Organization of Mixtures of Fluorinated and Hydrogenated Alkanethiolates on the Surface of a Gold Core *Acs Nano* **2016**, *10*, 9316-9325.
- (218) Liu, X.; Yu, M.; Kim, H.; Marnett, M.; Stellacci, F. Determination of Monolayer-Protected Gold Nanoparticle Ligand-Shell Morphology Using Nmr *Nat Commun* **2012**, *3*.

VITA

Rachel D. Harris

414-731-7732 ▪ rachel.dory.harris@gmail.com ▪ rachel.dory.harris.com ▪ Chicago, IL

Education

NORTHWESTERN UNIVERSITY ▪ Ph.D., Chemistry ▪ Evanston, IL ▪ Expected May 2017

- Specialization: Materials Chemistry, GPA: 3.93/4.0

KELLOGG SCHOOL OF MANAGEMENT ▪ Certificate ▪ Evanston, IL ▪ Aug 2016

- Management for Scientists and Engineers, an intensive and selective (50 of 150 applicants) program covering finance, accounting, business strategy, marketing, management, and leadership skills.

UNIVERSITY OF PITTSBURGH ▪ B.S., Chemistry ▪ Pittsburgh, PA ▪ Apr 2012

- *summa cum laude*, Honors in Chemistry; ACS Certified; GPA: 3.85/4.0

Skills

Instrumentation

1D and 2D NMR, FTIR, MALDI, ICP-OES, SEM, TEM, UV-VIS, photoluminescence

Laboratory

Air-free, polymerization, quantum dot synthesis, surface chemistry, thin film fabrication, safety

Software

R/RStudio, SQL, Origin, Avogadro, MestReNova, Excel, PowerPoint

Research Experience

GRADUATE RESEARCH ASSISTANT ▪ Dr. Emily Weiss, Northwestern ▪ Evanston, IL ▪ Nov 2012 - May 2017

- Selected for two prestigious national fellowships from the NSF (GRFP, \$132k) and Dept. of Defense (NDSEG, \$96k) based on academic achievement, leadership, and outreach experience, as well as an original research proposal (only the NSF-GRFP was accepted).
- Developed a novel quantitative NMR technique to characterize the relationship between bound exciton-delocalizing ligands on quantum dots and the degree of delocalization as measured by optical spectroscopy, which resulted in a first-author publication.
- Directed a team of eight graduate students and postdocs in the writing of a 587-reference literature review by supervising edits and facilitating progress update meetings.
- Mentored three undergraduate students and a dozen junior graduate students on their research projects, best laboratory practices, and success in graduate school.

UNDERGRADUATE RESEARCH ASSISTANT ▪ Dr. Tara Meyer, Pitt ▪ Pittsburgh, PA ▪ Aug 2010 - Jul 2012

- Earned five merit-based chemistry awards, totaling \$5800, as well as a four-year, full-tuition scholarship.
- Presented experimental results to an interdisciplinary team of scientists and engineers at biweekly meetings.
- Developed a dual-responsive Cu-chelating polymer hydrogel that becomes softer when reduced electrochemically (Cu⁺) and harder when oxidized in atmospheric oxygen (Cu²⁺).
- Published a first-author paper describing and characterizing this novel material, which has been cited 20 times, and earned authorship on a patent application as a result of this work.

Publications

1. **Harris, R.D.***; Homan, S.B.*; Kodaimati, M. *et al.* Electronic Processes within Quantum Dot-Molecule Complexes, *Chem. Rev.*, **2016**, *116* (21), 12865-12919.
2. Lian, S.; Weinberg, D.J.; **Harris, R.D.** *et al.* Subpicosecond Photoinduced Hole Transfer from a CdS Quantum Dot to a Molecular Acceptor Bound Through an Exciton-Delocalizing Ligand. *ACS Nano*, **2016**, *10* (6), 6372-6382.
3. **Harris, R.D.**; Amin, V.A.; Lau, B.; Weiss, E.A. Role of Interligand Coupling in Determining the Interfacial Electronic Structure of Colloidal CdS Quantum Dots, *ACS Nano*, **2016**, *10* (1), 1395-1403.
4. Nepomnyashchii, A. B.; **Harris, R.D.**; Weiss, E.A. The Composition and Permeability of Oleate Adlayers of CdS Quantum Dots upon Dilution to Photoluminescence-Relevant Concentrations, *Anal. Chem.*, **2016**, *88* (6), 3310-3316.
5. Jin, S.; Tagliacruzchi, M.; Son, H-J.; **Harris, R.D.** *et al.* Enhancement of the Yield of Photoinduced Charge Separation in Zinc Porphyrin-Quantum Dot Complexes by a Bis(dithiocarbamate) Linkage. *J. Phys. Chem. C*, **2015**, *119* (9), 5195-5202.
6. Jin, S.; **Harris, R.D.**; Lau, B.; Aruda, K.O.; Amin, V.A.; Weiss, E.A. Enhanced Rate of Radiative Decay in CdSe Quantum Dots upon Adsorption of an Exciton-Delocalizing Ligand, *Nano Lett.* **2014**, *14*, 5323-5328.
7. Peterson, M.D.; Cass, L.C.; **Harris, R.D.**; Edme, K.; Sung, K.; Weiss, E.A. The Role of Ligands in Determining the Exciton Relaxation Dynamics in Semiconductor Quantum Dots, *Ann. Rev. Phys. Chem.*, **2014**, *65*, 317-339.
8. **Harris, R.D.**; Auletta, J.T.; Motlagh, S.A.; *et al.* Chemical and Electrical Manipulation of Mechanical Properties in Stimuli-Responsive Copper-Crosslinked Hydrogels. *ACS Macro Lett.*, **2013**, *2* (12), 1095-1099.

Presentations and Patents

9. **Harris, R.D.**; Amin, V.A.; Lau, B.; Weiss, E.A. The Relationship between the Spatial Distribution of an Exciton-Delocalizing Ligand and the Radius of Delocalization for CdS Quantum Dots. 2016 MRS Spring Meeting, poster presentation.
10. Meyer, T.Y.; Clark, W.W.; Waldeck, D.; Weiland, L.M.; Calvo-Marzal, P; Pan, T; **Harris, R.D.**; Liu, H. Redox-Stimulated Variable-Modulus Material. U.S. Patent Application No. 20130146821. Issued June 13, 2013.

Leadership, Communication, and Outreach Experience

READY, SET, GO ▪ Northwestern ▪ Evanston, IL ▪ Jun 2016 - Sep 2016

- Honed communication skills by participating in an intensive science communications workshop for 12 weeks.
 - Developed an original seven-minute presentation on my research geared towards a general audience.
- "CHEMUNITY" PEER MENTOR** ▪ Northwestern Chemistry Dept. ▪ Evanston, IL ▪ Aug 2015 - May 2017
- Mentored two first-year graduate students as they transitioned into the department.
 - Gained mentoring skills by attending quarterly workshops throughout the year.
 - Advised first-year students during one-on-one meetings as needed.

PRESIDENT ▪ Northwestern Energy Technology Group ▪ Northwestern ▪ Aug 2014- Jun 2016

- Led a collaborative, 8+ student steering committee of scientists and engineers to promote energy awareness and education.
- Planned and executed social and professional development activities with other student groups at Northwestern, with some events totaling over 100 attendees.

CO-PRESIDENT ▪ American Chemical Society, Pitt Student Chapter ▪ Pittsburgh, PA ▪ Aug 2011 - Apr 2012

- Conducted weekly meetings of 50+ undergraduates to increase awareness of ongoing research, upcoming outreach events, and post-graduation opportunities.
- Planned and participated in outreach programs to improve interest in chemistry among local K-12 students.

OUTREACH COORDINATOR ▪ Pittsburgh Area Women Chemists Committee ▪ Pittsburgh, PA ▪ Jun 2011 - May 2012

- Developed outreach programs emphasizing science education for girls and young women.
- Organized the inaugural Couture, Cosmetics, and Chemistry event, a collaborative effort with the Girl Scouts.
- Coordinated 30+ volunteers in the preparation and execution of this event.

ORGANIC CHEMISTRY TEACHING ASSISTANT ▪ Various ▪ Sep 2010 - Nov 2013

- Educated students in laboratory and classroom settings for sophomores, juniors, and seniors in introductory and advanced organic chemistry courses.
- Mentored small groups on independent research projects.

Professional Affiliations

AMERICAN CHEMICAL SOCIETY ▪ Aug 2011 - Present**PHI LAMBDA UPSILON** ▪ Aug 2014 - Present